NASA Technical Memorandum 89438 USAAVSCOM TM 87-A-3

A Piloted Simulation of Helicopter Air Combat to Investigate Effects of Variations in Selected Performance and Control Response Characteristics

Michael S. Lewis, M. Hossein Mansur,
and Robert T. N. Chen

August 1987

NASA
National Aeronautics and
Space Administration

US ARMY
AVIATION
SYSTEMS COMMAND
AVIATION RESEARCH AND
TECHNOLOGY ACTIVITY

NASA Technical Memorandum 89438

USAAVSCOM TM 87-A-3

A Piloted Simulation of Helicopter Air Combat to Investigate Effects of Variations in Selected Performance and Control Response Characteristics

Michael S. Lewis,
M. Hossein Mansur, Aeroflight Directorate, U. S. Army Aviation Research and Technology Activity, Ames Research Center, Moffett Field, California
Robert T. N. Chen, Ames Research Center, Moffett Field, California

August 1987

National Aeronautics and Space Administration

Ames Research Center
Moffett Field, California 94035

US ARMY
AVIATION
SYSTEMS COMMAND

AVIATION RESEARCH AND TECHNOLOGY ACTIVITY
MOFFETT FIELD, CA 94305-1099

A PILOTED SIMULATION OF HELICOPTER AIR COMBAT TO INVESTIGATE EFFECTS OF VARIATIONS IN SELECTED PERFORMANCE AND CONTROL RESPONSE CHARACTERISTICS

Michael S. Lewis M. Hossein Mansur Robert T. N. Chen

ABSTRACT

A piloted simulation study investigating handling qualities and flight characteristics required for helicopter air-to-air combat is discussed. The Helicopter Air Combat system, developed on the Vertical Motion Simulator at NASA Ames Research Center, was used to investigate this important new role for Army rotorcraft.

Experimental variables for the study were the maneuver envelope size (load factor and sideslip), directional axis handling qualities, and pitch and roll control-response type of the test aircraft. Over 450 simulated, low altitude, one-on-one engagements were conducted utilizing evaluation pilots from the Army, NASA, and industry.

Data from the simulation are shown and compared for each of the configurations evaluated, including control response time histories, pilot handling-qualities ratings, weapons scoring, load factor and sideslip envelope excursions, control movements, and flight variable time histories.

Results from the experiment indicate that a well-damped directional response, low sideforce caused by sideslip, and some effective dihedral are all desirable for weapon system performance, good handling qualities, and low pilot workload. A rate command system was favored over the attitude-type pitch and roll response for most applications, and an enhanced maneuver envelope size over current generation aircraft was found to be advantageous. Pilot technique, background, and experience are additional factors which had a significant effect on performance in the air combat tasks investigated. The implication of these results on design requirements for future helicopters is discussed.

INTRODUCTION

Helicopter air combat has continued to be a dominant factor in driving both new military helicopter designs and current rotorcraft research since the air combat mission was identified as a high priority Army deficiency in 1982. Flight tests sponsored by the U.S. Army Aviation Research and Technology Activity have generated data pertaining to clear-air, one-on-one, maneuvering between selected current aircraft [1]. The Army also conducted flight-test exercises involving air combat with multiple participants in early 1986 at Fort Hunter Liggett, California. Various helicopter

manufacturers are also familiarizing company pilots and engineers with air combat maneuvering flight.

In order to investigate fully many of the important factors involved with successful helicopter air combat, parametric variations of vehicle performance and handling qualities characteristics are required. Both variable stability aircraft and research simulators are needed to manipulate selected variables, although only simulation studies can effectively vary performance-related parameters. In addition, at this relatively early stage of study, the great flexibility, high equivalent flight time, and comparably low cost of simulation is preferable to flight test, although final flight testing of selected configurations is required to validate specific results.

In early 1984, the Vertical Motion Simulator (VMS) at NASA Ames Research Center was modified to allow real time simulation of low-level, one-on-one, helicopter air combat. The Helicopter Air Combat (HAC) simulator system designed for this capability and the original experiment conducted (HAC I) are described in [2]. Following that experiment, several other studies using the Ames HAC system involving the air combat task have been conducted. One simulation [3] focused on required roll axis response, and another investigated the advantage gained by independent X-force control in a compound or tilt-rotor configuration. Additionally, a study [4] aimed at evaluating an advanced single-pilot cockpit design used the air combat task as a high workload portion of the flight mission.

All of these studies focused attention on the longitudinal and lateral axes, with no experimental variations in the directional axis. The directional axis, however, plays an important role during air-to-air engagements, as was indicated when the tail of an S-76 helicopter was damaged as a result of overstress during air-to-air combat tests (AACT II) [5] air combat maneuvering (ACM) tests. Therefore, the experiment described in this report was designed to explore the directional handling qualities and envelope requirements for air combat. In addition, a more comprehensive study of the control-response type issue (rate command/attitude hold vs attitude command/attitude hold) was conducted to validate, or otherwise generate data to modify, the results obtained during HAC-I. Finally, to provide information on fundamental performance design, the realistically maneuvering envelope size required for air combat was investigated.

In the sections below, the experimental design and conduct are discussed; test data are presented and results summarized. Conclusions regarding the test variables and other factors found to be important to this task are stated. An appendix is also included in this report which details a linear analysis of the helicopter math model used.

EXPERIMENTAL DESIGN

Experimental Variables

Experimental variables for this test were the directional axis dynamic characteristics, aircraft maneuver envelope size, and cyclic control-response type. Each of these variables and the configurations tested are discussed below. The configurations are identified with a three or four digit number; the first digit corresponds to envelope size, the second corresponds to cyclic control response, the third and fourth to directional axis response. Three different maneuvering envelopes were modeled and generally correspond to an early model attack aircraft (low baseline, 1xx), a typical modern utility aircraft (high baseline, 2xx), and a possible advanced scout/attack aircraft (advanced, 3xx), all at light gross weights. A diagram of the maximum steady load factor capability for these configurations, limited primarily by the power available, is shown in figure 1. A variety of

directional response characteristics were tested involving variations in natural frequency, damping, effective dihedral, and sideforce caused by sideslip. The pitch and roll responses were varied among three types as outlined below. Table 1 provides a summary of the characteristics of all the tested configurations.

Directional Response

A variety of directional axis responses were evaluated. The lateral-directional characteristics of the generic model may be represented by the following state-space representation:

$$\dot{x} = Fx + Gu$$

$$\begin{pmatrix} \dot{v} \\ \dot{r} \\ \dot{p} \\ \dot{\phi} \end{pmatrix} = \begin{pmatrix} Y_v & -U_\circ & 0 & g' \\ N_v & N_r & N_p & N_\phi \\ L_v & 0 & L_p & L_\phi \\ 0 & 0 & 1 & 0 \end{pmatrix} \begin{pmatrix} v \\ r \\ p \\ \phi \end{pmatrix} + \begin{pmatrix} 0 & 0 \\ N_{\delta_p} & 0 \\ 0 & L_{\delta_a} \\ 0 & 0 \end{pmatrix} \begin{pmatrix} \delta_p \\ \delta_a \end{pmatrix}$$

Tables 2(a-g) list the numerators and denominators of all the relevant transfer functions (longitudinal and lateral-directional) for both attitude and rate command systems at 30 and 60 knots airspeeds. It may be noted that the model was designed with automatic turn coordination above 50 knots leading to the $v/\delta_a = 0$ response listed for the 60 knots case. Parameters changed in the second order response realized at speeds above 50 knots were natural frequency, damping, sideforce caused by sideslip, and effective dihedral. The baseline configuration (xx1) had a natural frequency of 1.5 rad/sec, damping ratio of 0.71, Y_v derivative equal to -0.1 sec^{-1} and no effective dihedral. Natural frequencies above and below 1.5 rad/sec were examined while holding constant damping ratio values. Preliminary evaluations showed that a damping ratio of 0.71 was a relatively low value for the task and only additional higher values were subsequently used. Damping ratio changes were likewise made with the natural frequency held to constant values. As will be discussed in detail, pedal sensivity was always held constant despite changes in the directional natural frequency by setting N_{δ_p} to appropriate values.

Sideforce Caused by Sideslip

Since the effect on air combat handling qualities of variations in the Y_v derivative was unknown, an exaggerated high value (-0.3 sec^{-1}) was chosen for one configuration and a very low value (-0.05 sec^{-1}) was chosen for the other. The baseline value of -0.1 sec^{-1} is a typical value for a scout/attack helicopter.

Dihedral Effect

The effective dihedral derivative L_v, was made part of the roll acceleration equation and was nonzero in one configuration. Because of the turn coordination feature which caused a zero sideslip response to lateral control at speeds above 50 knots, the addition of this term did not change the characteristic response of the aircraft to lateral cyclic input or the directional response to a pedal input. The major difference between this configuration and an identical one with no effective

dihedral is the roll response to a pedal-induced sideslip. The configuration evaluated had a dihedral derivative value of $-0.07\ rad/ft - sec$, typical of the tested aircraft types. A complete discussion of the effect of the L_v term is included in the appendix.

Maneuver Envelope Size

Steady Load factor

Since a test variable in the simulation experiment was aircraft maneuverability (defined in reference [6] as the measure of the ability to change the velocity vector or energy state), it was desired to control the steady state load factor which various configurations could attain. The normal limitation to steady load factor in an actual helicopter is total power available. The math model used in the simulation did not have an engine model, however, and no "power available" term could be calculated. The steady state size of the thrust vector, and therefore the steady state load factor of the simulated aircraft could be controlled, though, by limiting the size of allowable collective inputs.

Values of maximum allowed collective inputs as a funtion of airspeed were programmed into the model. Maximum rate of climb data for typical existing and possible future aircraft designs were obtained as shown in figure 2. These curves are effectively plots of power available. By approximating the body-axis vertical velocity "w" as vertical climb speed, and assuming a first-order vertical response to collective input, maximum allowable collective inputs can be found. Letting

$$\frac{w}{\delta_c}(s) = \frac{Z_{\delta_c}}{(s - Z_w)}$$

where,

Z_{δ_c} = vertical control sensitivity $(ft/sec^2/\%)$
Z_w = vertical damping $(1/sec)$

the steady state response to a step input in collective is

$$\frac{w}{\delta_c} = \frac{-Z_{\delta_c}}{Z_w}$$

and therefore,

$$\delta_{c_{max}} = \frac{-(Z_w)(w_{max})}{Z_{\delta_c}}$$

Values for Z_{δ_c} and Z_w were set to be constant at 1.5 $ft/sec^2/\%$ and $-1.0\ sec^{-1}$, respectively. Similarly, a maximum rate of descent, and thus a minimum collective input, was set (fig. 3). A value of 1900 fpm was allowed for all configurations. Figure 3 also shows the effective ranges of collective stick travel for each configuration. If the collective was moved outside of this range, the added input above or below the limiting value was ignored. The steady load factors corresponding to the collective limits can be calculated as

$$n_{z_{max}} = \frac{Z_{\delta_c}\delta_{c_{max}}}{32.2} + 1$$

No indication was made to the pilot other than the lack of aircraft response when a steady load factor limit was reached.

Transient Load Factor

Transient load factor limiting was pilot controlled. If the measured value of aircraft normal load factor (n_z) exceeded limits for longer than 0.5 sec, a red warning light was automatically lit on the cockpit instrument panel, and the pilot would receive a high-pitched warning tone in his headset. An orange light on the instrument panel was used to indicate that the aircraft was within 10% of the limit values.

Transient load-factor limits were adjusted during the course of the experiment. Initial envelope sizes were obtained from flight-test documents [5] and ranges of values suggested by Lappos [6]. These load-factor limits, representative of structural limitations of the aircraft, are shown in figure 4. Limitations more representative of rotor-system capability were later implemented and are shown in figure 5. The values shown are typical for the aircraft loaded to design gross weight (DGW). As can be seen, there are significant differences from the original values. The majority of simulation evaluations were conducted with the latter limits modeled and driving the cockpit displays.

In comparing the steady and transient load factor limit curves, it can be seen that at airspeeds near 70 knots the steady load-factor capability exceeds the transient capability somewhat for the high and low baseline configurations. This result arises from the simple model used to transfer realistic maximum rate-of-climb values to load-factor capabilities. The steady load-factor curves roughly correspond to the aircraft types at light gross weights, while the transient load-factor limits correspond to these aircraft at design gross weight. In practice, the transient load factor was always the upper limit as the pilots were warned when this value was exceeded.

Sideslip Limits

A sideslip envelope for each configuration was implemented in a manner similar to the steady state normal load-factor limit. Maximum left and right pedal deflections as functions of airspeed were defined beyond which the added deflections were ignored.

The aircraft math model, in the absence of any dihedral effect, produces a sideslip angle response to pedal input as follows:

$$\frac{\beta}{\delta_p}(s) = \frac{-N_{\delta_p}}{s^2 - (Y_v + N_r)s + (Y_v N_r + U_\circ N_v)}$$

where,

N_{δ_p} = yaw control sensitivity $(rad/sec^2/\%)$
Y_v = lateral speed damping derivative $(1/sec)$
N_r = yaw rate damping derivative $(1/sec)$
$U_\circ$ = body axis longitudinal velocity component (ft/sec)
N_v = augmented directional stability derivative for automatic turn coordination $(rad/ft - sec)$

The derivative N_v was set to zero for hover and low speeds. In forward flight (i.e., airspeeds greater than 50 knots), however, N_v was set to $K_{N_v}/U_\circ$ so that any particular configuration would have a constant pedal response. The steady state pedal response to a step input is therefore:

$$\frac{\beta}{\delta_p} = \frac{-N_{\delta_p}}{(Y_v N_r + K_{N_v})}$$

Thus, a scheduling of allowable pedal deflections was implemented which effectively limited achievable sideslip angles. Pedal sensitivity was held constant despite configuration changes in the directional axis derivatives by setting

$$N_{\delta_p} = K(Y_v N_r + K_{N_v})$$

where

$$K = 0.0209$$

allowing 18.4° of sideslip per inch pedal deflection. Maximum sideslip angles for each of the vehicle types mentioned above are shown in figure 6.

Pitch and Roll Control Response

Three types of cyclic control responses were modeled for the blue (VMS) aircraft. The transfer functions for each of these responses are derived in the appendix. A summary of the small perturbation, linear dynamic characteristics of the model are discussed below.

Rate Command (RC)

The transfer functions for roll and pitch attitude response to lateral and longitudinal cyclic inputs respectively were:

$$\frac{\phi}{\delta_a}(s) = \frac{L_{\delta_a}}{s(s - L_p)}$$

$$\frac{\theta}{\delta_e}(s) = \frac{M_{\delta_e}}{s(s - M_q)}$$

where

L_{δ_a}, M_{δ_e} = roll, pitch control sensitivities
L_p, M_q = roll, pitch rate damping derivatives

Thus, the time constants in both the roll and pitch rate response were equal to 0.179 *sec*. This response is somewhat quicker in pitch and slower in roll than a typical hingeless helicopter. The roll response is comparable to that of the OH-6A articulated rotor system helicopter as shown in table 3. Original values of L_p and M_q in the model were both equal to $-2.8\ sec^{-1}$. Pitch and roll responses with these settings were deemed too slow by the evaluation pilots for the air-combat task. Since it was desired to keep an optimum cyclic response so that other characteristics could be evaluated independently, the rate damping values were changed to the -5.6 setting. Pitch and roll responses were then judged satisfactory for the task.

The control derivatives L_{δ_a} and M_{δ_e} were chosen to be 0.26 and 0.14 $rad/sec - \%$, respectively. These values are approximately equal to that of the BO-105C hingeless rotor system in both roll and pitch as shown in table 4. Steady state angular rates per unit cyclic can then be calculated for the model aircraft as follows:

$$\frac{p}{\delta_a}|_{ss} = \frac{L_{\delta_a}}{-L_p} = 0.26/5.6 = 0.0464\ (rad/sec - \%)$$

$$\frac{q}{\delta_e}|_{ss} = \frac{M_{\delta_e}}{-M_q} = -0.14/5.6 = -.025\ (rad/sec - \%)$$

Since full stick deflection in one direction is 50% of the total travel, and converting to degrees,

$$p_{max} = 132.9\ (deg/sec)$$

$$q_{max} = 71.6\ (deg/sec)$$

Attitude Command/Attitude Hold (AC/AH)

The transfer functions for roll and pitch attitude response to lateral and longitudinal cyclic inputs respectively were:

$$\frac{\phi}{\delta_a}(s) = \frac{L_{\delta_a}}{(s^2 - L_p s - L_\phi)}$$

$$\frac{\theta}{\delta_e}(s) = \frac{M_{\delta_e}}{(s^2 - M_q s - M_\theta)}$$

where,

L_ϕ, M_θ = roll, pitch attitude stability derivatives (nominally = $-6.25/sec^2$)

L_p and M_q values were held at the same values as the rate command system ($-5.6\ sec^{-1}$). To reduce the control sensitivity at low speeds and hover, L_{δ_a} and M_{δ_e} were scheduled as functions of airspeed as indicated in figure 7 (note the differences from the rate command system). Maximum roll and pitch angles attainable can be calculated as

$$\frac{\phi}{\delta_a}|_{ss} = \frac{-L_{\delta_a}}{L_\phi} = \frac{L_{\delta_a}}{6.25}\ (rad/\%)$$

$$\frac{\theta}{\delta_e}|_{ss} = \frac{-M_{\delta_e}}{M_\theta} = \frac{M_{\delta_e}}{6.25}\ (rad/\%)$$

With full stick deflection in one direction (50% of the total travel) and converting to degrees, maximum roll and pitch angles are shown in figure 8. The system has a natural frequency equal to 2.5 rad/sec and a damping ratio of 1.12.

Rate Command/Attitude Hold (RC/AH)

A rate command-type control response with an attitude-hold feature was modeled with the addition of an input shaping filter to the AC/AH system as shown in figure 9. The values of L_p and M_q were held at $-5.6\ sec^{-1}$ and L_ϕ and M_θ were held at $-6.25\ sec^{-2}$. Control sensitivities L_{δ_a} and M_{δ_e} were set equal to 0.26 and 0.14 $rad/sec^2 - \%$, respectively. Thus the roll and pitch responses of the RC/AH system were essentially identical to the RC system because of the pole-zero cancellation provided by the filter. The attitude feedback, however, provided the RC/AH system with a modified longitudinal response to a lateral stick input. The pitch attitude holds a constant value during turning flight following the removal of an input to the RC/AH system. Pitch attitude in the RC system is not held constant and altitude loss and an increase in airspeed can more easily occur in turning flight. This effect was noted by the evaluation pilots and will be discussed later in this report. A complete listing of the variable combinations selected and evaluated is given in table 1. Strip chart recordings of step input responses in each axis at 100 knots trim airspeed for each configuration are shown in figures 10 through 27.

FACILITY

As discussed in [2], the HAC simulator system utilizes the six-degree-of-freedom large amplitude motion VMS at NASA Ames Research Center (fig. 28) in conjunction with a fixed-base target control station for one-on-one air combat simulation. The VMS (or blue) cockpit is equipped with standard helicopter controls with adjustable force feel, full instrument panel including head-up and panel mounted CRT displays, and a three-window, wide field-of-view computer generated image (CGI) display (fig. 29). The target (or red) pilot is presented a single-window CGI with a superimposed head-up display and operates a three-axis joystick and collective lever to control the red aircraft (fig. 30) from a fixed-base station. Both aircraft flew over a 3×3 square kilometer CGI data base diagrammed in figure 31.

Blue Aircraft Model

The basic structure of the blue aircraft math model was that used for the target aircraft in the simulation described in [2]. A number of additions and changes were made, however, to make the response of the model more realistic and to incorporate various aspects of the experimental design. The changes include implementation of a power required curve, optimized turn coordination, and a turbulence model. These modifications are discussed in detail below.

Power Required

The Z-force equation in the math model of [2] reads in part:

$$FTZT = XMASS \times (\ldots + ZDCT * COLO + \ldots)$$

where,

$XMASS$ = aircraft mass ($slugs$, nominally= 310.56)
$ZDCT$ = vertical control sensitivity ($ft/sec^2/\%$, nominally = 1.5)
$COLO$ = collective input (%)

The term $COLO$ was set to be equal to the difference between the collective stick position and the collective trim value for the present airspeed. The collective trim value function was set as shown in figure 3, to provide a power required-airspeed relationship typical of conventional helicopters.

Turn Coordination

The turn coordination feature of the blue and red aicraft control system was optimized from the previous experiment. A discussion of the derivation and selection of turn coordination derivative values is also included in the appendix.

Turbulence

Turbulence disturbances were added to the aircraft model to further simulate realistic environmental conditions. A number of turbulence response derivatives were included in the equations of motion and are listed in table 5.

The turbulence inputs were disturbances ($UTURB$, $VTURB$, $WTURB$) to the u, v, and w body axis airspeeds used in the translational and rotational acceleration equations. Mean absolute values of the turbulence velocities were held constant throughout the test and set at the values 2.0, 2.0, and 3.0 ft/sec, respectively. There was no steady wind.

With controls fixed, the disturbances caused peak vertical accelerations of approximately $\pm.2$g and sideslip angles of $\pm 2°$. Strip chart records of these variables with controls fixed are shown in figure 32.

Red Aircraft Model

The red aircraft model was essentially identical to that used for the blue detailed above, though a simpler version. No turbulence or effective dihedral derivatives were included. The control system was permanently set to be an attitude-command/attitude-hold type with pitch and roll natural frequency equal to 2.0 rad/sec and damping ratio equal to 0.7. Cyclic control power was set to allow maximum roll angles of $\pm 66°$ and maximum pitch angles of $\pm 33°$. Collective control power was set to limit maximum rate of climb to 2250 ft/min and the load factor limit was set at 2.5 g. The model could be controlled manually through joystick control inputs, or automatically fly a series of preprogrammed, constant speed, constant altitude turns.

Head-Up Display

The pilot was provided with a head-up display modified from that used in the previous experiment (fig. 33). A philosophy of separating left- and right-hand controlled flightpath parameters onto the left- and right-hand sides of the display was used. Therefore, the digits and scales for altitude, rate-of-climb, and torque were shown on the left side of the display; airspeed, range-to-target, and rate-of-closure to the target on the right side. A heading tape and horizon indicator used previously were deemed unnecessary for air combat maneuvering and were removed from the display. Additions for this head-up display include a range-to-target digit, rate-of-closure scale, and target-position indicator. Each of these indicators were included to assist the pilot in locating and tracking the target displayed in the CGI monitors. From previous experience, pilots noted that one of the more difficult aspects of the task was modulating range to the target in order to stay within weapon

constraints. The range digit display presented the relative range to the target to the pilot. The rate-of-closure scale presented the pilot with the range rate to the target between ± 15 knots. When the target was within the weapon range parameters, the triangle indicator grew in size. Target position relative to the blue aircraft was indicated by a small cross which repeated the X-Y plane look-down scale used on the panel-mounted display (PMD). This feature was added to give the pilot a quick, rough indication of the target relative position without needing to refer to the panel-mounted display. All other information functioned identically to the HAC-I configuration.

The final modification to the HAC-I system was the addition of a switch function on the blue aircraft cyclic controller. This switch allowed the standard HUD display described above to be presented on the PMD screen and moved the standard PMD display to the HUD.

Blue Panel-Mounted Display/Red Head-Up Display

The blue panel-mounted and red head-up displays were also similar to the HAC-I developed displays and are shown in combined form in figure 34. Scoring displays of the probabilities of survival for both aircraft used in HAC-I were deleted from this experiment as unnecessary information. The scale on the right side of the display indicates relative altitude between the two aircraft along with the digits above the moving arrow. The functions of the other digits and scales are identical to the HAC-I displays. As with the HAC-I system, target information on the head-up and panel-mounted displays was presented only if a clear line-of-sight existed between the two aircraft.

Evaluation Pilots

Six pilots participated as evaluators in the experiment. Three of the pilots were employed by the helicopter industry, two were U.S. Army experimental test pilots, and one a NASA experimental test pilot. A summary of their flight experience and aircraft flown is given in table 6.

The experience level of the pilot subject group was divided into four categories. Pilots D, E, and F had significant actual flight time from various tests and training involving helicopter air combat. Pilots A and B had no real air combat training, but had previously participated in VMS air-to-air tests. One pilot (E) had both actual and VMS simulated air combat experience, and one (pilot C) had neither. A summary chart is presented in table 6. These background differences seemed to play an important role in pilot training time, technique, and engagement success as will be described in a later section.

EXPERIMENTAL CONDUCT

Task

The inherent variability of the tail-chase task has a significant effect on pilot ratings and performance. A means of standardizing the task to some extent was therefore desired. After experimenting with various schemes for automating the target aircraft, three automatic targets were selected, each consisting of various preprogrammed turning maneuvers at constant airspeed (85 knots) and altitude (100 ft) while avoiding the terrain obstacles. However, the repetitive nature of the automatic target shortly results in the pilots' anticipating the target's maneuvers, and leads to a loss in realism. Additionally, more aggressive offensive, and three-dimensional intelligent defensive, target maneuvering were desirable; therefore, both automatic and independently piloted targets

were used. Diagrams of the three flight paths flown by the automatic targets are shown in figure 35a, b, c.

The flight task for this experiment consisted of keeping the target aircraft within a firing cone, visible on the head-up display, for as great a percentage of the total run time as possible while trying to score as many hits as possible. For simplicity, a fixed forward-firing weapon was modeled. It was assumed that if one aircraft could successfully track the other within certain pitch-off and angle-off constraints for a representative time, then firing a shot was always equivalent to a hit. (Pitch-off and angle-off are defined as the angles between the blue aircraft body axis coordinates and the red aircraft in pitch and azimuth respectively. These constraints describe a truncated cone as depicted in figure 36). The cone size was set to $\pm 2^{\circ}$ in pitch and azimuth, and the effective range was between 250 and 750 ft. These constraints had to be held for two continuous seconds for a shot to be allowed. A series of panel lights and head set tones alerted the pilot to the tactical situation and to firing opportunities. When a successful shot was scored, the CGI displays flashed white for approximately 60 $msec$.

Because of the possibilty of attracting ground fire in actual air combat over threat terrain, the pilots were instructed to remain below 300 ft altitude as much as possible and to limit excursions above 300 ft to as short a time as possible. As noted previously, the pilots were also instructed to stay within the configuration load factor limits by responding to panel warning lights and headset tones.

PILOT BRIEFING

Each pilot was given a briefing of the design, objective, and approach of the simulation experiment. A set of written directives and definitions on the use of the Cooper-Harper handling qualities rating scale [7] and its application to this experiment was provided (table 7). The pilots were encouraged to make maximum use of the aircraft performance potential and of the available instrumentation, especially the head-up and panel-mounted displays. The pilots were also requested to make comments regarding the deficiencies of the simulation while evaluating the various experimental configurations.

Each pilot was given a 2-4 hour training session on the simulator during which he flew the entire matrix of test configurations, with the nature of each change explained. Exposure to various levels of target maneuvering was also given, as was a familiarization with the display symbology, audio tones, and the fire-control sequence. Despite these procedures, training was limited and learning and technique changes occured throughout the simulation to varying degrees for each pilot. As would be expected, those pilots with the least amount of simulated and actual air-to-air experience required the most training.

EVALUATION ORDER

All the pilots started each session with calibration runs using the baseline configuration (231). Following warm-up runs with this configuration, the pilots were cycled through the entire spectrum of directional axis characteristics. These included changes in the natural frequency and damping ratio, variations in the side-force due to sideslip, and finally addition of effective dihedral. Changes in the cyclic control system were then investigated followed by variations in the maneuvering capabilities of the aircraft.

Each time a change in the directional axis configuration was made, the pilot was advised only that a new configuration was to be evaluated without any reference to the actual nature of the change. The pilot was also given a few minutes to freely fly the aircraft around the database and familiarize himself with the characteristics of the new configuration. Generally, more than one engagement was flown with each configuration before a rating was assigned. Since the pilot would realistically always be aware of the performance capability and type of control system of the aircraft he flew, changes of these configuration variables were revealed to the pilot.

As explained previously, both automatic and manual targets were used. These were selected at random to minimize the effect of learning on the performance of the tail chase task against automatic targets.

DATA

Several means of data recording were employed. Three strip chart recorders, each receiving 16 channels of data, were used to record the time variation of a total of 48 variables. These included control inputs in each axis, blue and red aircraft roll, pitch, and yaw angles and rates, and cone times, among others. Cone time is defined as the total time a target aircraft is held within weapon parameters during a particular engagement. Instantaneous values of these and 12 other variables were simulatneously recorded on magnetic tapes so that computer analysis of the data could be performed. A listing of the recorded variables is given in table 8. Prior to the start of each run, a printout was made of the current value of most of the configuration variables, including each derivative being used in the math model (table 9). In addition, at the end of each run, a printout of the statistical results of the engagement such as cone time, average range to target, control movements in all axes, and total number of hits scored (table 10) was generated.

To facilitate data correlation, run number, configuration ID, target type, pilot rating, and major points of the pilots' post run comments were recorded on data sheets prepared for each pilot. Audio cassette tapes were also used to record the pilots' complete post run comments. Finally, video recordings of the blue pilot's center CGI window and HUD were made for some of the runs.

Data Analysis

As mentioned above, instantaneous values of all the relevant variables were recorded on magnetic tapes. These data were used for the subsequent data analysis in conjunction with pilots' post-run comments and the post-run statistical printouts. A database of all the statistical data, including pilot ratings, was created to facilitate quick access to the data and allow tabulation and/or plotting based on configuration(s), pilot(s), and target type(s), or any combination of the three.

Using the same data management system, it was also possible to search the available data and find the runs which satisfied the specified combination of configuration(s), pilot(s), and target type(s). This capability was used to make crossplots of normal load factor (n_z) and sideslip angle (β) vs airspeed for all the runs made with each maneuver envelope size. The envelopes were then superimposed on the plots to determine excursions beyond the established boundaries, if any.

Finally, time-percentage plots of normal load factor, sideslip angle, and turn rate were made as will be discussed in the results section.

RESULTS

This section presents the results of the experiment. First, the effects of variations in the directional handling qualities of the aircraft are discussed. Then, the results of an increase or decrease of the maneuver enevelope size are outlined. And finally, the suitability of each of the three control systems considered for the air combat task is discussed. Where possible, excerpts of the pilots' post-run comments are used to confirm the results.

Directional Axis Natural Frequency

The effects of changes in the natural frequency of the directional axis response on handling qualities were mixed. As the configuration natural frequency increased, the spread of assigned pilot ratings (for damping ratio of 0.71) grew larger (fig. 37). Pilot comments for all three configurations called for higher damping to avoid overshoots while attempting to point the aircraft at the target:

> I would have to say that for the close-in tracking ..., I'm still seeing (an) objectionable yaw property. It appears to be poor damping. I'm getting a considerable number of overshoots through the target, to the point where, when he did three roll reversals in a row, I had to just lay off entirely trying to use my pedals to fight him. (Pilot F, Configuration 231, HQR=6)

A closed-loop analysis of the linearized helicopter model with a simple pilot model (represented by a simple pilot gain (k) and a typical effective delay time (τ) of 0.3 sec.) shows that the aircraft yaw attitude responses to a yaw attitude command exhibit excessive overshoot for all the three configurations. A wide range of pilot gain was examined as shown in figure 38. Of the three configurations analyzed, configuration 232 ($\omega_n = 1.0\ rad/sec$) has the least overshoot, possibly explaining the better ratings the pilots assigned to it. Overall, the simple closed-loop analysis tends to confirm the pilot comments indicating that these three configurations were unsatisfactory because of inadequate damping and a resulting lack of directional predictability.

Tracking success as indicated by cone time (fig. 39) for most pilots was best for configuration 232 and approximately equal for configurations 231 and 233, slightly favoring 233. Again, though not satisfactory, configuration 232 had the least overshoot of the three, possibly explaining better tracking performance. Notice that although pilot E rated configuration 233 much better than the other pilots, his tracking performance was best on configuration 232 which was consistent with the general trend.

Directional Axis Damping

Pilot ratings and opinions on variations in the damping ratio of the directional axis pedal response were much more consistent than were those for natural frequency changes. A plot of pilot ratings for configurations 231, 235, and 234 ($\omega_{n_d} = 1.5\ rad/sec$) is shown in figure 40. Both configurations 235 and 234 show improvement over the baseline by 0.5 to 2 pilot ratings, while rating differences between 235 and 234 are mixed. A closed-loop analysis similar to the one performed for the natural frequency sweep above clearly explains the pilot ratings trend seen in figure 40 based on the extent of overshoot in the yaw attitude response (fig. 41). Tracking performance data (fig. 42) support these ratings. A large improvement can be seen between configurations 231 and 235, and the higher performance is maintained in configuration 234. Pedal-control movement data for these

configurations (figs. 43 and 44) show comparable numbers of control reversals, but somewhat fewer direction changes in the higher damping configurations, indicating a reduced workload.

Pilot ratings for configurations 233, 2310, and 2311 ($\omega_{n_d} = 2.0\ rad/sec$) show a similar trend (fig. 45). Pilot ratings improved with increasing damping in these configurations with a directional axis natural frequency of 2.0 rad/sec. Less spread is seen in the pilot ratings of the higher damping ratio configurations of these series compared with those for the natural frequency of 1.5 rad/sec. Pilot comments indicate that increased quickness of response was not a noticeable change and that the damping variation was the dominant parameter.

Tracking performance for this series (fig. 46) shows an interesting trend. Scores for configurations 233 and 2310 do not change significantly for any one pilot, while a dramatic improvement in tracking occurs for three pilots with configuration 2311. This same sort of increase occurs for these pilots between configurations 231 and 235. This result seems to indicate that an easing of the tracking task occurs as directional axis damping ratio is varied from 1.0 to 1.4.

Sideforce Caused by Sideslip

The effect on pilot ratings of increased sideforce caused by sideslip (Y_v) is shown in figure 47. The general trend is for poorer pilot ratings and a larger spread of ratings with increasing Y_v. Unfortunately, this series of configurations were marked by relatively poor yaw damping characteristics ($\zeta = 0.71$), which may have masked the influence of the sideforce characteristics. Pilot comments point toward the deficiencies of higher Y_v outweighing the benefits as significantly noted by pilot F:

> I can see it now. It is making a considerably faster turn capability than I had before, but there is something degrading the close-in task that is taking away its usefulness. I would also have to say that in this kind of battle, the turn is only part of it. I think that there are other simulators that would show that to be of value — Y_v. I'm concerned that at least part or most of its usefulness in enriching the turn is lost in the difficulties in tracking. (pilot F, Configuration 237, HQR=5)

Pilots who preferred to consistently fly in coordinated flight found the high sensitivity of the sideslip ball in configuration 237 unacceptable. Additionally, since lateral force cues were limited in the simulator, the full effect of uncoordinated flight was not perceived by any of the pilots.

Tracking performance data (fig. 48) are mixed. An equal number of pilots showed performance improvements, degradations, or no change between each of the configurations. These differences perhaps show the varying effects of the handling qualities trade-offs mentioned above.

Dihedral Effect

The effect on pilot ratings of changing the value of the L_v derivative from 0.0 to -0.07 was dramatically consistent (fig. 49). Each pilot noted an improvement in handling qualities with added effective dihedral. Overall pilot ratings for configuration 238 were among the best of any configuration tested. Tracking performance (fig. 50) was also highly consistent, showing improved scores for every pilot except pilot C. Pedal control movements were the lowest of any configuration (figs. 43 and 44).

Pilot comments noted the smooth and coordinated feel of the lateral directional response:

> The directional axis was well behaved. The aircraft exhibited a high degree of directional stability during the turns. A turn that was commanded with lateral stick only produced no out-of-trim condition and, therefore, no pedal requirement to help through the turn or the come around. The aircraft appeared to exhibit some slight amount of effective dihedral. It tended to help —seemed to help during the large amplitude maneuvering. (Pilot E, Configuration 238, HQR=3)

Although these results were not expected, they may be attributed to the more natural feel of the simulated aircraft because of the addition of the roll to yaw coupling which is typically present in an actual aircraft. Also, as figures 51a-d show, the dihedral effect results in better coordinated turns and probably makes pointing the weapon by using the pedals more comfortable.

Load-Factor Envelope

Figures 52a, b, and c show a crossplot of continuous time histories of load-factor variations with airspeed for the low, middle, and high envelope limit configurations respectively, with the RC/AH control system and either of two (xx1, and xx5) directional axis responses over all pilots. As can be seen, in all cases there were instances of the limits being exceeded. The increasing progression in the size of envelope utilized by the pilots show that high load-factor levels were being demanded for the task, but maneuvering was at times restricted by limit-violation warnings in the cockpit. The lack of any continuous envelope excursions indicates that the warning lights and tones were heeded by the pilots.

Interestingly, the -1 g lower limit for the largest envelope was sufficient for every encounter flown, and the lower load factor boundary of the middle configuration was only rarely exceeded. The $+0.5$ g limit allowed by the low limit configuration (typical of a teetering rotor design) is clearly not sufficient for the air combat task. However, a requirement for load factors less than -0.5 does not seem to be warranted for the maneuvers flown.

An alternate format for data is shown in figures 53a, b, and c. These time-percentage plots show the percentage of total run time spent at or above any load factor by pilots A, D, and F, respectively. Since all runs began almost immediately with air-to-air maneuvering, the data are unbiased by any initial nonengagement set-up time. Flat portions of the curves bracket values which were rarely reached, while highly sloped areas reflect frequent use. The curve shapes and values are remarkably alike. Each pilot consistently operated at load factors between approximately 0.5 g and 2.3 g. Only 5-6% of any particular run time would be spent above or below these values. That time, however, was likely to be at crucial moments during the encounter when high maneuverability levels were required. The crossplots discussed above should be used to determine load factor envelope requirements.

These time-percentage plots, however, present information which can be used for other purposes. The estimation of some of the structural loads likely to be placed upon the aircraft during air combat maneuvering can be judged. It is important to notice that 20% or more of an air-to-air engagement can be spent at load factor above 1.5 g. Requirements for maneuverability levels with the flight-control system operating in a "degraded mode" can be judged. Roughly 80% of the air combat capability is retained operating at load factors between 0.9 g and 2.0 g.

Sideslip Envelope

Figures 54a, b, and c show the variation in sideslip envelopes used with increasing capability. In the small envelope configuration, the entire allowed envelope was completely utilized and maneuvering was often limited. When that envelope was expanded to the modern utility aircraft range, the increased capability was used often, but these limits were only rarely reached. When the envelope was expanded still further, only a minor increase in the sideslip capability was used, and even then, the middle authority level was still sufficient.

These conclusions are substantiated by the time-percentage plots of figures 55a, b, and c. The sideslip levels used in the low limit configurations are noticeably less than the larger envelope cases, while the frequency of sideslip use with the larger envelopes is not significantly different. The larger spread of data in the sideslip histograms as compared to the load factor plots, demonstrates differences in pilot technique. These differences are discussed in a later section. Again, the information in these plots can provide some design data for structural load requirements and degraded mode conditions.

Cyclic Control Response

Comparisons of pilot evaluation data for variations in the type of control response with similar data from the HAC-I experiment yield mixed results. Like the HAC-I test, most pilots voiced a preference for the qualities of both the rate-command and attitude-command responses. The ability to quickly generate large roll rates and aggressively maneuver with the rate-response system was seen as an advantage during the initial chase-and-acquisition portion of the encounters while the added stability and fine pointing capabilities of the attitude-response system were desired for the final stages of the tracking task. The priority in which the pilots preferred these characteristics, however, was reversed from the HAC-I experiment. Whereas the attitude-response system was primarily desired earlier, the rate-response type was now preferred if a choice needed to be made. In the HAC-I test, both models had handling qualities deficiencies, and it was not surprising that of the two, the more stable attitude-response system was chosen. However for this test, both models were decoupled with extremely good basic-handling qualities and the superior maneuvering capability of the rate-command system was more important to the pilots. The large stick inputs necessary for the attitude-response system to generate large angles and rates were objectionable and overshadowed the enhanced pointing capability of the system. As would be expected, the attitude-response system configurations required only about half the control reversals as the rate-response systems (figs. 56a and b). However, the requirement to maintain a stick force and displacement in order to hold a roll or pitch angle was not entirely desirable.

Figures 57 and 58 show the pilot ratings for the configurations evaluated. Most pilots flew only directional axis configuration 1 or 5 while evaluating the cyclic response, while pilot D flew both. For all pilots but one, the ratings for both the RC and RC/AH systems were better than for the AC/AH system. Tracking success time results were mixed. Most of the pilots tracked best with the RC/AH system; some with the RC system (figs. 59 and 60). None of the pilots was most successful with the AC/AH system. In some cases, however, the final averages were very close and, therefore, are not definitive. The different benefits of both systems mentioned above probably contributed to mixing the spread of relative RC and AC success.

Figures 61 and 62 show summaries of roll-rate activity for all pilots in RC/AH and AC/AH configurations, respectively, with similar directional characteristics. No significant differences are

seen. Thus, the AC/AH system would seem to be capable of producing the roll rates required for the task. Again, the objection of the pilots was the large stick inputs (and the corresponding large stick force) needed to be maintained to produce the desired rates.

Some differences among different pilots in roll-rate usage can be seen, however. Probably because of different tracking techniques (which will be discussed later), pilot A was forced to use higher roll rates than the other pilots. Figures 63a, b, and c show roll-rate histograms for pilots A, D, and F, respectively, for all evaluation runs. Pilots D and F show similar magnitudes of roll-rate use while the rates of pilot A are noticeably higher. Figures 64a, b, and c show crossplots of roll rate and velocity for the three pilots. Several interesting results can be seen: Pilot A is again seen to use the highest rates, many times exceeding 70 *deg/sec*, while pilots D and F generally stayed within ± 65 *deg/sec*. On two occasions, pilot A exceeded 115 *deg/sec* roll rate. The characteristic sharp points on the crossplot graphs explain the very small percentage times seen at high rates on the time-percentage plots since for any particular aggressive bank angle change, the time spent at the maximum roll rate is a small percentage of the total time required to execute the maneuver.

Pitch-rate data for all pilots are shown in figure 65. Engagements were almost entirely flown with pitch rates under 20 *deg/sec*. Rates above 30 *deg/sec* were extremely rare. Differences among individual pilots were minimal as can be seen in figures 66a, b, and c.

Effects of Pilot Experience and Technique

As noted in an earlier section, although each evaluation pilot was a highly experienced helicopter pilot, the experience and training of each in helicopter air combat varied. This factor seems to be quite important in affecting the pilots' adaptability to, and success in, the simulated air combat task. Actual flight experience in air combat maneuvering tests seems to have been the best training, followed by VMS simulated air combat experience. Qualitatively, there were also indications that individual motivation and competitiveness varied among the group. Some of the pilots felt their primary task was to evaluate configuration changes while attempting to track the target. In contrast, others felt their primary task was to track and score on the target while evaluating the configuration changes. Although the wording is subtle, the differences were significant. Since two of the authors also shared the adversary pilot role for each of the over 300 pilot vs. pilot engagements, this subjective opinion is based on more than the feelings of observers of the experiment.

The four most experienced pilots were also the most consistent in their tracking performance and the handling qualities ratings assigned to various configurations. The trend in any of figures 39, 42, 45, 46, 48, or 50 becomes significantly clearer when the ratings and scores of pilots B and C are removed. These two pilots were also perceived to have the most difficulties tracking the target. These difficulties are not readily apparent in their overall tracking times, however, since the aggressivenes of the target was scaled in order to make the task difficult for each pilot, yet allow him enough of a chance to track the target so as to assign a configuration rating in a reasonable amount of time. Thus if a pilot was "shaken" enough by the target, the target pilot would generally allow the evaluation pilot to reacquire a track by maneuvering less aggressively for a period of time. However, since all pilots also maneuvered against identical pre-recorded target flight paths, a comparison of tracking scores for these runs only is revealing.

Figure 67 shows the mean and standard deviation of the tracking scores of each pilot for the pre-recorded target runs. Pilot F was by far the most successful of the pilots, followed by a grouping of pilots B, D, and E, and then a drop-off to pilot A and then C. It seems to be no coincidence that

pilot C was the least aggressive and most inexperienced in ACM flying of the group, while pilot F was highly motivated and had a significant amount of ACM test experience.

Reasons and support for these differences can be found in the tracking range plot of figure 68. The average tracking range from the target for each of the directional axis configuration data runs is plotted for eack pilot. Pilot C was the least aggressive pilot and consistently trailed the target at ranges generally greater than 700 ft. Since this was close to the maximum range of the simulated weapon, firing solutions were often missed. Pilot A adopted a very different strategy but also was relatively unsuccessful. He attempted to follow the target at very close range (usually under 500 ft) and mirror the target's maneuvers. This strategy, along with very little pedal usage (as will be discussed), forced pilot A to use aggressive maneuvering and the high roll rates shown in figure 64a. Pilots D, E, and F generally stayed in the 550 to 650 ft average range, resulting in an easier tracking task than pilot A experienced, while keeping within gun range with more aggresive maneuvering than pilot C. Each of these pilots was more successful than were pilots A and C. Pilot B was characterized by inconsistent tracking success, and this is reflected in the variable range strategy shown in figure 68. At times pilot B stayed beyond gun range as did pilot C, while at other times, he attempted to track closely like pilot A. Thus, as might be obvious from geometric considerations, the best tracking strategy seems to be to remain just within maximum weapon range.

An even stronger correlation with tracking success is found by examining the amount of sideslip used to point the blue aircraft at the target. The extremes ranged from pilot A who preferred to allow the turn coordination feature of the flight control system establish directional pointing almost exclusively, to pilot F who used large amounts of pedal control to sideslip the aircraft into a firing solution. A comparison of the envelopes used (all runs, all configurations, figs. 69a-e) by five of the evaluation pilots (data for pilot C are not available) shows a direct correlation with their tracking success ranking of figure 67. Figure 69 clearly shows these sideslip envelopes expanding from pilot A to B to E to D to F. It is felt that had data been available for pilot C, the sideslip envelope used would have been relatively small, though probably not as small as that of pilot A.

The reason for differences in sideslip usage was not simply different levels of pilot aggressiveness, but more of a difference of tracking philosophy. Those pilots who used little sideslip felt that better ballistic solutions would result if the gun was fired with the aircraft close to trimmed flight, even though the simulation design assumed that a sophisticated fire control computer would solve for uncoordinated firing conditions. The very large benefits which result from having and using such a fire control computer along with a large sideslip envelope are obvious from the success of pilots D, E, and F.

Similar to the HAC-I experiment, simulator limitations on field-of-view and other visual system characteristics were important to understand. However, in general, pilot reactions were very favorable toward the usefulness of the test and the ability to gain new insights into the air combat task. The comments of one pilot who had recently finished actual air tracking training flying H-3 helicopters over the Arizona desert provide a good summary of the capabilities of the HAC simulation.

> I have to think that one of the tricks to helicopter air-to-air is getting very firmly in everybody's mind not so much exactly how we used to do it in a fixed wing aircraft–the dog fights of World War II and Vietnam–but here there's a sort of a relative motion thing, a way of exploiting the center of mass of the aircraft. There are some points

where I just chase you around. I never really get consistent long term solutions on you, and then there are other times where I am in the right position where it doesn't make any difference what you do. I just sit there and keep pumping rounds, and I'm not quite sure how to define that, but I think if we could figure that out, that's something you need to teach everybody- how to work for that position. It is not so much being at six o'clock, it's having a whole bunch of things come together at once that make up the angular difference. It doesn't make much difference what the target does, the delta angle will never increase much. I think that probably has a lot to do with proximity as well as a lot of the other things. It seems like I had a tendency to follow you closer on this run. That does show the tendency when you are being successful by getting shots off to continue to keep the power in there and continue to follow you, especially if it looks like you're not getting away from me. Then I have a real problem of jamming you, which could be pretty lethal to both of us. It is very interesting. It is really quite good and it looks very interesting from what I've seen in the last couple of weeks (flying actual ACM training). I find that this machine I'm flying tends to be pretty maneuverable. If you could get a helicopter to do some of the things you can do in this machine in terms of angle of bank and trim, you'd have a very, very capable air-to-air machine. It strikes me, as I'm flying these things, that there's a real art to assessing exactly where the target aircraft is going. I found that when I was flying down in the desert with the H-3 that very seldom could you ever fake somebody out by rolling in one direction and going hard in the other direction, becouse you can't roll an H-3 fast enough to get it to change its velocity vector, but here, I find that you can do that. Unlike the 'real world' that I just came from, here it is critical to watch the target fuselage very carefully because you pulled a couple of things that were hard to follow. That didn't mess me up for very long, but just a hard roll in one direction and then an immediate reversal does, in fact, break the lock and its real hard to keep you locked up. I found a bunch of times, probably four or five times, where I had you right up to the point of being able to fire and then you did something. I would be sitting there listening to the tones and watching the lights, and bang!, just as I was ready to pull the trigger, you would be gone. In the 'real world', of course, that's really what counts. There seems to be some magnificent premium placed on the ability to have sustained maneuvering capability- to be able to just continue to fight back and forth laterally and vertically with a lot of excess power to defeat the guy behind you. I didn't see much of that in the desert, but here, it's really obvioiusly essential.

CONCLUDING REMARKS

A moving-base simulation was conducted using the NASA Ames VMS facility to investigate parameters affecting helicopter handling qualities in air combat. The variables for the study were the maneuver envelope size (load factor and sideslip), directional axis handling qualities, and pitch and roll control response type. Over 450 simulated, low altitude, one-on-one engagements were conducted by pilots from the Army, NASA, and industry.

The data and results set forth in this report support a number of conclusions regarding this new helicopter role and are listed below. The general close correlation between subjective pilot opinions and actual tracking performance adds a degree of confidence to the data evaluation.

1. Relatively high directional axis damping ratios were desired by the evaluation pilots for the air-to-air tracking task. Yaw damping ratio values between 1.0 and 1.4 received the best ratings.

2. Some degree of effective dihedral was found to significantly enhance tracking performance and pilot handling qualites ratings. Since the L_v derivative is a coupling term, the resulting benefits were not expected.

3. The handling qualities drawbacks of large values of sideforce caused by sideslip outweighed increased twining performance potential.

4. A number of insights into load factors required for helicopter air combat were gained. A lower limit of $-0.5\ g$ was adequate for almost all maneuvering performed and a value lower than $-1.0\ g$ was never required. A lower limit of $+0.5\ g$ typical of unrestrained teetering rotor designs is clearly not adequate. Maximum load factor values greater than that achievable by present designs were often used by the pilots. Limits presented to the pilot were at times exceeded in all configurations, revealing the need for automatic envelope limiting to avoid critical limit violations. Though data presented in this report reveal a trend of relative usage of increasing load factor values, further investigations are needed to determine the cost/benefit of maximum load factor limit design.

5. Though the degree of sideslip used by individual pilots varied, the most successful pilots used aircraft sideslip performance to significant advantage. For these pilots, the sideslip envelope typical of early attack helicopters is clearly not sufficiently large. The envelope afforded by modern utility aircraft is close to adequate if the entire envelope can be exploited without consequence. If the assumed ability of fire control computers to compensate for sideslip velocities is correct, the skillful use of sideslip weapon pointing is a distinct tactical advantage.

6. An angular rate-command-type cyclic control response was desired by the evaluation pilots, although the fine pointing capability of an attitude-command response type is also beneficial.

7. Time history and statistical summary charts of roll and pitch rates show relatively large values often used. They may serve as design data for pitch-and-roll control power needed in this highly dynamic maneuvering task.

8. Pilot experience and technique were found to be important factors in air-to-air tracking success. Pilots with actual air combat test experience performed better than those with little or no experience. In addition, pilots who optimized relative range to the target and effectively used the sideslip pointing capability of the helicopter were consistently the most successful fighters.

APPENDIX A

Derivation of transfer functions from equations of motion:

Lateral/Directional

The linearized lateral directional equations of motion for the blue aircraft model are:

$$\dot{p} = L_p p + L_\phi \phi + L_v v + L_{\delta_a} \delta_a$$

$$\dot{r} = N_r r + N_v v + N_p p + N_\phi \phi + N_{\delta_p} \delta_p$$

$$\dot{v} = Y_v v + g' \phi - U_o r$$

where the L, N, and Y derivatives are for $p,r = (rad/sec)$, $\phi = (rad)$, $v = (ft/sec)$, δ_a, $\delta_p = (\%)$, $g' = g \cos \phi_o$ In state equation form: $(\dot{x} = Fx + Gu)$

$$\begin{pmatrix} \dot{v} \\ \dot{r} \\ \dot{p} \\ \dot{\phi} \end{pmatrix} = \begin{pmatrix} Y_v & -U_o & 0 & g' \\ N_v & N_r & N_p & N_\phi \\ L_v & 0 & L_p & L_\phi \\ 0 & 0 & 1 & 0 \end{pmatrix} \begin{pmatrix} v \\ r \\ p \\ \phi \end{pmatrix} + \begin{pmatrix} 0 & 0 \\ N_{\delta_p} & 0 \\ 0 & L_{\delta_a} \\ 0 & 0 \end{pmatrix} \begin{pmatrix} \delta_p \\ \delta_a \end{pmatrix}$$

so, from:

$$X(s) = (sI - F)^{-1} G U(s)$$

the characteristic equation of the system is:

$$\left| sI - F \right| = \begin{vmatrix} s - Y_v & U_o & 0 & -g' \\ -N_v & s - N_r & -N_p & -N_\phi \\ -L_v & 0 & s - L_p & -L_\phi \\ 0 & 0 & -1 & s \end{vmatrix} = 0$$

$$[s^2 - (Y_v + N_r)s + (Y_v N_r + U_o N_v)](s^2 - L_p s - L_\phi) + L_v[(U_o N_p - g')s + (U_o N_\phi + N_r g')] = 0$$

For this simulation experiment, L_v was set equal to zero for all configurations but one. For these configurations, the characteristic equation is:

$$[s^2 - (Y_v + N_r)s + (Y_v N_r + U_\circ N_v)](s^2 - L_p s - L_\phi) = 0$$

The transfer functions for these configurations are therefore as follow:

$$\frac{\beta}{\delta_p}(s) = \frac{-N_{\delta_p}}{s^2 - (Y_v + N_r)s + (Y_v N_r + U_\circ N_v)}$$

$$\frac{r}{\delta_p}(s) = \frac{N_{\delta_p}(s - Y_v)}{s^2 - (Y_v + N_r)s + (Y_v N_r + U_\circ N_v)}$$

$$\frac{p}{\delta_p}(s) = 0$$

$$\frac{\phi}{\delta_p}(s) = 0$$

$$\frac{v}{\delta_a}(s) = \frac{L_{\delta_a}[s(g' - U_\circ N_p) - (U_\circ N_\phi + g' N_r)]}{[s^2 - (Y_v + N_r)s + (Y_v N_r + U_\circ N_v)](s^2 - L_p s - L_\phi)}$$

$$\frac{r}{\delta_a}(s) = \frac{L_{\delta_a}[N_p s^2 + (N_\phi - Y_v N_p)s + (g' N_v - Y_v N_\phi)]}{[s^2 - (Y_v + N_r)s + (Y_v N_r + U_\circ N_v)](s^2 - L_p s - L_\phi)}$$

$$\frac{p}{\delta_a}(s) = \frac{s L_{\delta_a}}{s^2 - L_p s - L_\phi}$$

$$\frac{\phi}{\delta_a}(s) = \frac{L_{\delta_a}}{s^2 - L_p s - L_\phi}$$

Values of particular derivatives can be set to allow for a number of desirable characteristics:

- By setting $N_v = \frac{K_{N_\theta}}{U_\circ}$, constant yaw damping and natural frequency can be set independent of $U_\circ$ for constant Y_v and N_r.
- For automatic transient and steady coordinated turns, $\frac{v}{\delta_a} = 0$. Setting $N_p = \frac{g'}{U_\circ}$ and $N_\phi = -N_p N_r$ adjusts the response:

$$\frac{r}{\delta_a}(s) = \frac{L_{\delta_a} N_p}{s^2 - L_p s - L_\phi} = N_p \frac{\phi}{\delta_a}(s)$$

  so $\frac{r}{\phi} = N_p = \frac{g'}{U_\circ}$ and the turn is always in phase as desired.
- In hover and low speeds, $N_v = N_p = N_\phi = 0$. Therefore:

$$\frac{r}{\delta_p}|_{U_\circ = 0}(s) = \frac{N_{\delta_p}}{(s - N_r)}$$

$$\frac{v}{\delta_a}|_{U_\circ = 0}(s) = \frac{L_{\delta_a} g'}{(s - Y_v)(s^2 - L_p s - L_\phi)}$$

  N_v, N_p, N_ϕ varied linearly from zero values at speeds less than 30 ($knots$) to their respective full values at 50($knots$). They then were set as the functions described above.

Effect of dihedral on lateral/directional response

The addition of a nonzero L_v (configuration 238) changes the transfer functions in an interesting way. With the N_r, N_p, and N_ϕ derivatives augmented for turn coordination as described above, the characteristic equation is unchanged since the coefficients of L_v sum to zero. The transfer function numerators become modified, however, as listed below:

$$\frac{\beta}{\delta_p}(s) = \frac{-N_{\delta_p}}{s^2 - (Y_v + N_r)s + (Y_v N_r + U_o N_v)}$$

$$\frac{r}{\delta_p}(s) = \frac{N_{\delta_p}[(s - Y_v)(s^2 - L_p s - L_\phi) - L_v g]}{[s^2 - (Y_v + N_r)s + (Y_v N_r + U_o N_v)](s^2 - L_p s - L_\phi)}$$

$$\frac{p}{\delta_p}(s) = \frac{-L_v U_o N_{\delta_p} s}{[s^2 - (Y_v + N_r)s + (Y_v N_r + U_o N_v)](s^2 - L_p s - L_\phi)}$$

$$\frac{\phi}{\delta_p}(s) = \frac{-L_v U_o N_{\delta_p}}{[s^2 - (Y_v + N_r)s + (Y_v N_r + U_o N_v)](s^2 - L_p s - L_\phi)}$$

The responses to δ_a remain unchanged. Thus the addition of the L_v derivative does not change the yaw damping or natural frequency, but couples the roll axis to pedal inputs.

Longitudinal

The longitudinal equations of motion (from trim) are:

$$\dot{u} = X_u u - g \sin\theta$$

$$\dot{w} = Z_w w + g \cos\theta + U_o q + Z_{\delta_e}\delta_e$$

$$\dot{q} = M_q q + M_\theta \delta\theta + M_{\delta_e}\delta_e$$

where,

$\delta\theta = \theta - \theta_{trim}$

In state equation form, and assuming small angles, the equations become:

$$\begin{pmatrix} \dot{u} \\ \dot{w} \\ \dot{q} \\ \delta\dot{\theta} \end{pmatrix} = \begin{pmatrix} X_u & 0 & 0 & -g' \\ 0 & Z_w & U_o & 0 \\ 0 & 0 & M_q & M_\theta \\ 0 & 0 & 1 & 0 \end{pmatrix} \begin{pmatrix} u \\ w \\ q \\ \delta\theta \end{pmatrix} + \begin{pmatrix} 0 & 0 \\ Z_{\delta_e} & 0 \\ 0 & M_{\delta_e} \\ 0 & 0 \end{pmatrix} \begin{pmatrix} \delta_c \\ \delta_e \end{pmatrix}$$

The characteristic equation is thus:

$$(s - X_u)(s - Z_w)(s^2 - M_q s - M_\theta) = 0$$

and the transfer functions are therefore:

$$\frac{u}{\delta_c}(s) = \frac{q}{\delta_c}(s) = \frac{\theta}{\delta_c}(s) = 0$$

$$\frac{w}{\delta_c}(s) = \frac{Z_{\delta_c}}{(s - Z_w)}$$

$$\frac{u}{\delta_e}(s) = \frac{-g' M_{\delta_e}}{(s - X_u)(s^2 - M_q s - M_\theta)}$$

$$\frac{w}{\delta_e}(s) = \frac{M_{\delta_e} U_o s}{(s - Z_w)(s^2 - M_q s - M_\theta)}$$

$$\frac{q}{\delta_e}(s) = \frac{M_{\delta_e} s}{(s^2 - M_q s - M_\theta)}$$

$$\frac{\theta}{\delta_e}(s) = \frac{M_{\delta_e}}{(s^2 - M_q s - M_\theta)}$$

References

[1] Wolfrom, Joseph A.; and Fisher, Chris E.: Data Presentation from Air-To-Air Combat Maneuvering Between an S-76 and a UH-60A. USA AVSCOM TR-85-D-17, 1985.

[2] Lewis, Michael S.; and Aiken, Edwin W.: Piloted Simulation of One-On-One Helicopter Air Combat at NOE Flight Levels. NASA TM-86686, Apr. 1985.

[3] Heffley, Robert K.; Bourne, Simon M.; Curtiss, Howard C., Jr.; Hindson, William S.; and Hess, Ronald A.: Study of Helicopter Roll Control Effectiveness Criteria. NASA Contractor Report 177404, 1986.

[4] Haworth, L. A.; Bivens, C. C.; and Shively, R. J.: An Investigation of Single-Piloted Advanced Cockpit and Control Configurations for Nap-Of-the-Earth Helicopter Combat Mission Tasks. AHS 42nd Annual Forum Proceedings, 1986, pp. 657-672.

[5] Anon.: Air-to-Air Combat Test Flight Test Plan (AACT II), Applied Technology Laboratory, U.S. Army Research and Technology Laboratories (AVSCOM), Fort Eustis, VA, 1983.

[6] Lappos, N. D.: Insight Into Helicopter Air Combat Maneuverability. Presented at the 40th Annual Forum of the American Helicopter Society, Crystal City, VA, 1984.

[7] Cooper, G. E.; and Harper, R. P.: The Use of Pilot Rating in the Evaluation of Aircraft Handling Qualities. NASA TN D-5153, 1969.

[8] Heffley, Robert K.; Jewell, Wayne F.; Lehman, John M.; and Van Winkle, Richard A.: A Compilation and Analysis of Helicopter Handling Qualities Data, Volume One: Data Compilation. NASA Contractor Report 3144, 1979.

TABLE 1 TESTED CONFIGURATIONS

IDENTIFIER	MANEUVERABILITY	CONTROL SYSTEM	Y_v	N_r	K_{N_v}	L_v	ω_n	ζ
131	LOW	RC/AH	-0.10	-2.00	2.05	0	1.50	0.71
135	LOW	RC/AH	-0.10	-4.00	1.85	0	1.50	1.37
211	MIDDLE	RC	-0.10	-2.00	2.05	0	1.50	0.71
215	MIDDLE	RC	-0.10	-4.00	1.85	0	1.50	1.37
221	MIDDLE	AC/AH	-0.10	-2.00	2.05	0	1.50	0.71
224	MIDDLE	AC/AH	-0.10	-6.00	1.65	0	1.50	2.03
225	MIDDLE	AC/AH	-0.10	-4.00	1.85	0	1.50	1.37
231	MIDDLE	RC/AH	-0.10	-2.00	2.05	0	1.50	0.71
232	MIDDLE	RC/AH	-0.10	-1.32	0.87	0	1.00	0.71
233	MIDDLE	RC/AH	-0.10	-2.70	3.73	0	2.00	0.71
234	MIDDLE	RC/AH	-0.10	-6.00	1.65	0	1.50	2.03
235	MIDDLE	RC/AH	-0.10	-4.00	1.85	0	1.50	1.37
236	MIDDLE	RC/AH	-0.05	-2.08	2.15	0	1.50	0.71
237	MIDDLE	RC/AH	-0.30	-1.83	1.70	0	1.50	0.71
238	MIDDLE	RC/AH	-0.10	-2.00	2.05	-0.07	1.50	0.71
239	MIDDLE	RC/AH	-0.10	-4.00	7.90	0	2.90	0.71
2310	MIDDLE	RC/AH	-0.10	-4.00	3.60	0	2.00	1.03
2311	MIDDLE	RC/AH	-0.10	-6.00	3.40	0	2.00	1.53
331	HIGH	RC/AH	-0.10	-2.00	2.05	0	1.50	0.71
335	HIGH	RC/AH	-0.10	-4.00	1.85	0	1.50	1.37

Table 2a LONGITUDINAL TRANSFER FUNCTION NUMERATORS FOR ATTITUDE COMMAND SYSTEM
RATE COMMAND → $N^{\omega}_{\delta_c}$ = 1.5(0.01)(0)(5.6)

TF NUM / A/S, knots	$N^{u}_{\delta_c}$	$N^{q}_{\delta_c}$	$N^{\theta}_{\delta_c}$	$N^{\omega}_{\delta_c}$	$N^{u}_{\delta_e}$	$N^{\omega}_{\delta_e}$	$N^{q}_{\delta_e}$	$N^{\theta}_{\delta_e}$
30	0	0	0	1.5(0.01)(4.061)(1.539)	-2.576(1)	4.053(0)(0.01)	0.08(0)(0.01)(1)	0.08(0.01)(1)
60	0	0	0	1.5(0.01)(4.061)(1.539)	-4.508(1)	14.187(0)(0.01)	0.14(0)(0.01)(1)	0.14(0.01)(1)

LONGITUDINAL TRANSFER FUNCTION DENOMINATORS
FOR BOTH 30 knots AND 60 knots AIRSPEED

TF DEN	AC	RC
	(0.01)(1)(4.061)(1.539)	(0.01)(1)(0)(5.6)

Table 2b LATERAL DIRECTIONAL TRANSFER FUNCTION NUMERATORS FOR ATTITUDE COMMAND SYSTEM AT 60 knots AIRSPEED

TF NUM / DIR CONFIG.	$N^{\beta}_{\delta_p}$	$N^{r}_{\delta_p}$	$N^{p}_{\delta_p}$	$N^{\phi}_{\delta_p}$	$N^{v}_{\delta_a}$	$N^{r}_{\delta_a}$	$N^{p}_{\delta_a}$	$N^{\phi}_{\delta_a}$
1	-0.047(4.061)(1.539)	0.047(0.1)(4.061)(1.539)	0	0	0	0.083(0.70;1.5)	0.26(0)(0.70;1.5)	0.26(0.70;1.5)
2	-0.021(4.061)(1.539)	0.021(0.1)(4.061)(1.539)	0	0	0	0.083(0.71;1.0)	0.26(0)(0.71;1.0)	0.26(0.71;1.0)
3	-0.084(4.061)(1.539)	0.084(0.1)(4.061)(1.539)	0	0	0	0.083(0.70;2.0)	0.26(0)(0.70;2.0)	0.26(0.70;2.0)
4	-0.047(4.061)(1.539)	0.047(0.1)(4.061)(1.539)	0	0	0	0.083(5.706)(0.394)	0.26(0)(5.706)(0.394)	0.26(5.706)(0.394)
5	-0.047(4.061)(1.539)	0.047(0.1)(4.061)(1.539)	0	0	0	0.083(3.447)(0.653)	0.26(0)(3.447)(0.653)	0.26(3.447)(0.653)
6	-0.047(4.061)(1.539)	0.047(0.05)(4.061)(1.539)	0	0	0	0.083(0.71;1.5)	0.26(0)(0.71;1.5)	0.26(0.71;1.5)
7	-0.047(4.061)(1.539)	0.047(0.3)(4.061)(1.539)	0	0	0	0.083(0.71;1.5)	0.26(0)(0.71;1.5)	0.26(0.71;1.5)
9	-0.174(4.061)(1.539)	0.174(0.1)(4.061)(1.539)	0	0	0	0.083(0.71;2.88)	0.26(0)(0.71;2.88)	0.26(0.71;2.88)
10	-0.084(4.061)(1.539)	0.084(0.1)(4.061)(1.539)	0	0	0	0.083(2.554)(1.566)	0.26(0)(2.554)(1.566)	0.26(2.554)(1.566)
11	-0.084(4.061)(1.539)	0.084(0.1)(4.061)(1.539)	0	0	0	0.083(5.376)(0.744)	0.26(0)(5.376)(0.744)	0.26(5.376)(0.744)
8	-0.047(4.061)(1.539)	0.047(4.260)(0.876;0.822)	0.334(0)	0.334	0	0.083(0.70;1.5)	0.26(0)(0.70;1.5)	0.26(0.70;1.5)

TABLE 2c LATERAL DIRECTIONAL TRANSFER FUNCTION NUMERATORS FOR RATE COMMAND SYSTEM AT 60 knots AIRSPEED

TF NUM / DIR. CONFIG.	$N^{\beta}_{\delta_p}$	$N^{r}_{\delta_p}$	$N^{p}_{\delta_p}$	$N^{\phi}_{\delta_p}$	$N^{v}_{\delta_a}$	$N^{r}_{\delta_a}$	$N^{p}_{\delta_a}$	$N^{\phi}_{\delta_a}$
1	-0.047(0)(5.6)	0.047(0.1)(0)(5.6)	0	0	0	0.083(0.70;1.5)	0.26(0)(0.70;1.5)	0.26(0.70;1.5)
2	-0.021(0)(5.6)	0.021(0.1)(0)(5.6)	0	0	0	0.083(0.71;1.0)	0.26(0)(0.71;1.0)	0.26(0.71;1.0)
3	-0.084(0)(5.6)	0.084(0.1)(0)(5.6)	0	0	0	0.083(0.70;2.0)	0.26(0)(0.70;2.0)	0.26(0.70;2.0)
4	-0.047(0)(5.6)	0.047(0.1)(0)(5.6)	0	0	0	0.083(5.706)(0.394)	0.26(0)(5.706)(0.394)	0.26(5.706)(0.394)
5	-0.047(0)(5.6)	0.047(0.1)(0)(5.6)	0	0	0	0.083(3.447)(0.653)	0.26(0)(3.447)(0.653)	0.26(3.447)(0.653)
6	-0.047(0)(5.6)	0.047(0.05)(0)(5.6)	0	0	0	0.083(0.71;1.5)	0.26(0)(0.71;1.5)	0.26(0.71;1.5)
7	-0.047(0)(5.6)	0.047(0.3)(0)(5.6)	0	0	0	0.083(0.71;1.5)	0.26(0)(0.71,1.5)	0.26(0.71;1.5)
9	-0.174(0)(5.6)	0.174(0.1)(0)(5.6)	0	0	0	0.083(0.71;2.88)	0.26(0)(0.71;2.88)	0.26(0.71;2.88)
10	-0.084(0)(5.6)	0.084(0.1)(0)(5.6)	0	0	0	0.083(2.554)(1.566)	0.26(0)(2.554)(1.566)	0.26(2.554)(1.566)
11	-0.084(0)(5.6)	0.084(0.1)(0)(5.6)	0	0	0	0.083(5.376)(0.744)	0.26(0)(5.376)(0.749)	0.26(5.376)(0.744)
8	-0.047(0)(5.6)	0.047(5.671)(0.023;0.631)	0.334(0)	0.334	0	0.083(0.70;1.5)	0.26(0)(0.70;1.5)	0.26(0.70;1.5)

TABLE 2d LATERAL DIRECTIONAL TRANSFER FUNCTION DENOMINATORS FOR BOTH ATTITUDE COMMAND AND RATE COMMAND AT 60 knots AIRSPEED

DIR CONFIG. / TF DEN	AC	RC
1	(0.70;1.5)(4.061)(1.539)	(0.70;1.5)(0)(5.6)
2	(0.71;1.0)(4.061)(1.539)	(0.71;1.0)(0)(5.6)
3	(0.70;2.0)(4.061)(1.539)	(0.70;2.0)(0)(5.6)
4	(5.706)(0.394)(4.061)(1.539)	(5.706)(0.394)(0)(5.6)
5	(3.447)(0.653)(4.061)(1.539)	(3.447)(0.653)(0)(5.6)
6	(0.71;1.5)(4.061)(1.539)	(0.71;1.5)(0)(5.6)
7	(0.71;1.5)(4.061)(1.539)	(0.71;1.5)(0)(5.6)
9	(0.71;2.88)(4.061)(1.539)	(0.71;2.88)(0)(5.6)
10	(2.554)(1.566)(4.061)(1.539)	(2.554)(1.566)(0)(5.6)
11	(5.376)(0.744)(4.061)(1.539)	(5.376)(0.744)(0)(5.6)
8	(0.70;1.5)(4.061)(1.539)	(0.70;1.5)(0)(5.6)

TABLE 2e

LATERAL DIRECTIONAL TRANSFER FUNCTION NUMERATORS FOR
ATTITUDE-COMMAND SYSTEM AT 30 knots AIRSPEED

TF NUM / DIR. CONFIG.	$N^{\beta}_{\delta_p}$	$N^{r}_{\delta_\rho}$	$N^{p}_{\delta_p}$	$N^{\phi}_{\delta_p}$	$N^{v}_{\delta_a}$	$N^{r}_{\delta_a}$	$N^{p}_{\delta_a}$	$N^{\phi}_{\delta_a}$
1	-0.0042(4.061)(1.539)	0.0042(0.1)(4.061)(1.539)	0	0	4.508(2.0)	0	0.14(0)(0.1)(2.0)	0.14(0.1)(2.0)
2	-0.0028(4.061)(1.539)	0.0028(0.1)(4.061)(1.539)	0	0	4.508(1.32)	0	0.14(0)(1.32)(0.1)	0.14(1.32)(0.1)
3	-0.0056(4.061)(1.539)	0.0056(0.1)(4.061)(1.539)	0	0	4.508(2.7)	0	0.14(0)(0.1)(2.70)	0.14(0.1)(2.70)
4	-0.0125(4.061)(1.539)	0.0125(0.1)(4.061)(1.539)	0	0	4.508(6.0)	0	0.14(0)(6.0)(0.1)	0.14(6.0(0.1)
5	-0.0084(4.061)(1.539)	0.0084(0.1)(4.061)(1.539)	0	0	4.508(4.0)	0	0.14(0)(0.1)(4.0)	0.14(0.1)(4.0)
6	-0.0022(4.061)(1.539)	0.0022(0.05)(4.061)(1.539)	0	0	4.508(2.08)	0	0.14(0)(0.05)(2.08)	0.14(0.05)(2.08)
7	-0.0115(4.061)(1.539)	0.0115(0.3)(4.061)(1.539)	0	0	4.508(1.83)	0	0.14(0)(1.83)(0.3)	0.14(1.83)(0.3)
9	-0.0084(4.061)(1.539)	0.0084(0.1)(4.061)(1.539)	0	0	4.508(4.0)	0	0.14(0)(4.0)(0.1)	0.14(4.0)(0.1)
10	-0.0084(4.061)(1.539)	0.0084(0.1)(4.061)(1.539)	0	0	4.508(4.0)	0	0.14(0)(4.0)(0.1)	0.14(4.0)(0.1)
11	-0.0125(4.061)(1.539)	0.0125(0.1)(4.061)(1.539)	0	0	4.508(6.0)	0	0.14(0)(6.0)(0.1)	0.14(6.0)(0.1)
8	-0.0042(4.061)(1.539)	0.0042(3.790)(2.114)(-0.203)	-0.0149(0)	-0.0149	4.508(2.0)	0	0.14(0)(0.1)(2.0)	0.14(0.1)(2.0)

TABLE 2f LATERAL DIRECTIONAL TRANSFER FUNCTION NUMERATORS FOR RATE-COMMAND SYSTEM AT 30 knots AIRSPEED

TF NUM / DIR CONFIG.	$N^{\beta}_{\delta_p}$	$N^{r}_{\delta_\rho}$	$N^{p}_{\delta_p}$	$N^{\phi}_{\delta_p}$	$N^{v}_{\delta_a}$	$N^{r}_{\delta_a}$	$N^{p}_{\delta_a}$	$N^{\phi}_{\delta_a}$
1	-0.0042(0)(5.6)	0.0042(0.1)(0)(5.6)	0	0	4.508(2.0)	0	0.14(0)(0.1)(2.0)	0.14(0.1)(2.0)
2	-0.0028(0)(5.6)	0.0028(0.1)(0)(5.6)	0	0	4.508(1.32)	0	0.14(0)(1.32)(0.1)	0.14(1.32)(0.1)
3	-0.0056(0)(5.6)	0.0056(0.1)(0)(5.6)	0	0	4.508(2.7)	0	0.14(0)(0.1)(2.7)	0.14(0.1)(2.70)
4	-0.0125(0)(5.6)	0.0125(0.1)(0)(5.6)	0	0	4.508(6.0)	0	0.14(0)(6.0)(0.1)	0.14(6.0)(0.1)
5	-0.0084(0)(5.6)	0.0084(0.1)(0)(5.6)	0	0	4.508(4.0)	0	0.14(0)(0.1)(4.0)	0.14(0.1)(4.0)
6	-0.0022(0)(5.6)	0.0022(0.05)(0)(5.6)	0	0	4.508(2.08)	0	0.14(0)(0.05)(2.08)	0.14(0.05)(2.08)
7	-0.0115(0)(5.6)	0.0115(0.3)(0)(5.6)	0	0	4.508(1.83)	0	0.14(0)(1.83)(0.3)	0.14(1.83)(0.3)
9	-0.0084(0)(5.6)	0.0084(0.1)(0)(5.6)	0	0	4.508(4.0)	0	0.14(0)(4.0)(0.1)	0.14(4.0)(0.1)
10	-0.0084(0)(5.6)	0.0084(0.1)(0)(5.6)	0	0	4.508(4.0)	0	0.14(0)(4.0)(0.1)	0.14(4.0)(0.1)
11	-0.0125(0)(5.6)	0.0125(0.1)(0)(5.6)	0	0	4.508(6.0)	0	0.14(0)(6.0)(0.1)	0.14(6.0)(0.1)
8	-0.0042(0)(5.6)	0.0042(5.525) (0.732)(-0.557)	-0.0149(0)	-0.0149	4.508(2.0)	0	0.14(0)(0.1)(2.0)	0.14(0.1)(2.0)

TABLE 2g LATERAL DIRECTIONAL TRANSFER FUNCTION DENOMINATORS FOR BOTH ATTITUDE COMMAND AND RATE COMMAND AT 30 knots

TF DEN / DIR CONFIG.	AC	RC
1	(0.1)(2.0)(4.061)(1.539)	(0.1)(2.0)(0)(5.6)
2	(1.32)(0.1)(4.061)(1.539)	(1.32)(0.1)(0)(5.6)
3	(0.1)(2.70)(4.061)(1.539)	(0.1)(2.70)(0)(5.6)
4	(6.0)(0.1)(4.061)(1.539)	(6.0)(0.1)(0)(5.6)
5	(0.1)(4.0)(4.061)(1.539)	(0.1)(4.0)(0)(5.6)
6	(0.05)(2.08)(4.061)(1.539)	(0.05)(2.08)(0)(5.6)
7	(1.83)(0.3)(4.061)(1.539)	(1.83)(0.3)(0)(5.6)
9	(4.0)(0.1)(4.061)(1.539)	(4.0)(0.1)(0)(5.6)
10	(4.0)(0.1)(4.061)(1.539)	(4.0)(0.1)(0)(5.6)
11	(6.0)(0.1)(4.061)(1.539)	(6.0)(0.1)(0)(5.6)
8	(4.260)(2.0)(0.876;0.822)	(5.671)(2.0)(0.023;0.630)

TABLE 3 HELICOPTER ROLL AND PITCH DAMPING DERIVATIVES (LEVEL FLIGHT, MID-CG, SEA LEVEL, 80 knots)

	BO-105C*	OH-6A*	AH-1G*	MODEL
L_p, 1/sec	-9.18	-5.4	-1.23	-5.6
M_q, 1/sec	-3.6	-2.68	-0.37	-5.6

*FROM REF. 8

TABLE 4 HELICOPTER CONTROL SENSITIVITY DERIVATIVES (LEVEL FLIGHT, MID-CG, SEA LEVEL, 80 knots)

	BO-105C*	OH-6A*	AH-1G*	MODEL
L_{δ_a}, rad/sec^2-%	0.23	0.15	0.06	0.26
M_{δ_e}, rad/sec^2-%	0.13	0.09	0.02	0.14

*FROM REF. 8

TABLE 5 TURBULENCE RESPONSE DERIVATIVES

DERIVATIVE	VALUE	UNIT
$L_{v_{turb}}$	-0.011	rad/ft-sec
$M_{u_{turb}}$	0.007	rad/ft-sec
$M_{w_{turb}}$	-0.014	rad/ft-sec
$N_{v_{turb}}$	0.049	rad/ft-sec
$X_{u_{turb}}$	-0.01	1/sec
$Y_{v_{turb}}$	CONFIG. Y_v	1/sec
$Z_{u_{turb}}$	-0.073	1/sec
$Z_{w_{turb}}$	-0.924	1/sec

TABLE 6 EVALUATION PILOTS

PILOT	TOTAL TIME		ACM TIME		PRIMARY A/C FLOWN	OTHER A/C FLOWN
	HELICOPTER	FIXED WING	ACTUAL	SIMULATOR		
A	3450	1550	5	20	CH-46, HH-3 UH-1, CH-53D/E AH-1, C-141	XV-15, SH-3 OH-6, T-28
B	1183	3000	3	20	UH-1, AH-1 LEAR 24, C-130 01G, T-42A	YAH-64, RSRA SH-3, OH-58
C	8500	2000	0	0	BELL UH-1 AH-1, 214, 222 400 HUGHES 300, 500 BELL XV-15	H-13, H-34 H-19, T-33 CESSNA 310, 320 401, 500, 550
D	3700	500	14	0	BELL UH-1 AH-1, OH-58 HUGHES AH-64 500, 530	30-40 MISC. TYPES
E	5000	1500	35	25	AH-1, UH-1 UH-60	OH-58, CH-47 OV-1, CH-46 ABC, OTHERS
F	3700	465	35	0	S-76, UH-60 AH-1, H-53 H-34, H-3	XH-59A, S-67 H-13, OTHERS

TABLE 7.– EVALUATION TASK DEFINITION

	Task	Cooper-Harper term	Definition
1.	Initial long-range tracking	Control task	Maneuver the aircraft as aggressively as necessary to obtain a tail-chase position and begin tracking in the quickest time possible.
		Auxiliary task	Maintain an awareness and use of terrain masking to avoid detection.
		Uncontrollable	Control of the aircraft will be lost during aggressive, large amplitude maneuvers.
		Adequate performance	The aircraft is able to establish a tail-chase position.
		Satisfactory performance	The aircraft is able to establish and hold a tail-chase position.
		Tolerable workload	During the tracking engagement, pilot workload will be such that the task can be accomplished with sufficient reserve capacity for tactical maneuvering and communication with friendly forces and situational awareness of altitude constraints, ground position and air and ground threat locations.
2.	Close-in gun tracking	Control task	Track the target aircraft within weapon parameters for as much a percentage of the total engagement time as possible. Maximum use of the aircraft's performance potential, instruments, and displays is expected.
		Auxiliary task	Maintain a good defensive awareness and position, i.e., a six-o'clock tail position is better than a head-on pass. Maintain a maximum altitude of 300 ft above ground level unless forced to higher altitude by the target aircraft.
		Uncontrollable	Control of the aircraft will be lost if the air-to-air tracking task is attempted.
		Adequate performance	The aircraft can be expected to attain a tactical advantage and effect a firing solution over the target aircraft.
		Satisfactory performance	The aircraft can be expected to maintain a tactical advantage and effect a large number of firing solutions against the target aircraft.
		Tolerable workload	Same as Task No. 1

TABLE 8.– RECORDED VARIABLES

Computer Mnemonic	Description
XCG	X position of the CG of the blue aircraft with respect to the origin of the CGI data base, ft
YCG	Y position of the CG of the blue aircraft with respect to the origin of the CGI data base, ft
HCG	Z (height) position of the CG of the blue aircraft
ALTD	Rate of climb, blue aircraft, ft/sec
FTX	Sum of forces in the X direction, blue aircraft, lbf
FTY	Sum of forces in the Y direction, blue aircraft, lbf
FTZ	Sum of forces in the Z direction, exluding gravity, blue aircraft, lbf
UB	Velocity in the X direction, blue aircraft body axis, ft/sec
VB	Velocity in the Y direction, blue aircraft body axis, ft/sec
WB	Velocity in the Z direction, blue aircraft body axis, ft/sec
VEQ	Airspeed, knots
4MAIN	Phi, roll angle, deg
THET	Pitch angle, deg
PSI	Heading, blue aircraft, deg
BETA	Sideslip angle, deg
PHID	Phi dot, roll rate, rad/sec
THED	Theta dot, pitch rate, rad/sec
PSID	Psi dot, yaw rate, rad/sec
ROLLO	Lateral cyclic input, percent
PITCHO	Longitudinal cyclic input, percent
COLO	Collective input, percent
VN	North component of airspeed, ft/sec
VE	East component of airspeed, ft/sec
XCGT	X position of the CG of the red aircraft, ft
YCGT	Y position of the CG of the red aircraft, ft

TABLE 8.– CONTINUED

Computer Mnemonic	Description
HCGT	Z position of the CG of the red aircraft, ft
FTXT	Sum of forces in the X direction, red aircraft, lbf
FTYT	Sum of forces in the Y direction, red aircraft, lbf
FTZT	Sum of forces in the Z direction, red aircraft, lbf
UBT	Velocity in the X direction, red aircraft body axis, ft/sec
VBT	Velocity in the Y direction, red aircraft body axis, ft/sec
WBT	Velocity in the Z direction, red aircraft body axis, ft/sec
VEQT	Airspeed, red aircraft, knots
XH	Roll angle, red aircraft, deg
THETAT	Pitch angle, red aircraft, deg
PSIT	Heading, red aircraft, deg
BETAT	Sideslip angle, red aircraft, deg
PBTDEG	Roll rate, red aircraft, deg/sec
QBTDEG	Pitch rate, red aircraft, deg/sec
RBTDEG	Yaw rate, red aircraft, deg/sec
ROLLT	Roll input, red aircraft, percent
PITCHT	Pitch input, red aircraft, percent
YAWT	Yaw input, red aircraft, percent
COLT	Collective input, red aircraft
VNT	North component of velocity, red aircraft, ft/sec
VET	East component of velocity, red aircraft, ft/sec
ALTDT	Rate of climb, red aircraft, ft/sec
UTURB	X component of turbulence, body axis
VTURB	Y component of turbulence, body axis
WTURB	Z component of turbulence, body axis

TABLE 8.– CONCLUDED

Computer Mnemonic	Description
OWNTIM	Cone time of blue aircraft, sec
TARTIM1	Cone time of red aircraft, sec
ISEE	Clear line of sight flag
SRANGE	Range from blue aircraft to red aircraft, ft
AOFFO	Angle off, azimuth, blue aircraft view, deg
POFFO	Angle off, pitch blue aircraft view, deg
AOFFT	Angle off, azimuth, red aircraft view, deg
POFFT	Angle off, pitch, red aircraft view, deg

TABLE 9

RUN NUMBER = 99 09:13 JUL 09, 85

CONFIGURATION = HIGH BASELINE UH-60
PILOT = STEVE HANVEY
CONFIGURATION I.D. NUMBER = 23 1
CONTROL SYSTEM TYPE = RATE COMM/ ATT. HOLD

----------INITIAL CONDITIONS----------

	OWNSHIP	TARGET
XCG (FT) =	-4.583300	.000000
YCG (FT) =	.000000	2899.000000
HCG (FT) =	200.000000	100.000000
PSI (DEG) =	.000000	325.000000
VEQ (KTS) =	79.99988	80.000000
WEIGHT (LB) =	10000.000000	10000.000000

----------OWNSHIP VARIABLES----------

XLPHIO =	-6.250000	FT.LB/(R/S)	XNDPT =	.003866	FT.LB/%
XLDAT =	.266700	FT.LB/%	ZWT =	-1.000000	LB/(FT/S)
ZMQT =	-5.600000	FT.LB/(R/S)	ZDCT =	1.500000	LB/%
XMTHETO =	-6.250000	FT.LB/RAD	XUT =	-.010000	LB/(FT/S)
XMDET =	.133300	FT.LB/%	YVT =	-.100000	LB/(FT/S)
ZNRT =	-2.000000	FT.LB/(R/S)	ZMU =	.000000	FT.LB/(FT/S)
ZMUT =	.007100	-N.D-	ZMWT =	-.001390	-N.D-
ZNVT =	.004920	-N.D-	ZUT =	-.007310	-N.D-
ZWTT =	-.92426	-N.D-	ZLPT =	-5.600000	FT.LB/(R/S)
XNVO =	.001515	RAD/FT.SEC	ZNPO =	.238000	RAD/FT.SEC
ZLVT =	-.001070	-N.D-	ZLV =	.000000	FT.LB/(FT/S)
XNPHIO =	.476001	FT.LB/RAD	XNV =	2.005000	RAD

----------WIND CONDITIONS----------

	(KTS)	(FT/SEC)	
VW =	.000000	.000000	PSIW = 90.000000 (DEG)
UDISP =	1.200006	2.02547	
VDISP =	1.200006	2.02547	
WDISP =	1.800000	3.03805	

TABLE 10

RUN NUMBER = 99 ØØ9:18 JUL Ø9,'85

CONFIGURATION = HIGH BASELINE UH-6Ø
PILOT = STEVE HANVEY
CONFIGURATION I.D. NUMBER = 23 1
CONTROL SYSTEM TYPE = RATE COMM/ ATT. HOLD
RUN TIME = 1ØØ.Ø7999 SECONDS

	BLUE	RED
SHOTS FIRED =	3	Ø
CONE TIME (% RUN TIME) =	2Ø.74258 (RED IN BLUE)	.ØØØØØ (BLUE IN RED)
SURVIVABILITY PROBABILITY =	1.ØØØØØ	.729ØØ

MAX. AIRSPEED =	89.39215	KTS
MIN. AIRSPEED =	53.97937	KTS
AVG. AIRSPEED =	77.96951	KTS
MAX. ROLL RATE =	37.199Ø7	DEG/SEC
MAX. PITCH RATE =	9.72498	DEG/SEC
MIN. PITCH RATE =	-8.67966	DEG/SEC
MAX. BETA RATE =	18.44327	DEG/SEC
MIN. BETA RATE =	-7.77612	DEG/SEC
MAX. ROLL ANGLE =	61.7885Ø	DEG
MAX. PITCH ANGLE =	9.17992	DEG
MIN. PITCH ANGLE =	-2Ø.84877	DEG
MAX. BETA ANGLE =	28.12988	DEG
MIN. BETA ANGLE =	-37.57Ø37	DEG
MAX. NORMAL FORCE =	2.42486	G
AVG. NORMAL FORCE =	1.15466	G
MIN. NORMAL FORCE =	.38546	G
MAX. SIDE FORCE =	.16413	G
MAX. ALTITUDE =	259.Ø5444	FT
MIN. ALTITUDE =	36.98796	FT
AVG. ALTITUDE =	127.91222	FT
AVG. RANGE TO TARGET =	793.34473	FT
MAX. G. MANEUVERS =	Ø	
ROLL AXIS REVERSALS =	45	
YAW AXIS REVERSALS =	3	
PITCH AXIS REVERSALS =	43	
ROLL AXIS DIRECTION CHANGES =	88	
YAW AXIS DIRECTION CHANGES =	73	
PITCH AXIS DIRECTION CHANGES =	1Ø7	
COLLECTIVE AXIS DIRECTION CHANGES =	4Ø	

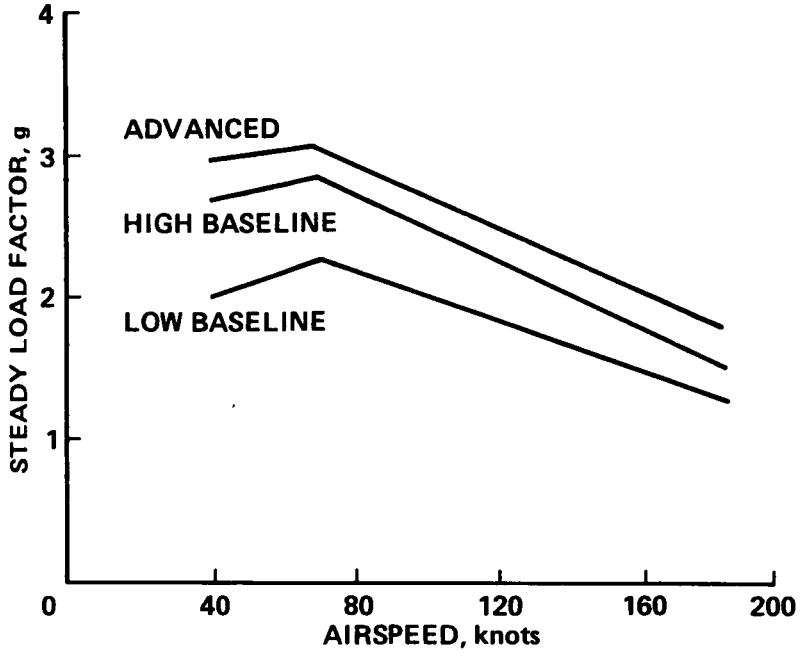

Figure 1.- Maximum steady load factor capability.

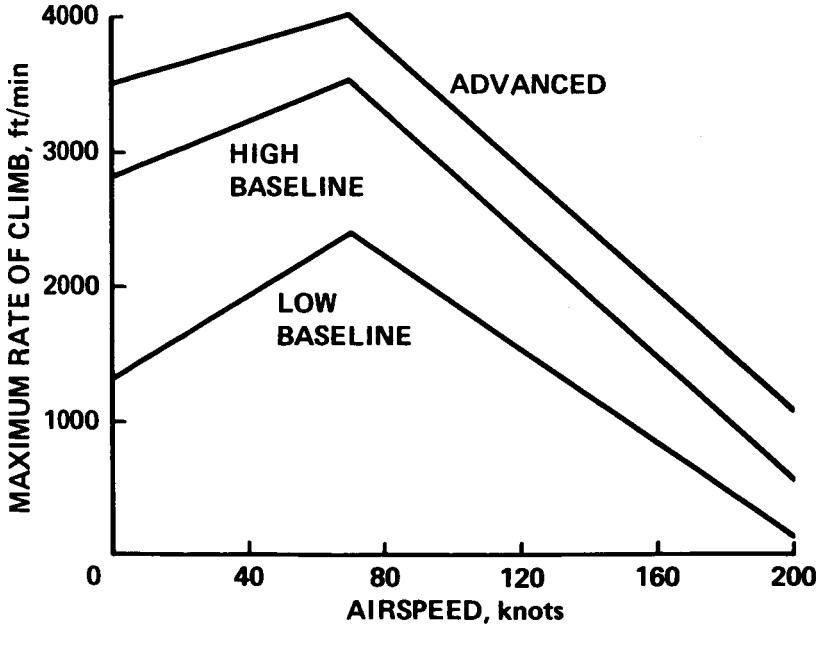

Figure 2.- Maximum rate of climb data.

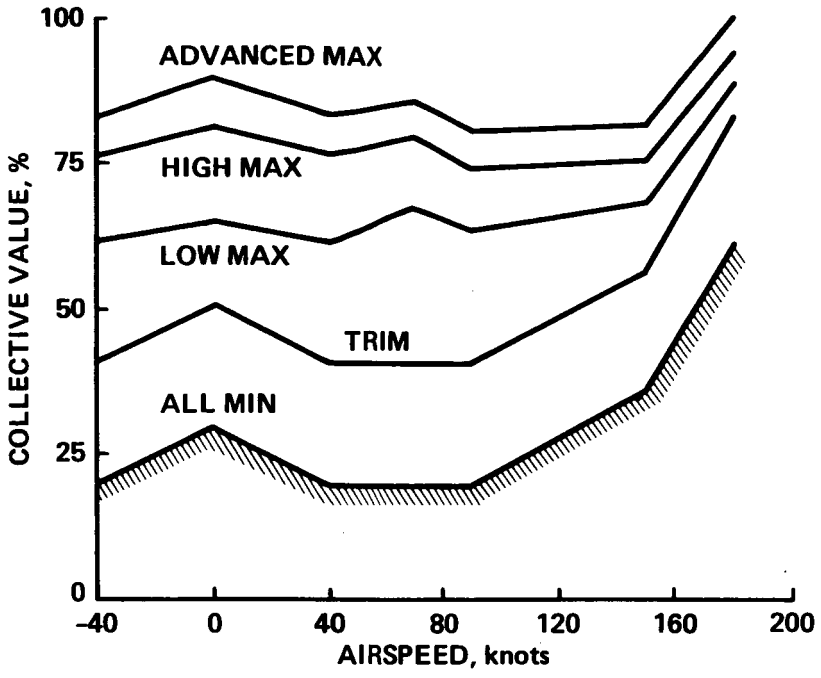

Figure 3.- Collective scheduling and trim to limit sideslip capability.

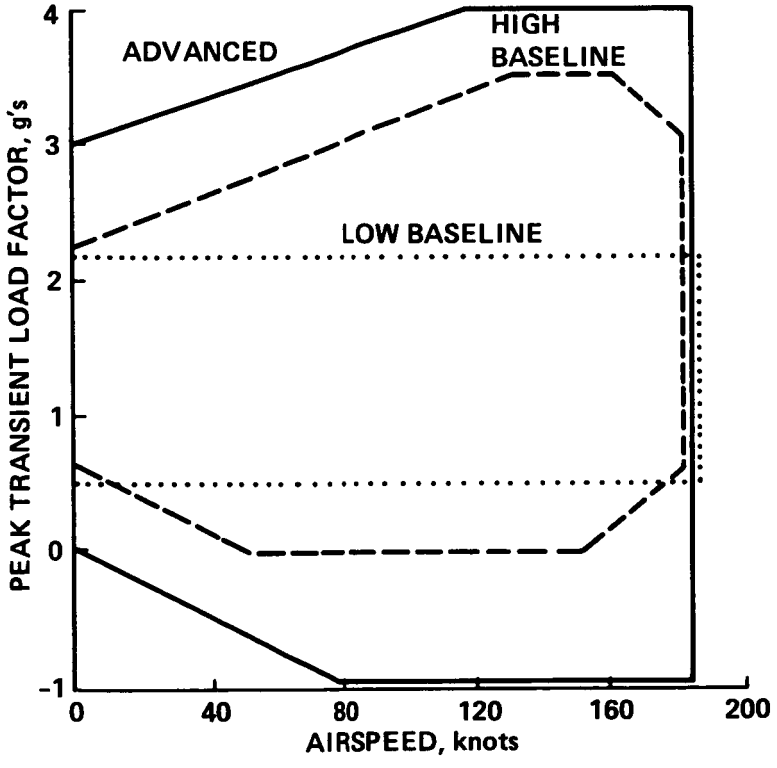

Figure 4.- Transient load factor limits, structural.

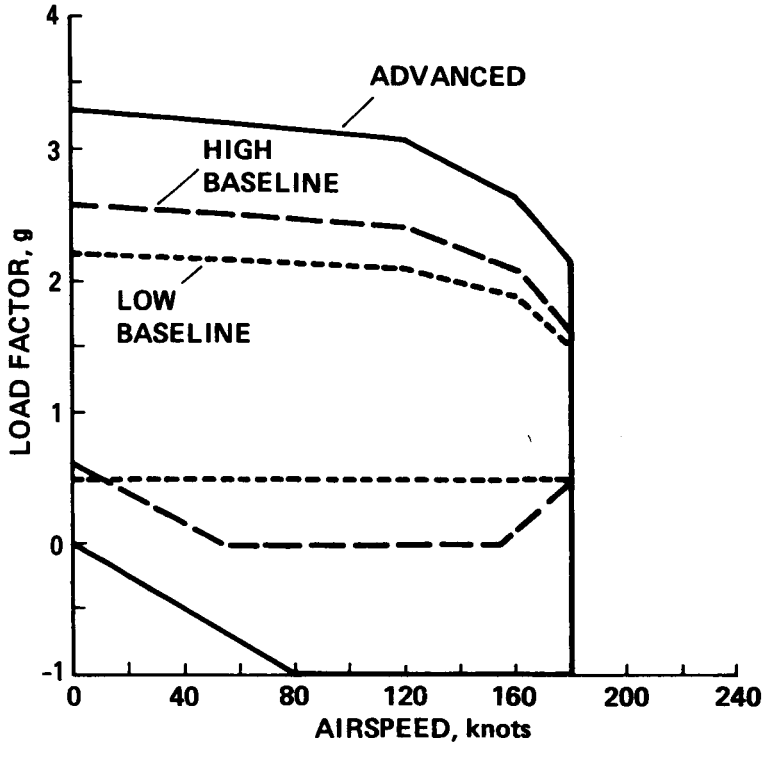

Figure 5.- Transient load factor limits, rotor system capability at DGW.

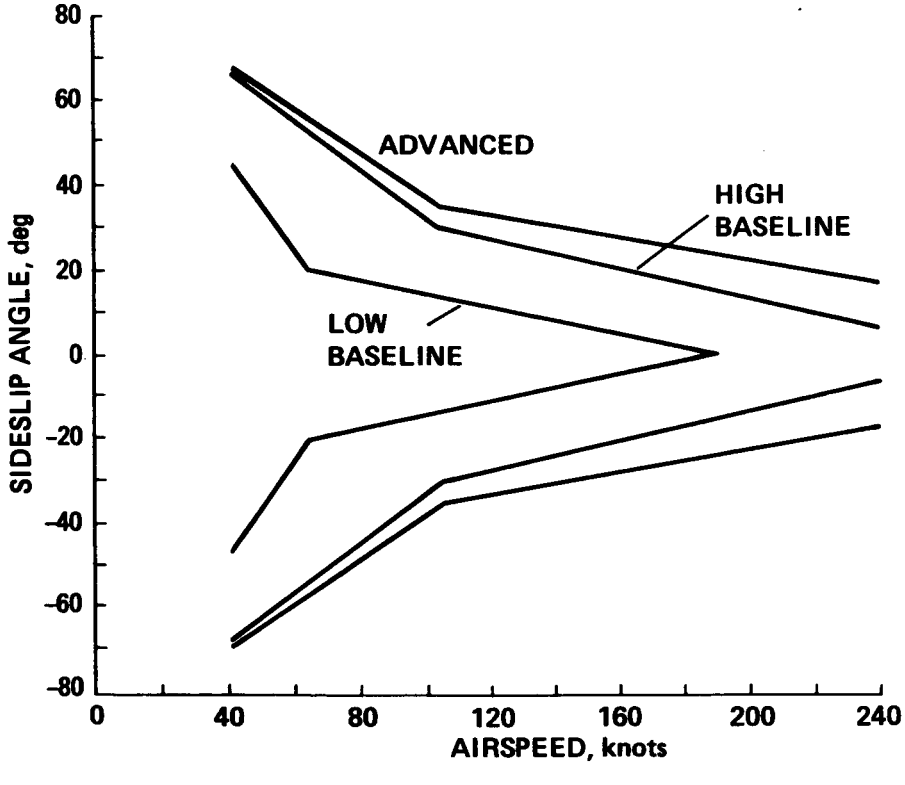

Figure 6.- Sideslip envelopes.

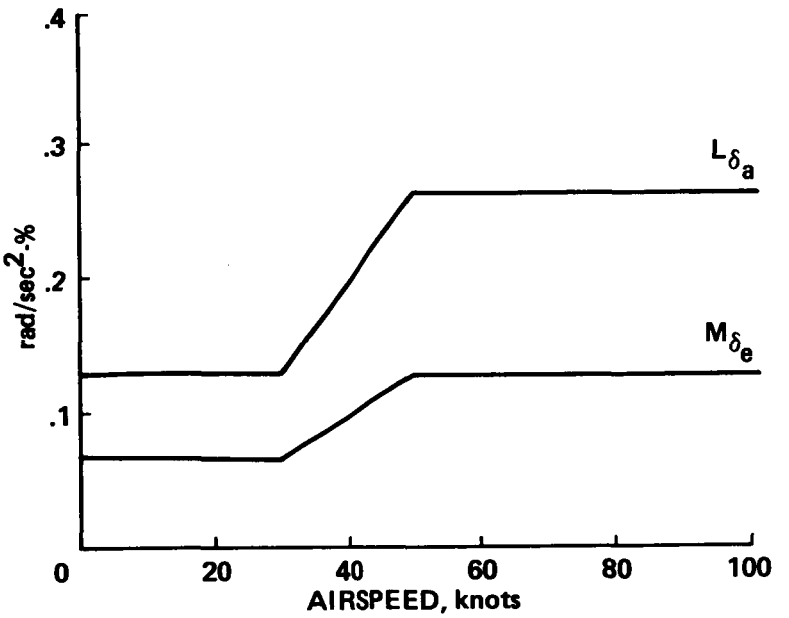

Figure 7.- Scheduling of roll and pitch control sensitivity derivatives.

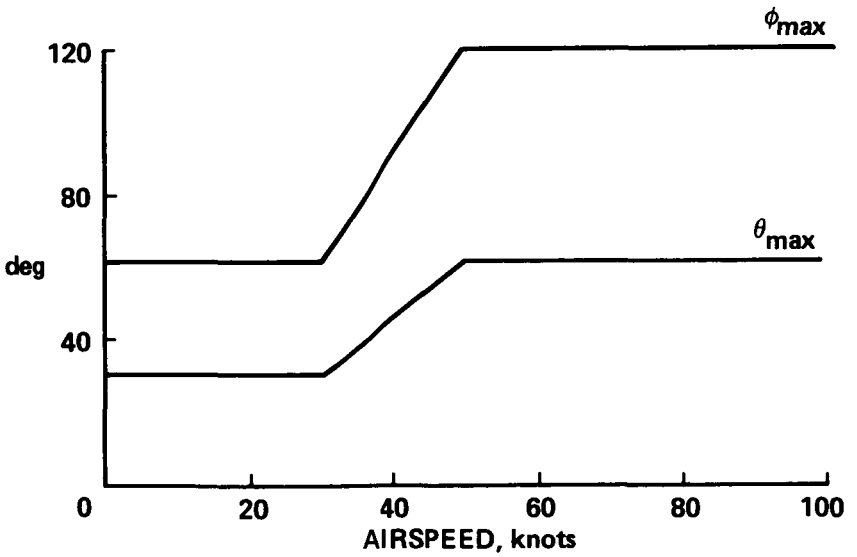

Figure 8.- Maximum roll and pitch angles, AC/AH.

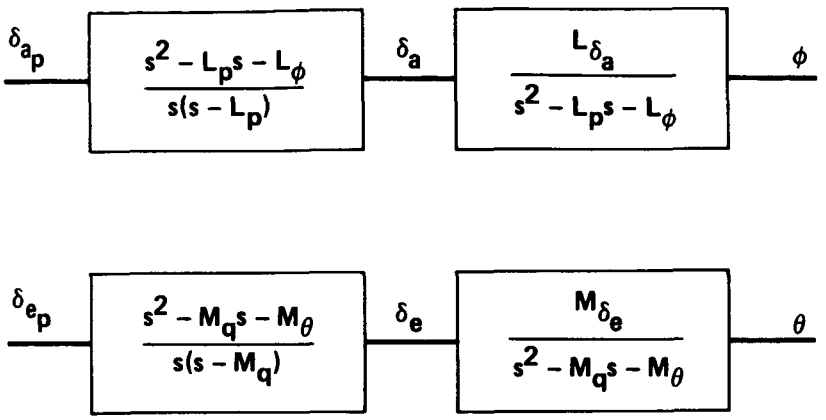

Figure 9.- Input shaping filter (added to AC/AH to get RC/AH).

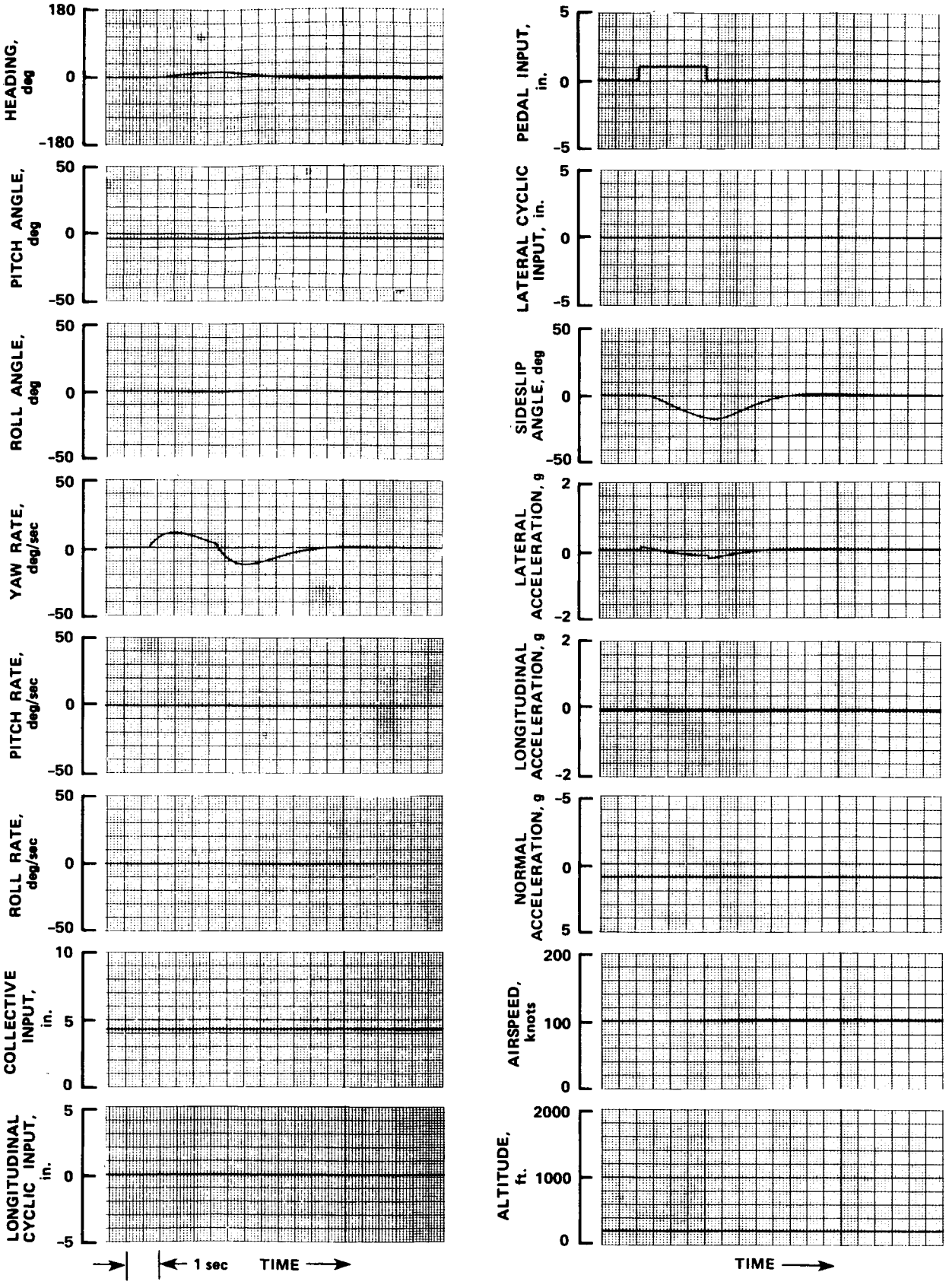

Figure 10.- Strip chart recording of step input responses. Step pedal input, configuration 231, 100 knots.

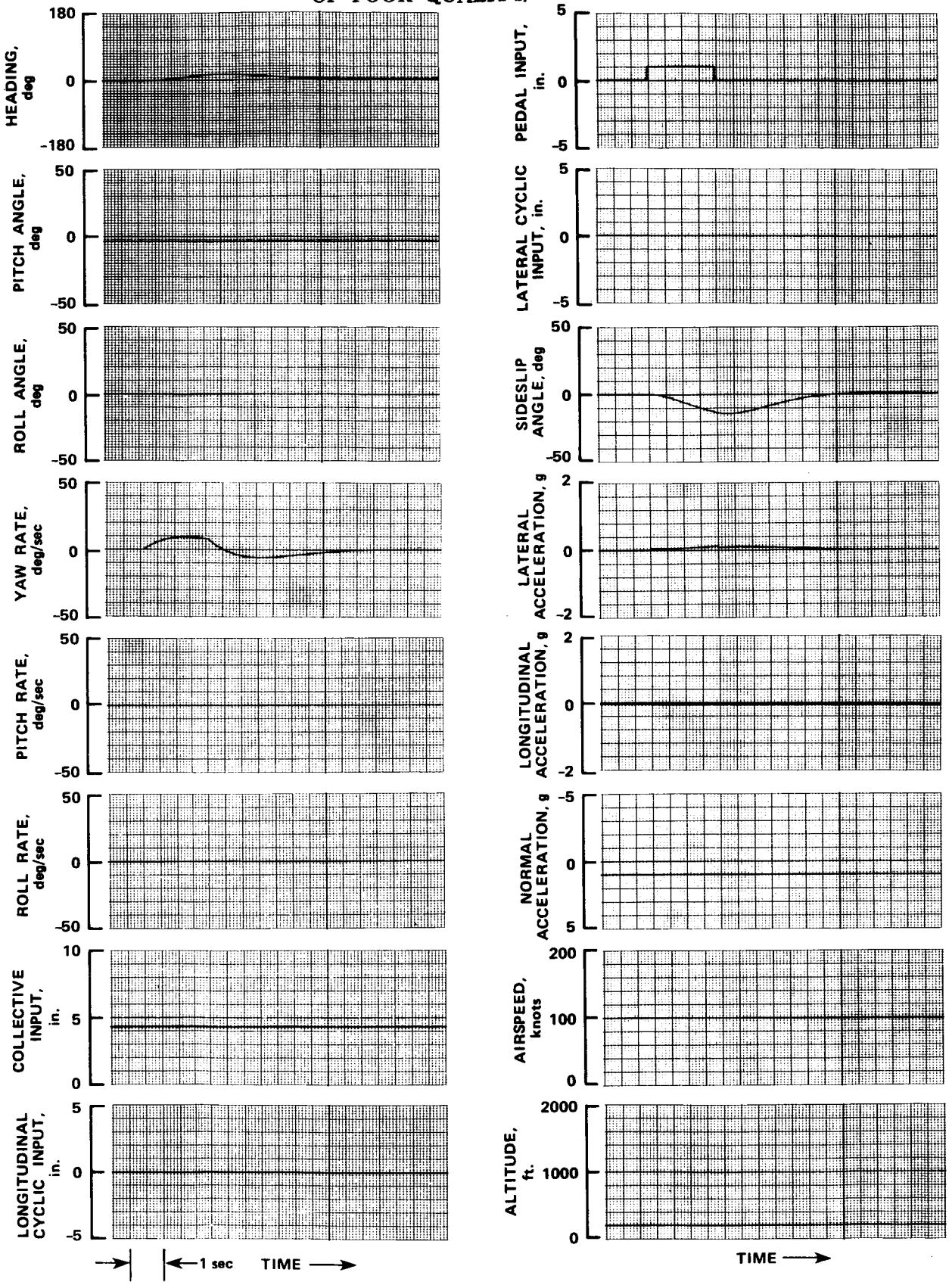

Figure 11.- Strip chart recording of step input responses. Step pedal input, configuration 232, 100 knots.

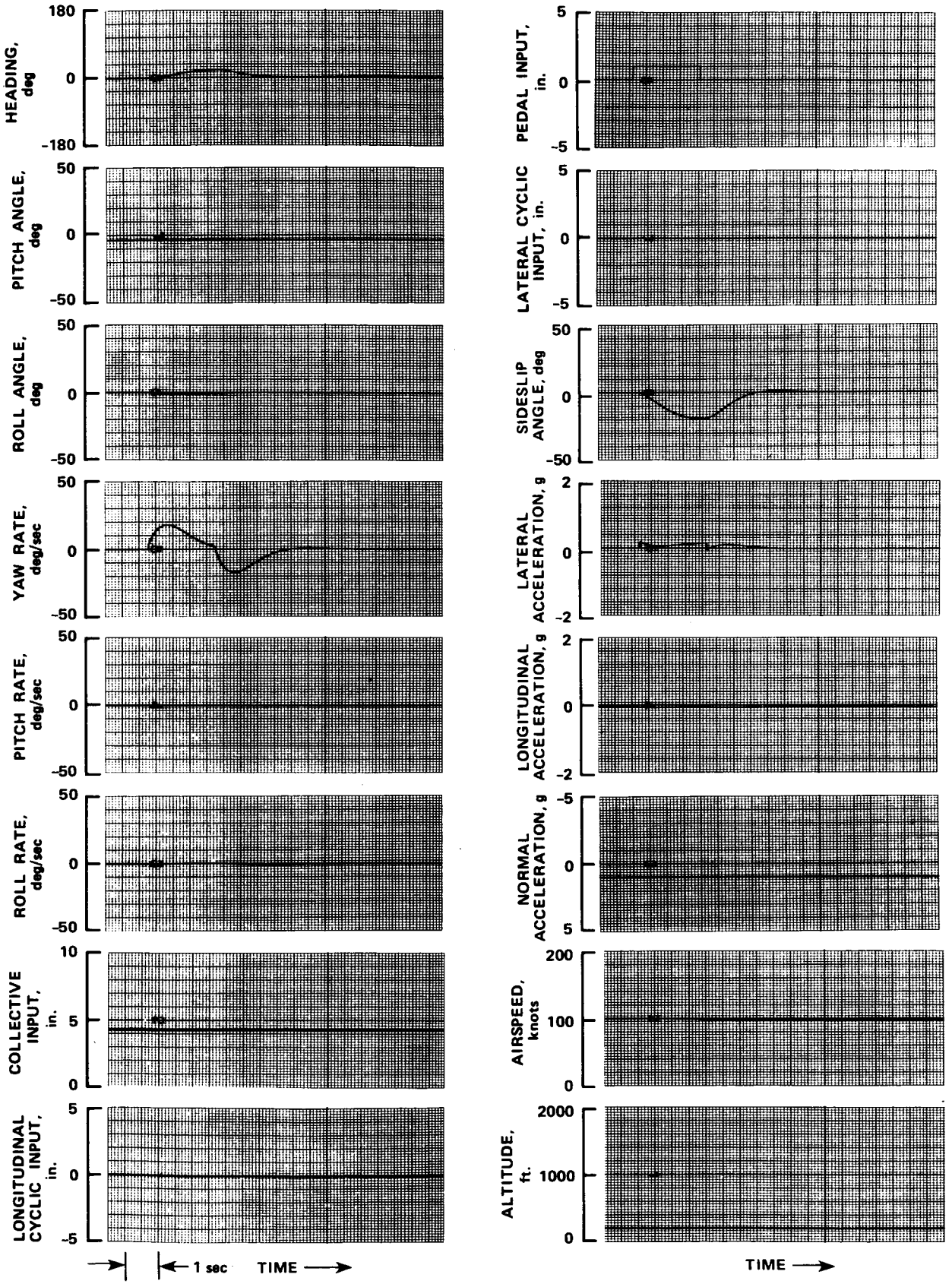

Figure 12.- Strip chart recording of step input responses. Step pedal input, configuration 233, 100 knots.

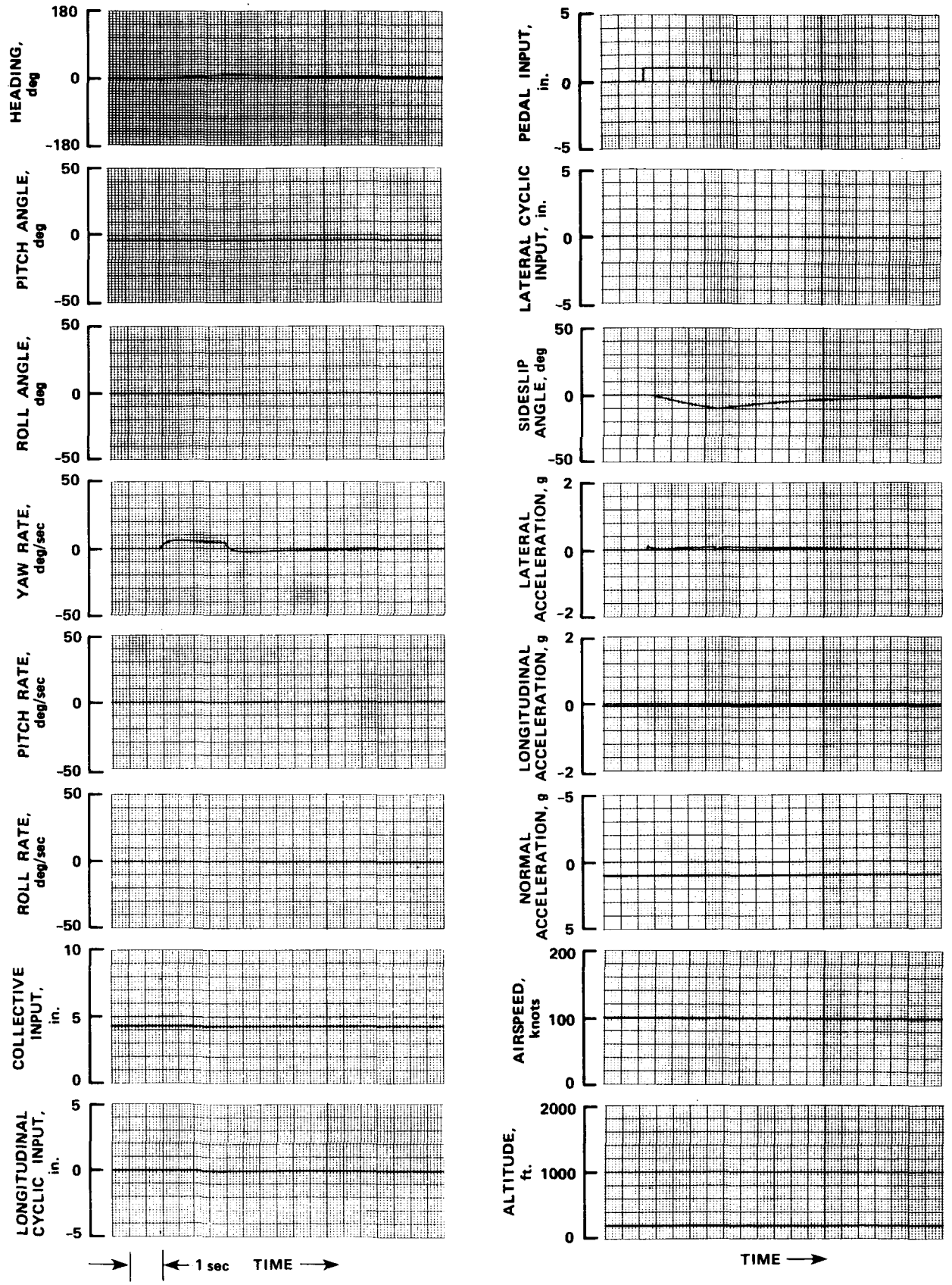

Figure 13.- Strip chart recording of step input responses. Step pedal input, configuration 234, 100 knots.

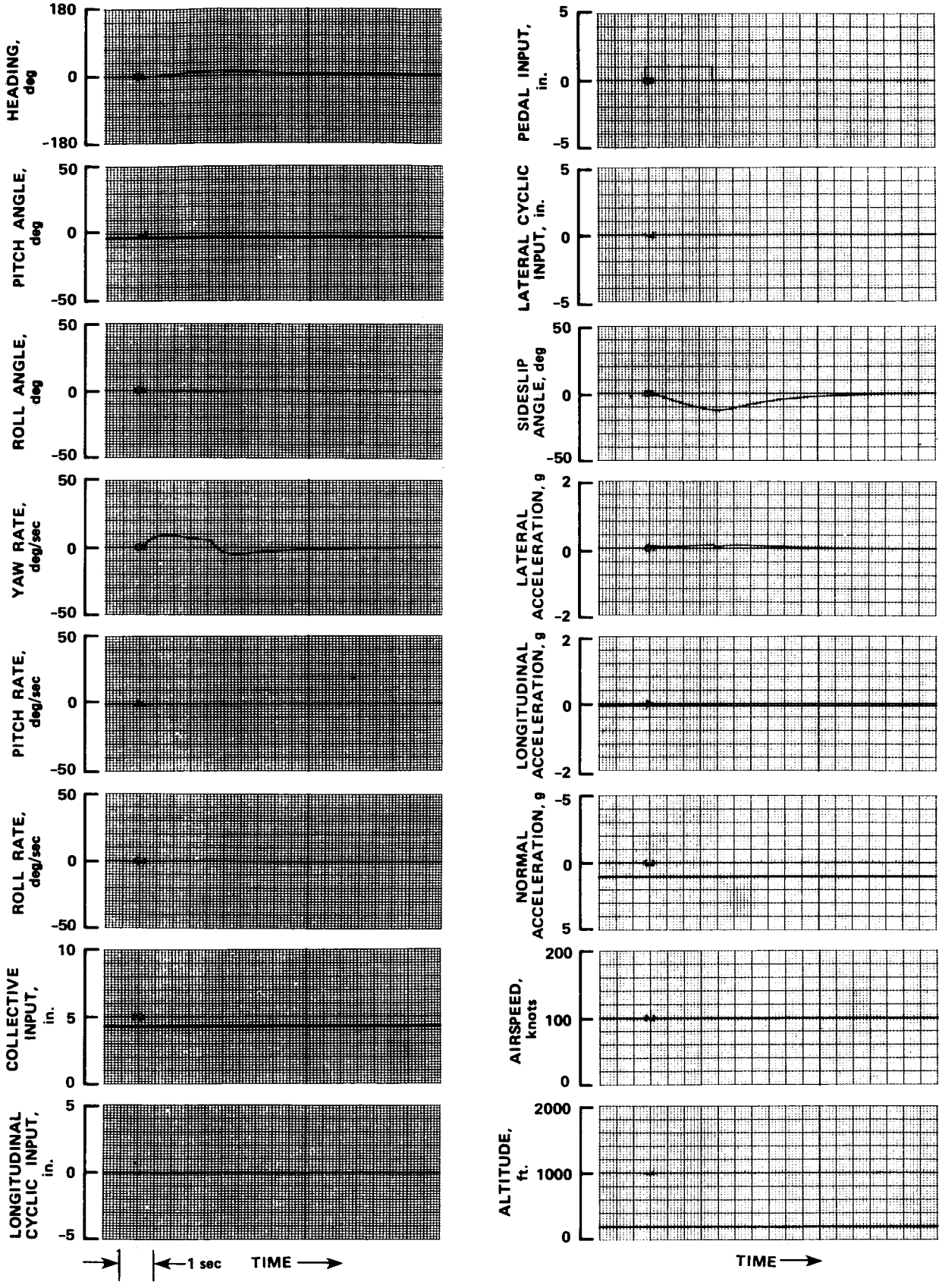

Figure 14.- Strip chart recording of step input responses. Step pedal input, configuration 235, 100 knots.

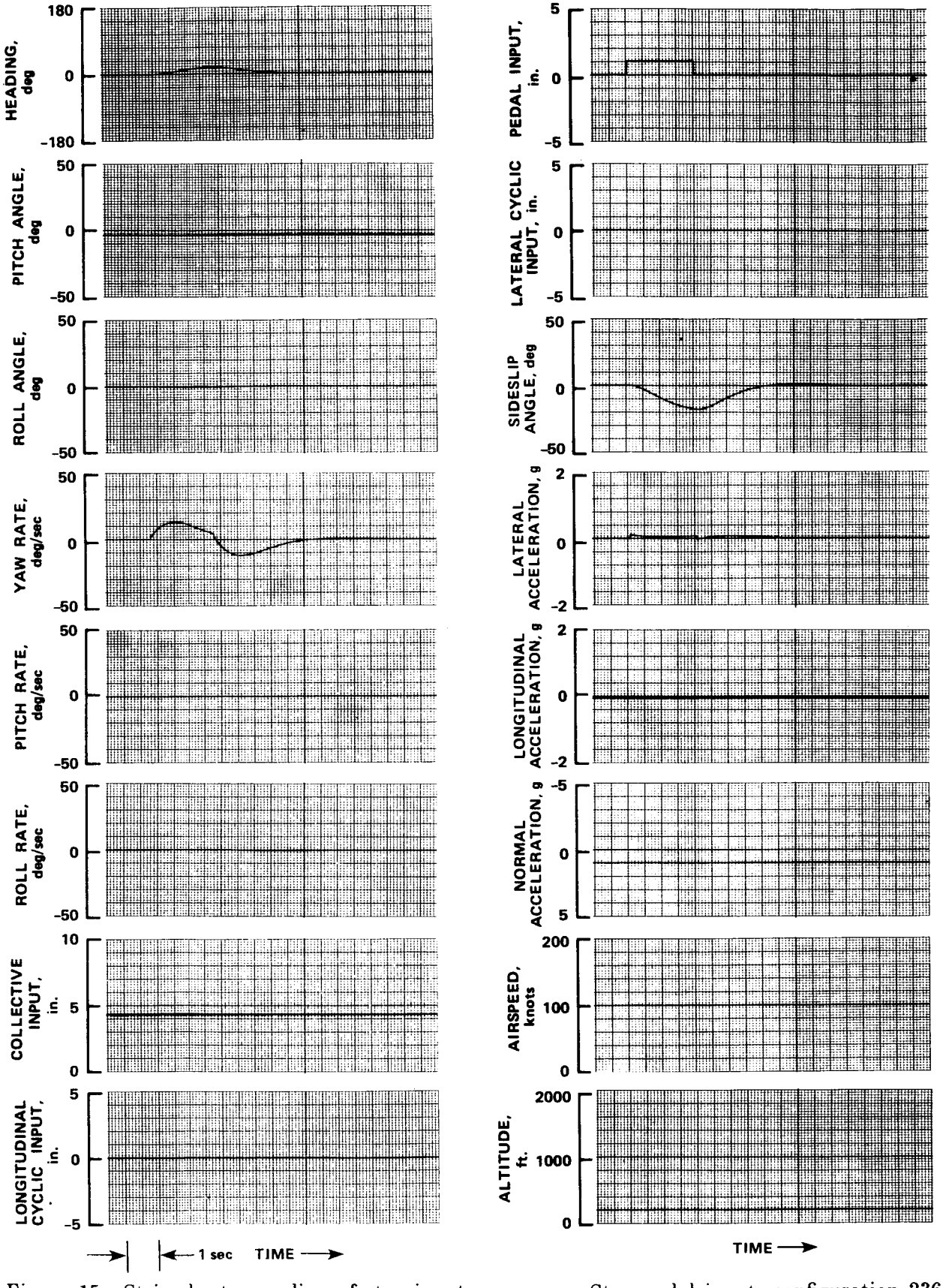

Figure 15.- Strip chart recording of step input responses. Step pedal input, configuration 236, 100 knots.

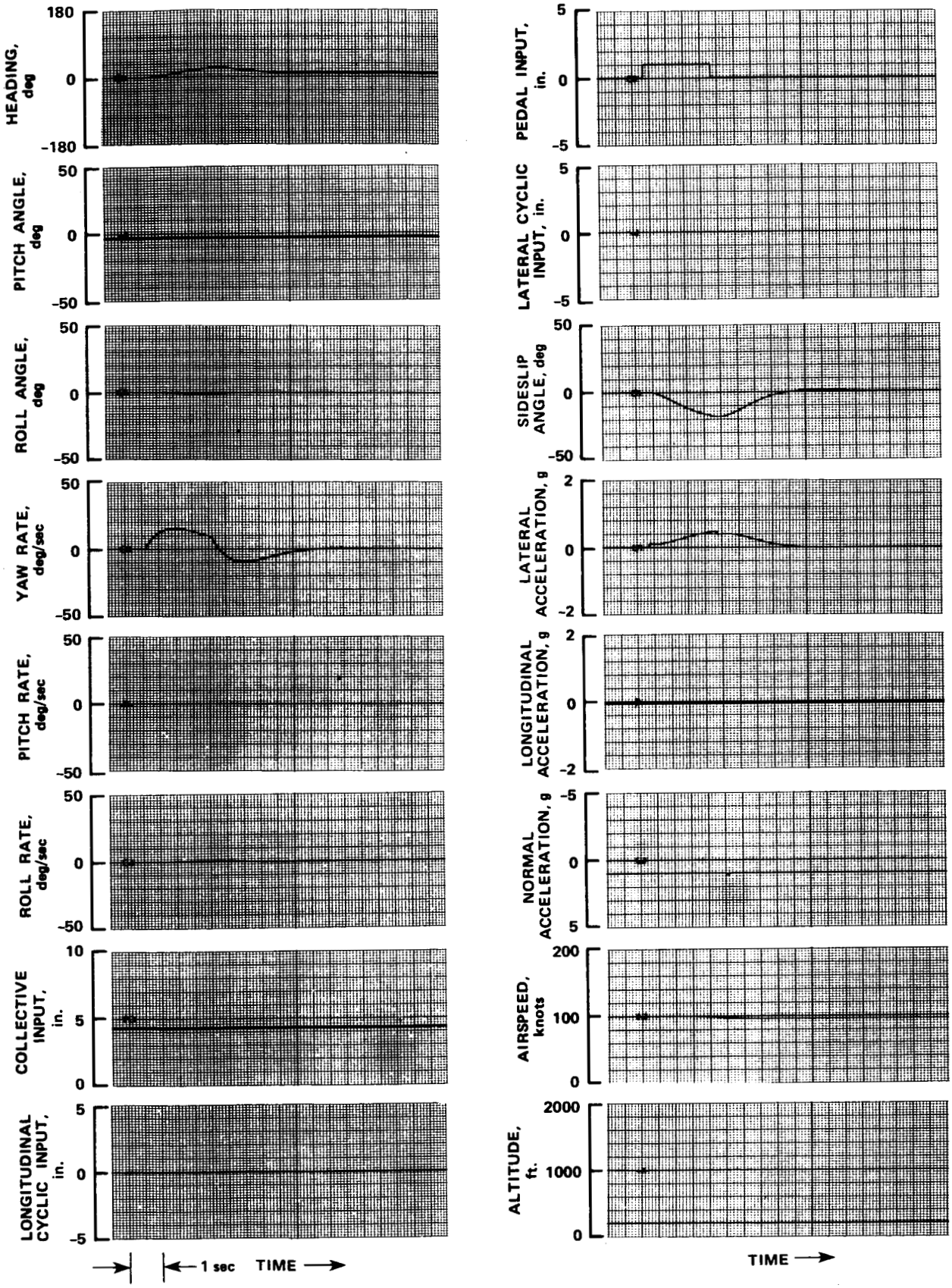

Figure 16.- Strip chart recording of step input responses. Step pedal input, configuration 237, 100 knots.

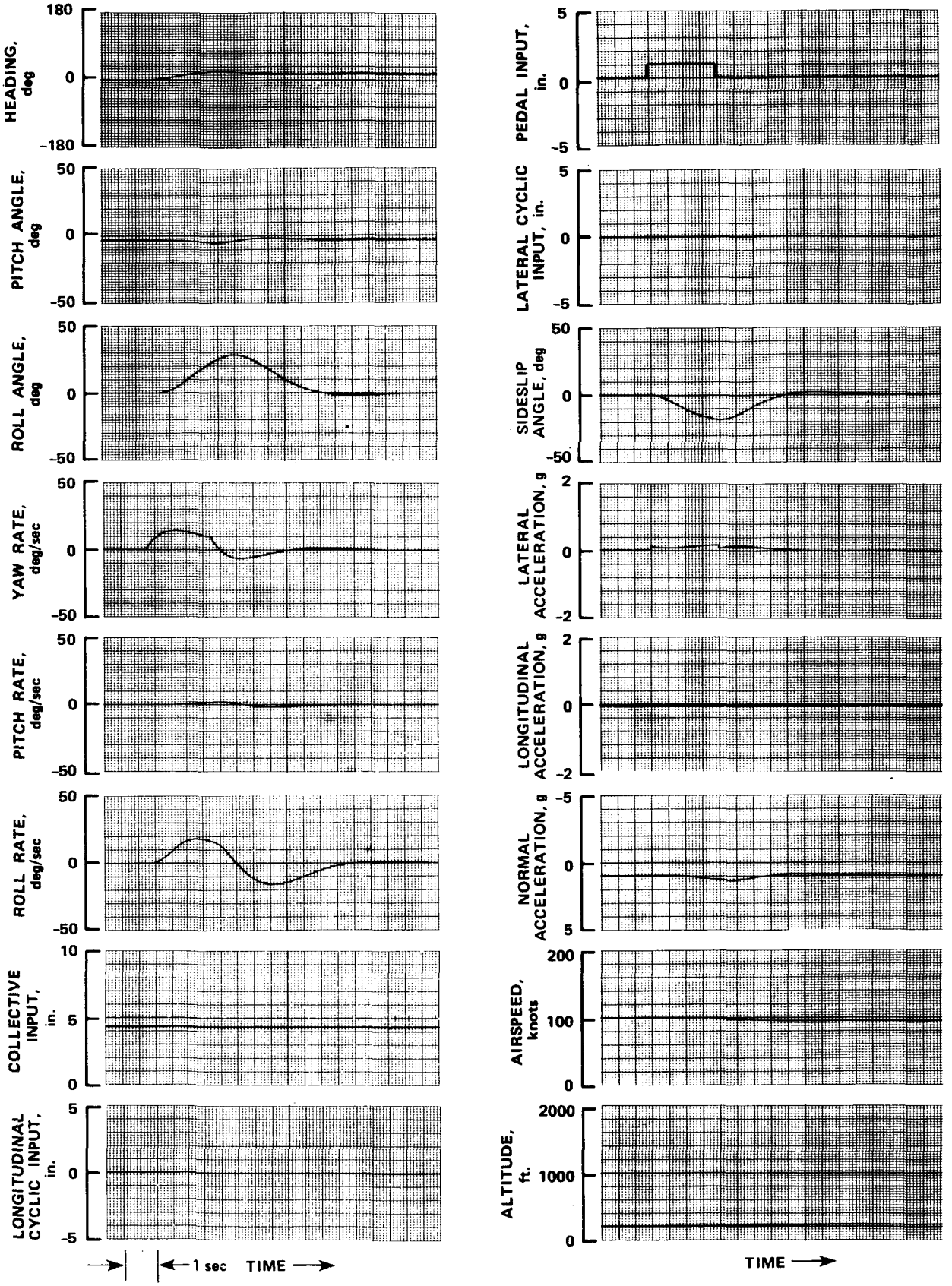

Figure 17.- Strip chart recording of step input responses. Step pedal input, configuration 238, 100 knots.

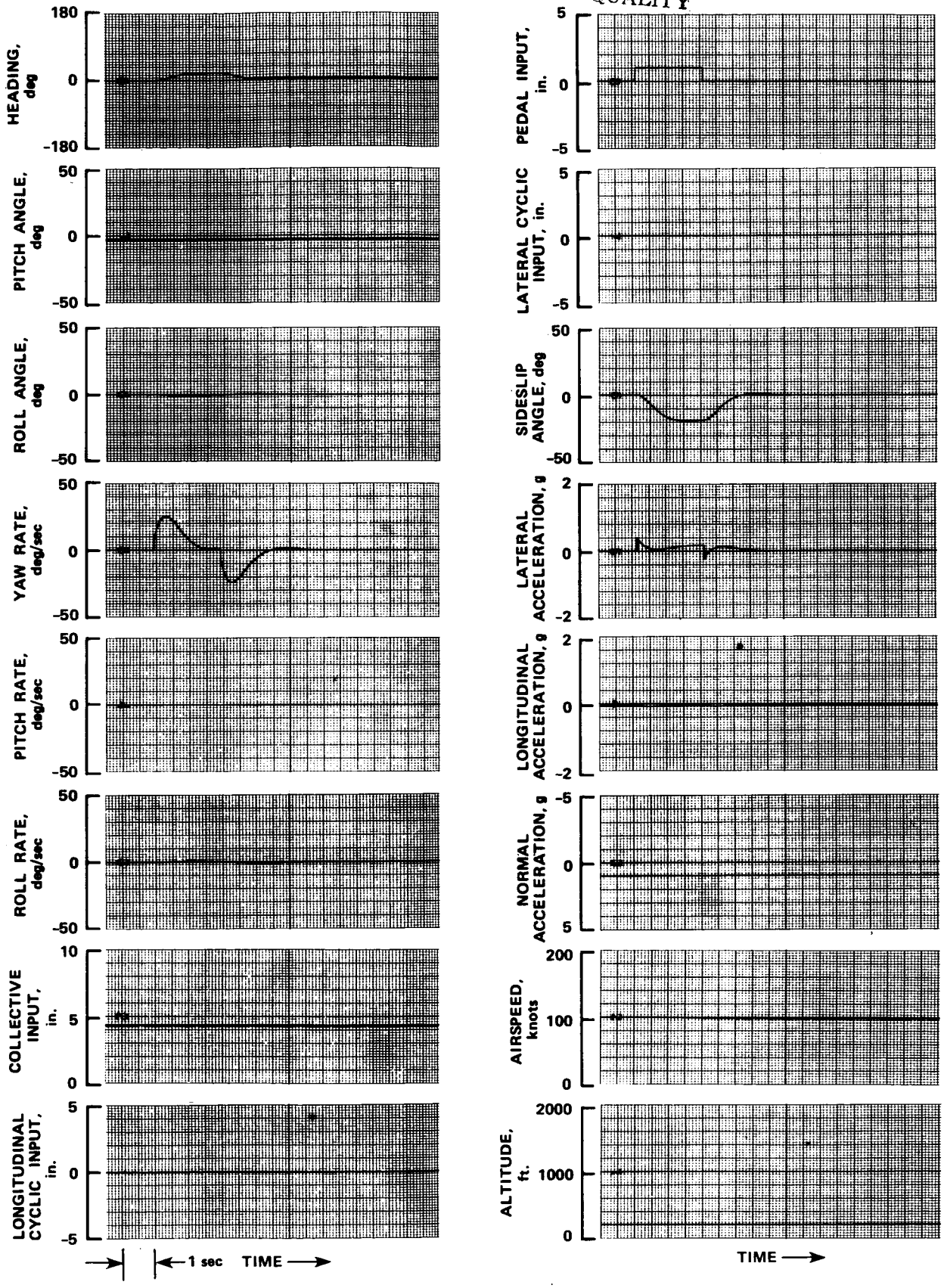

Figure 18.- Strip chart recording of step input responses. Step pedal input, configuration 239, 100 knots.

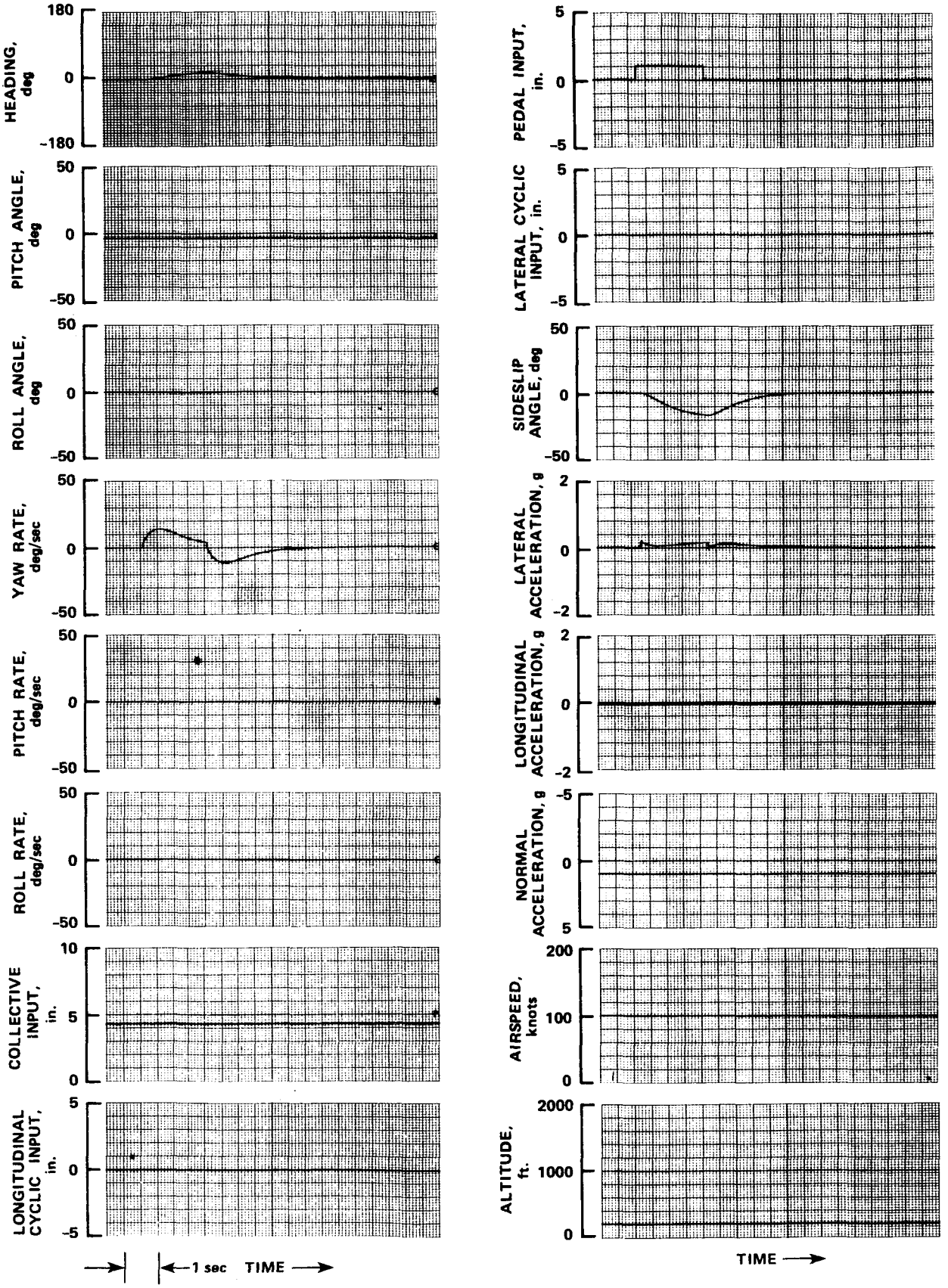

Figure 19.- Strip chart recording of step input responses. Step pedal input, configuration 2310, 100 knots.

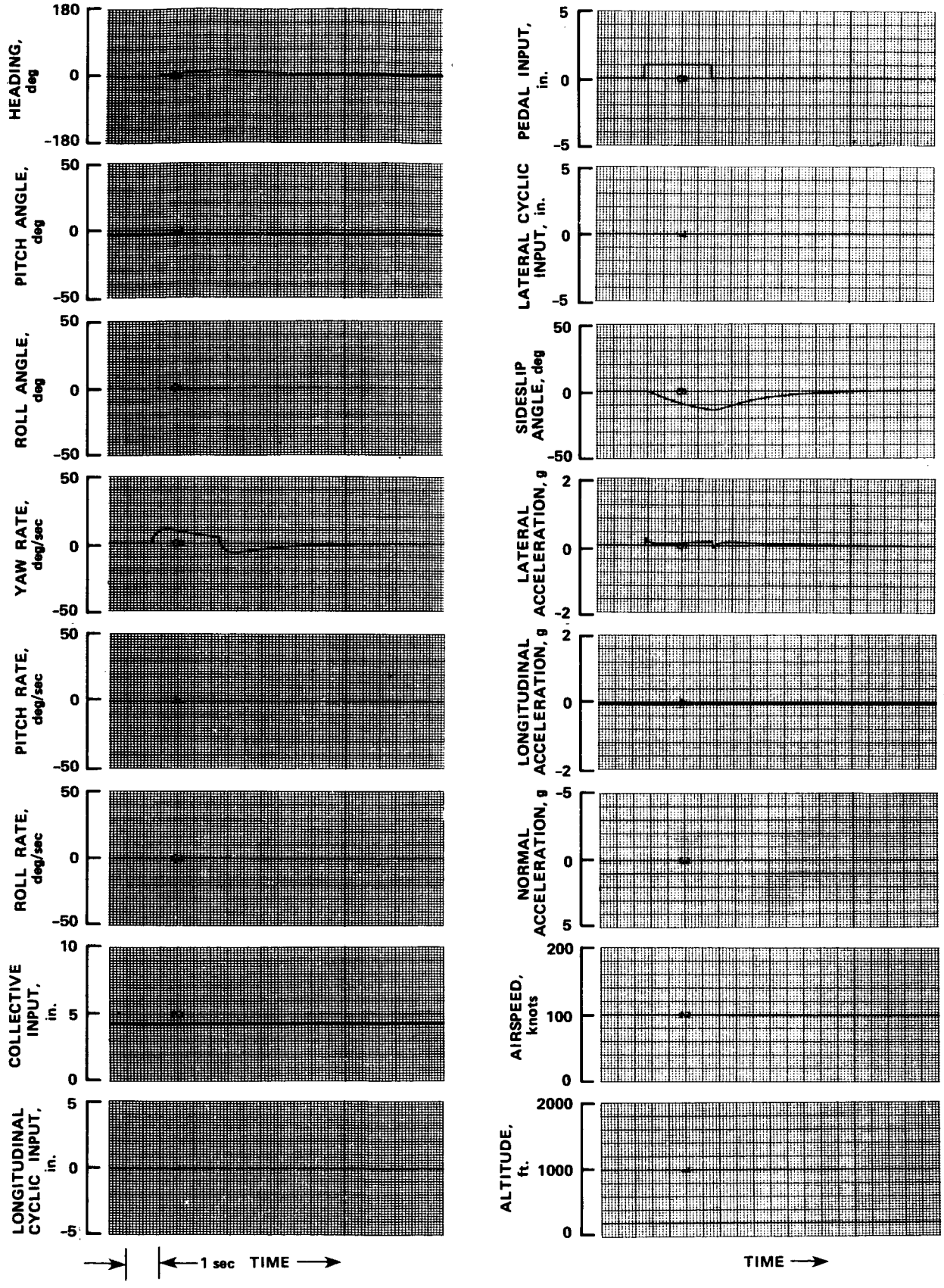

Figure 20.- Strip chart recording of step input responses. Step pedal input, configuration 2311, 100 knots.

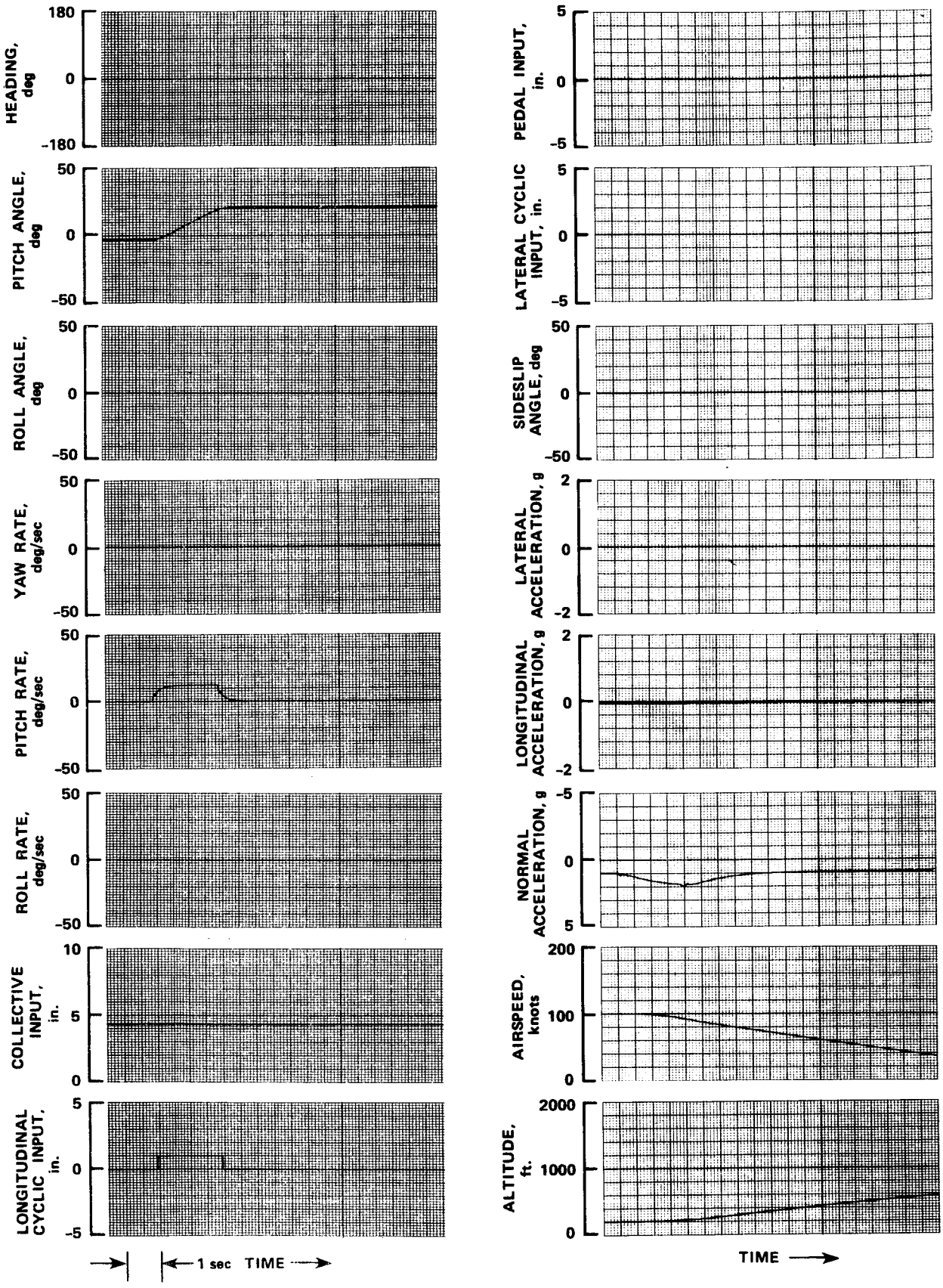

Figure 21.- Strip chart recording of step input responses. Step longitudinal cyclic, configuration 211, 100 knots.

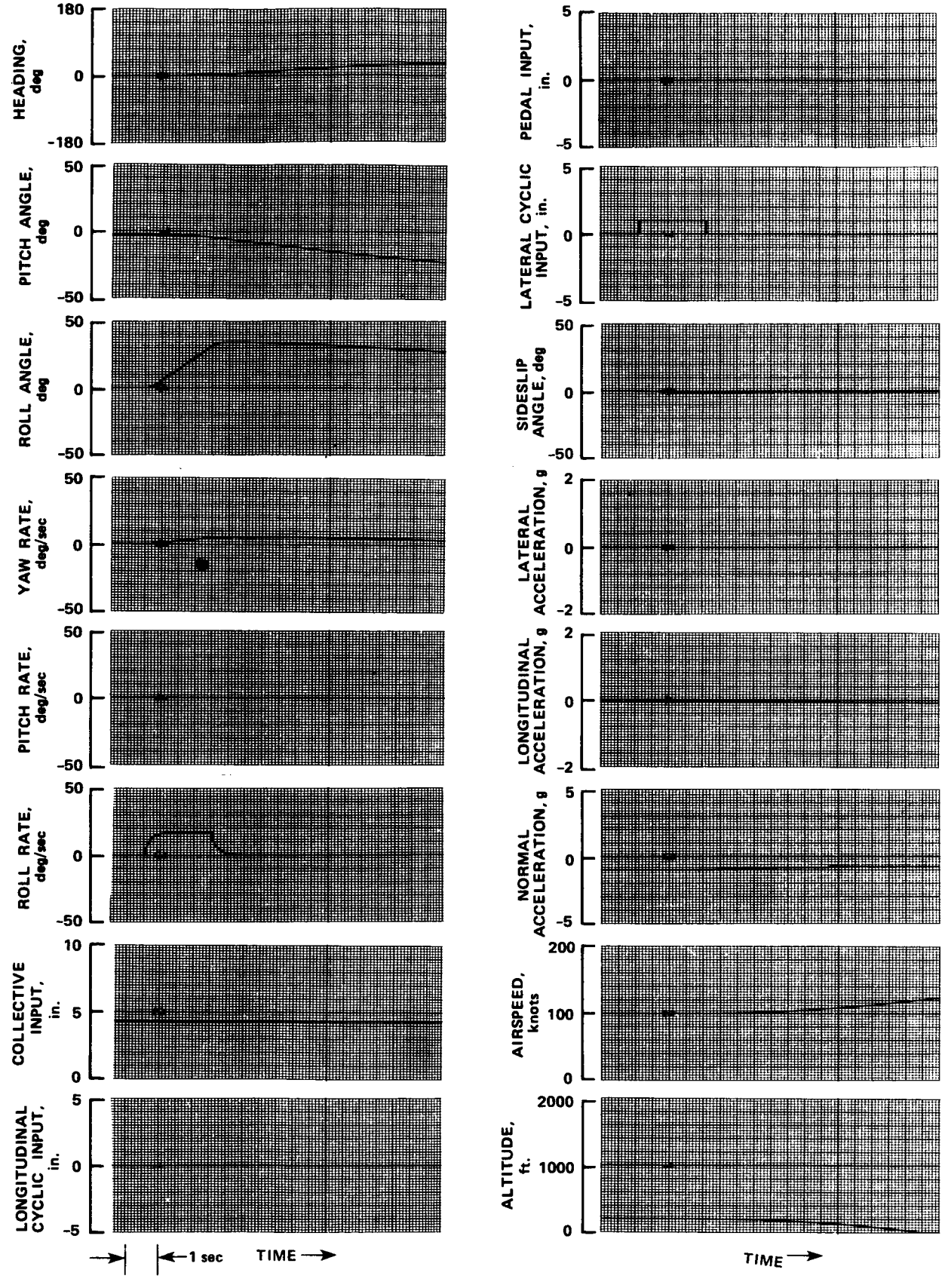

Figure 22.- Strip chart recording of step input responses. Step lateral cyclic, configuration 211, 100 knots.

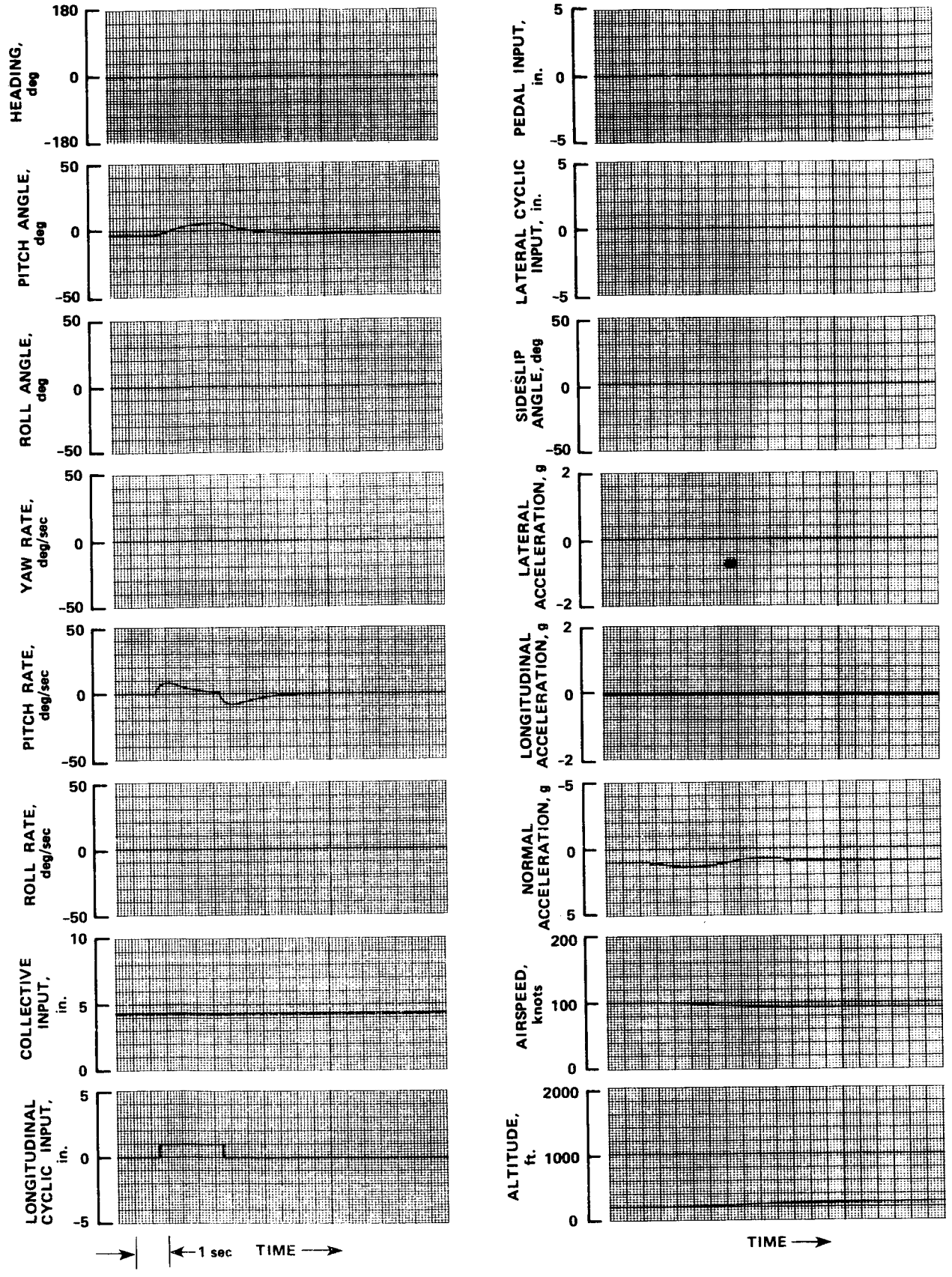

Figure 23.- Strip chart recording of step input responses. Step longitudinal cyclic, configuration 221, 100 knots.

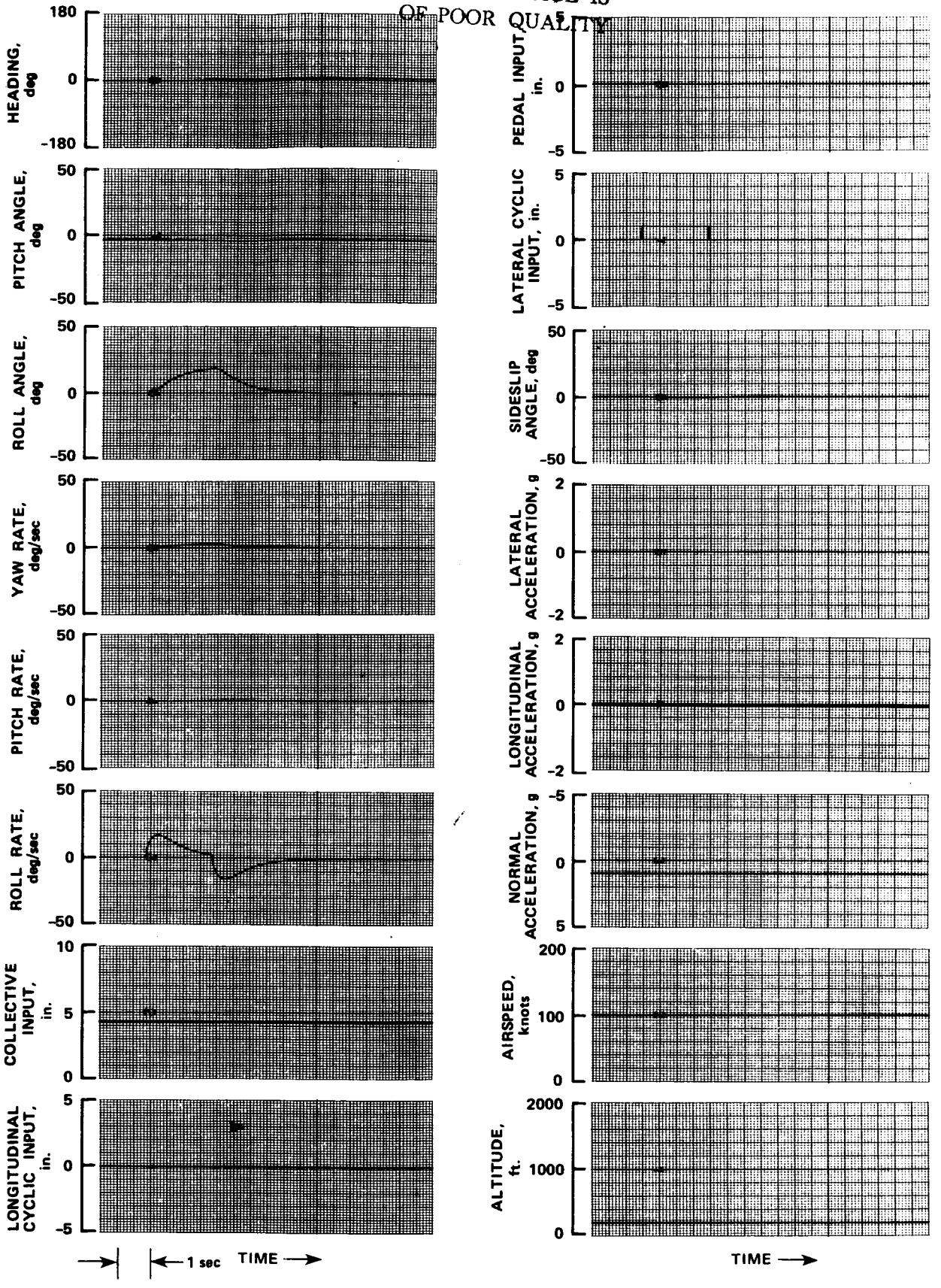

Figure 24.- Strip chart recording of step input responses. Step lateral cyclic, configuration 221, 100 knots.

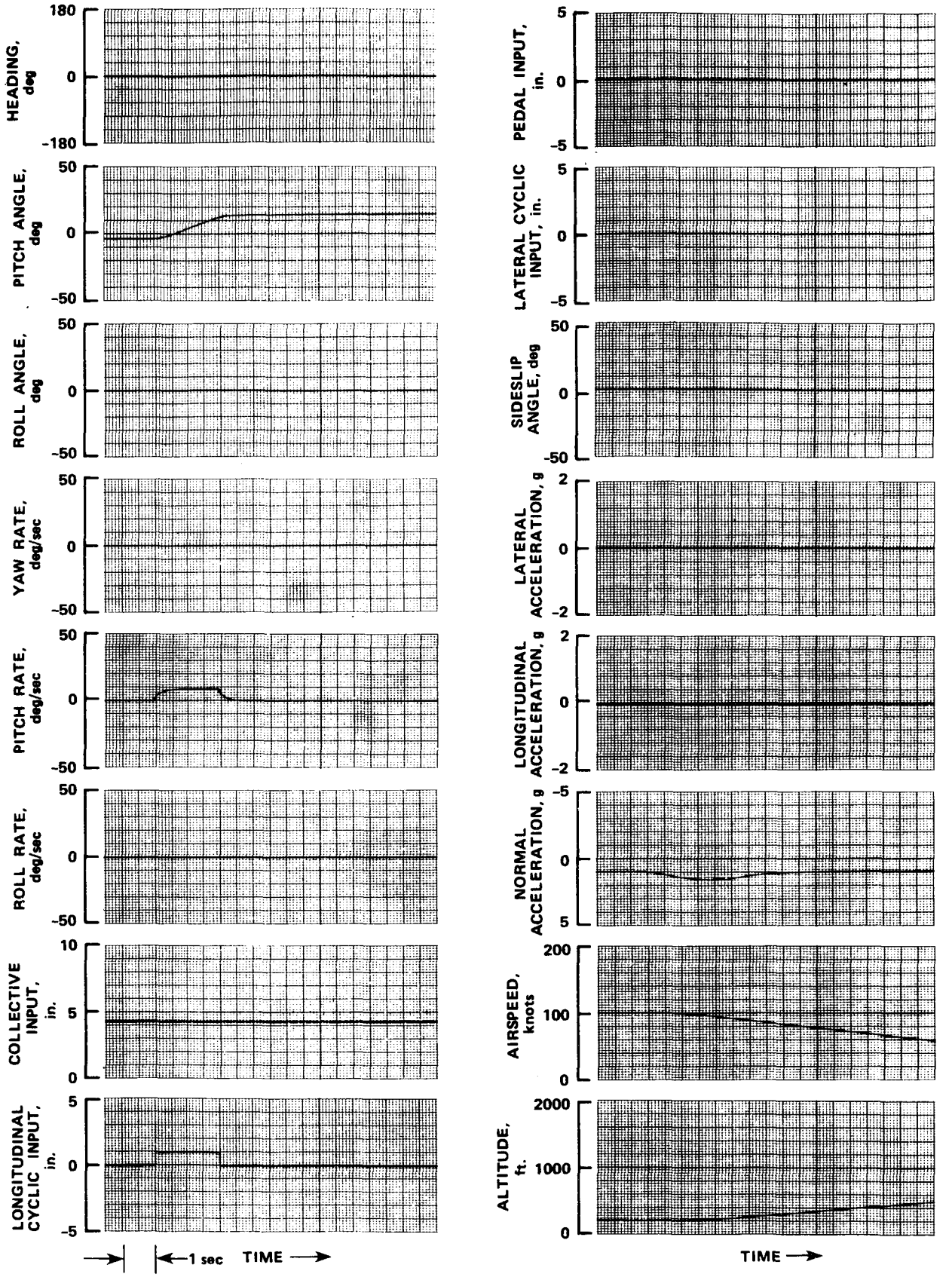

Figure 25.- Strip chart recording of step input responses. Step longitudinal cyclic, configuration 231, 100 knots.

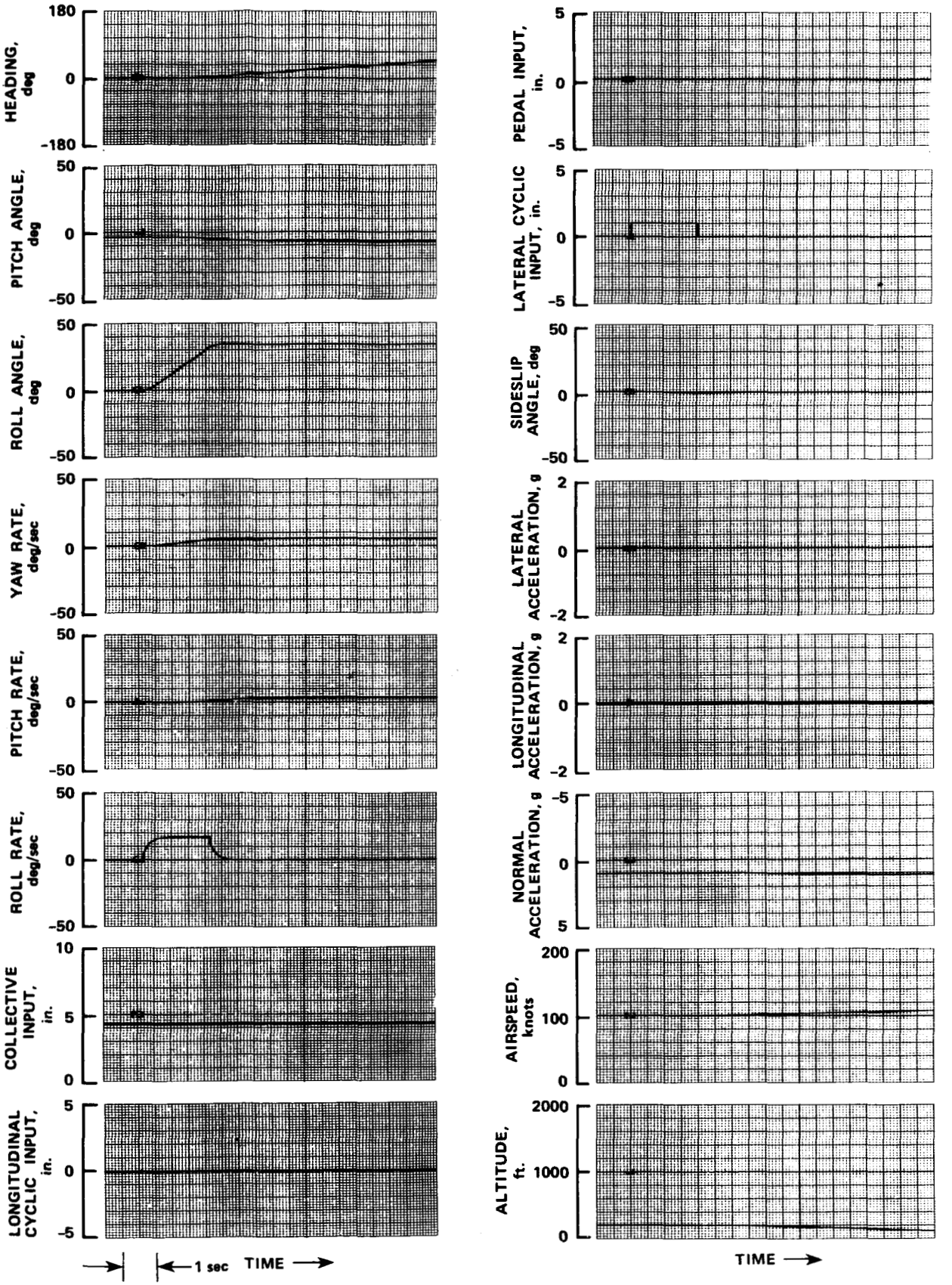

Figure 26.- Strip chart recording of step input responses. Step lateral cyclic, configuration 231, 100 knots.

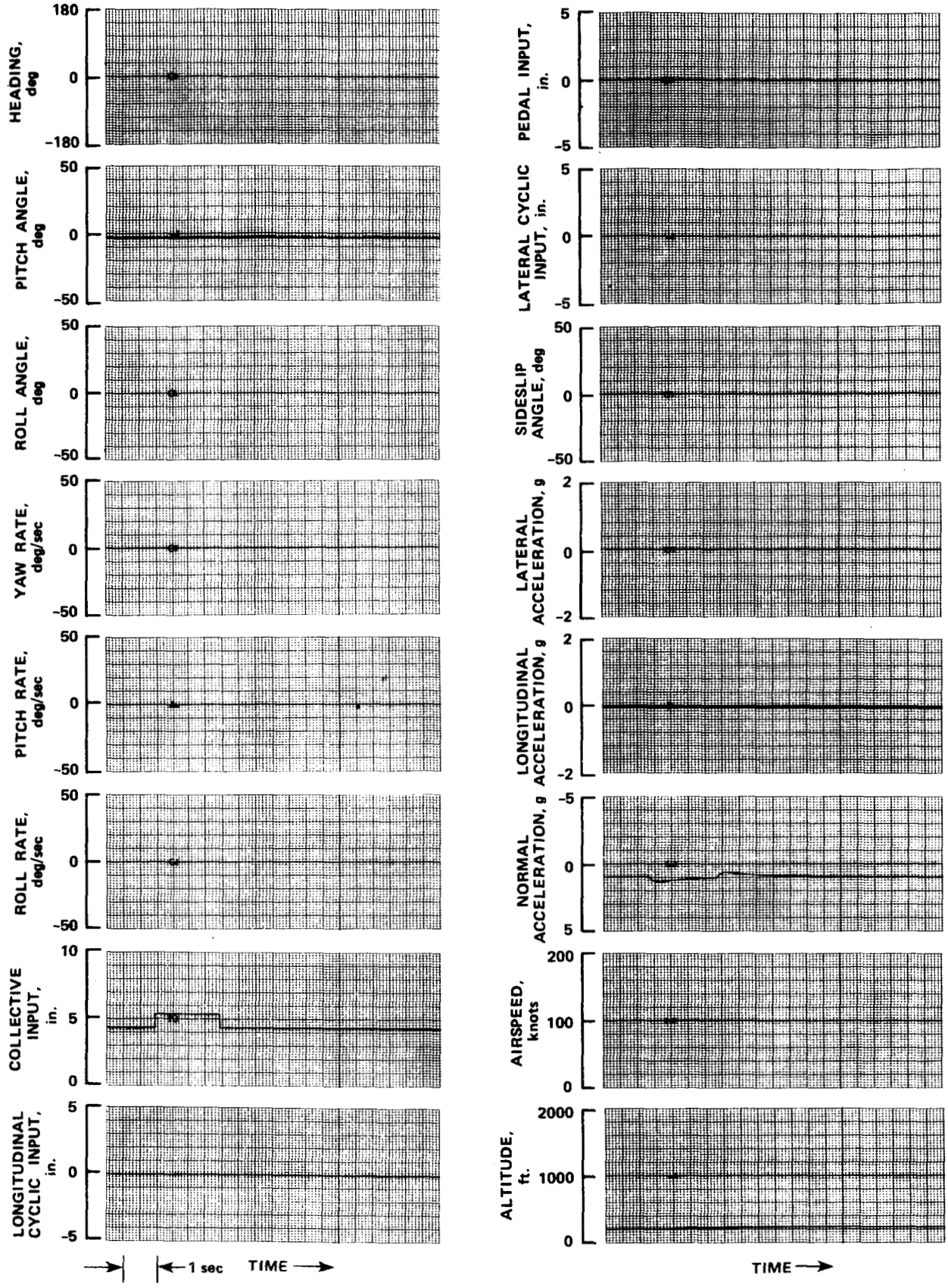

Figure 27.- Strip chart recording of step input responses. Step collective input, configuration 231, 100 knots.

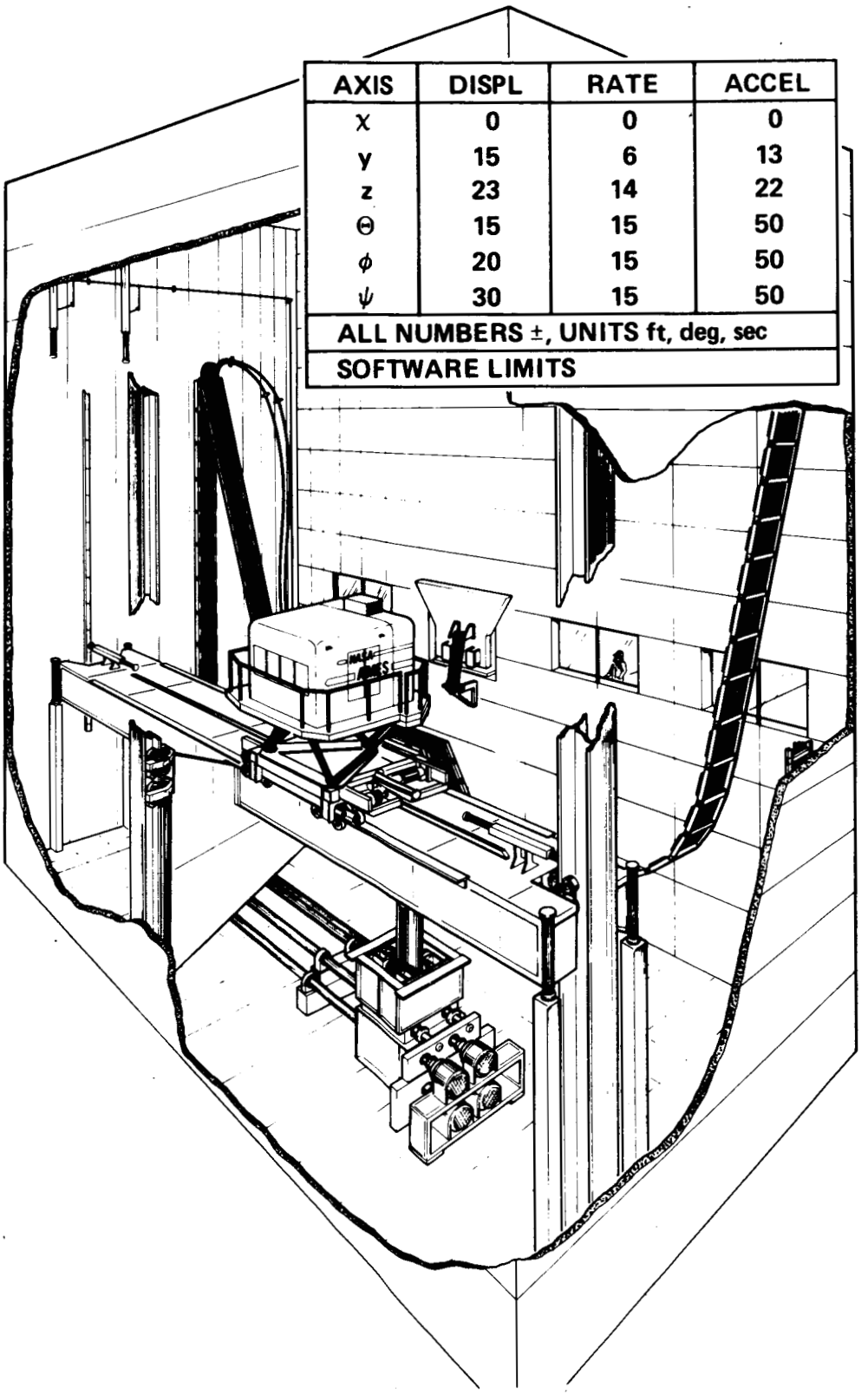

Figure 28.- NASA Ames Vertical Motion Simulator.

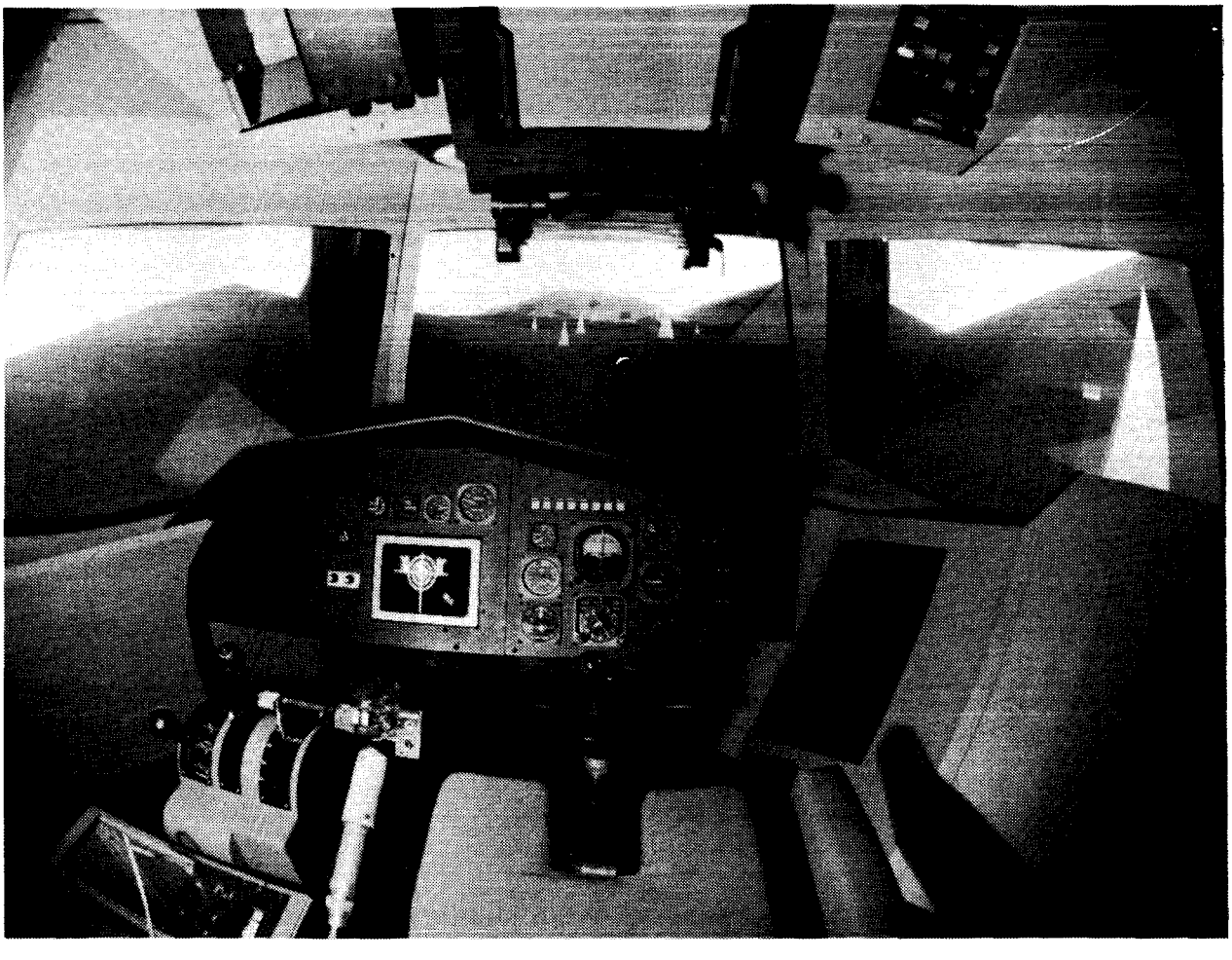

Figure 29.- Blue aircraft cockpit and CGI.

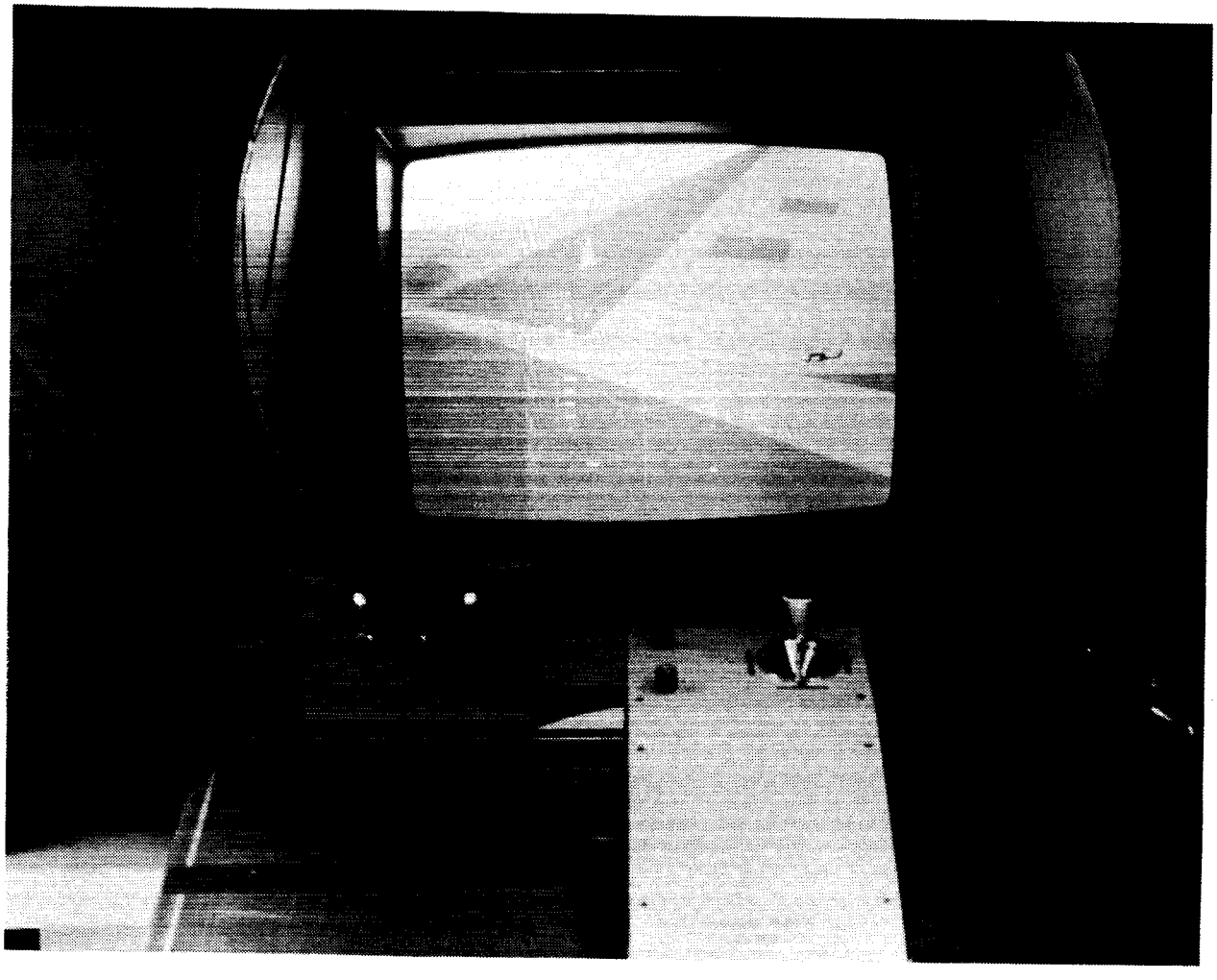

Figure 30.- Target station.

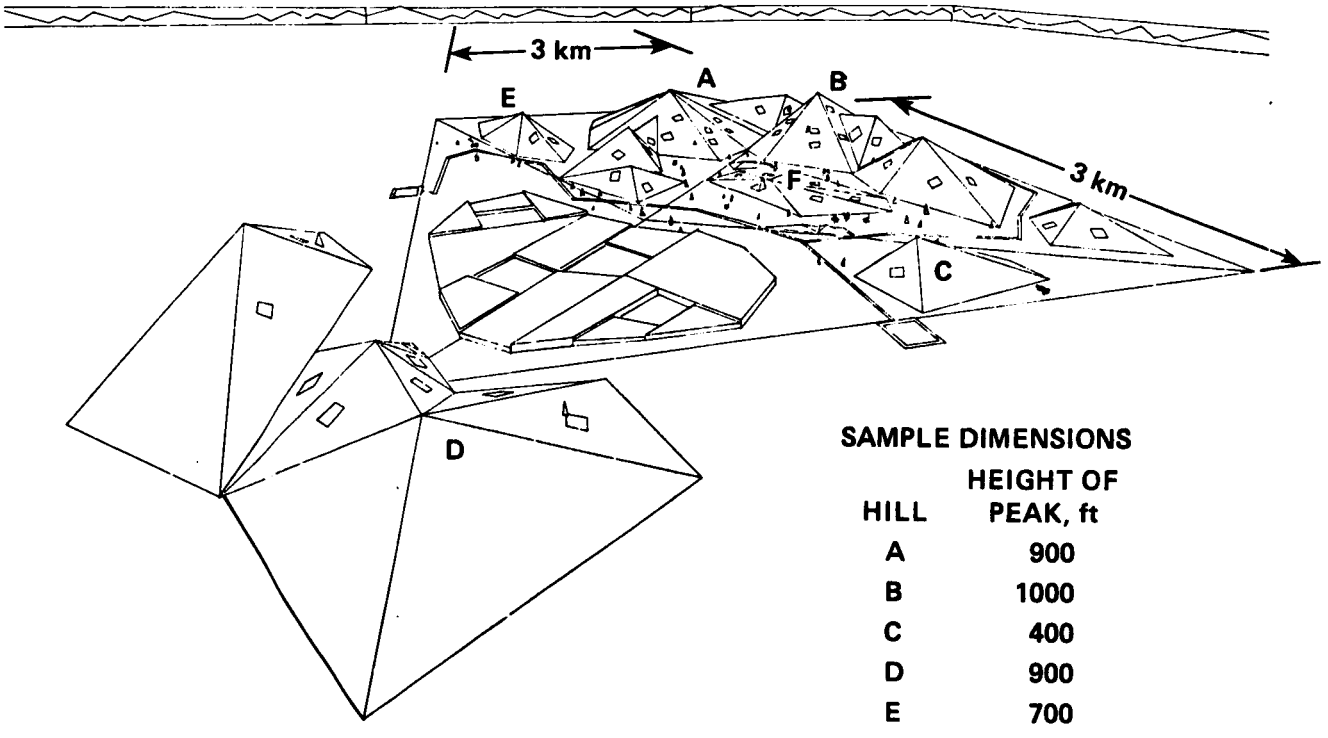

SAMPLE DIMENSIONS

HILL	HEIGHT OF PEAK, ft
A	900
B	1000
C	400
D	900
E	700
F	150

Figure 31.- HAC database.

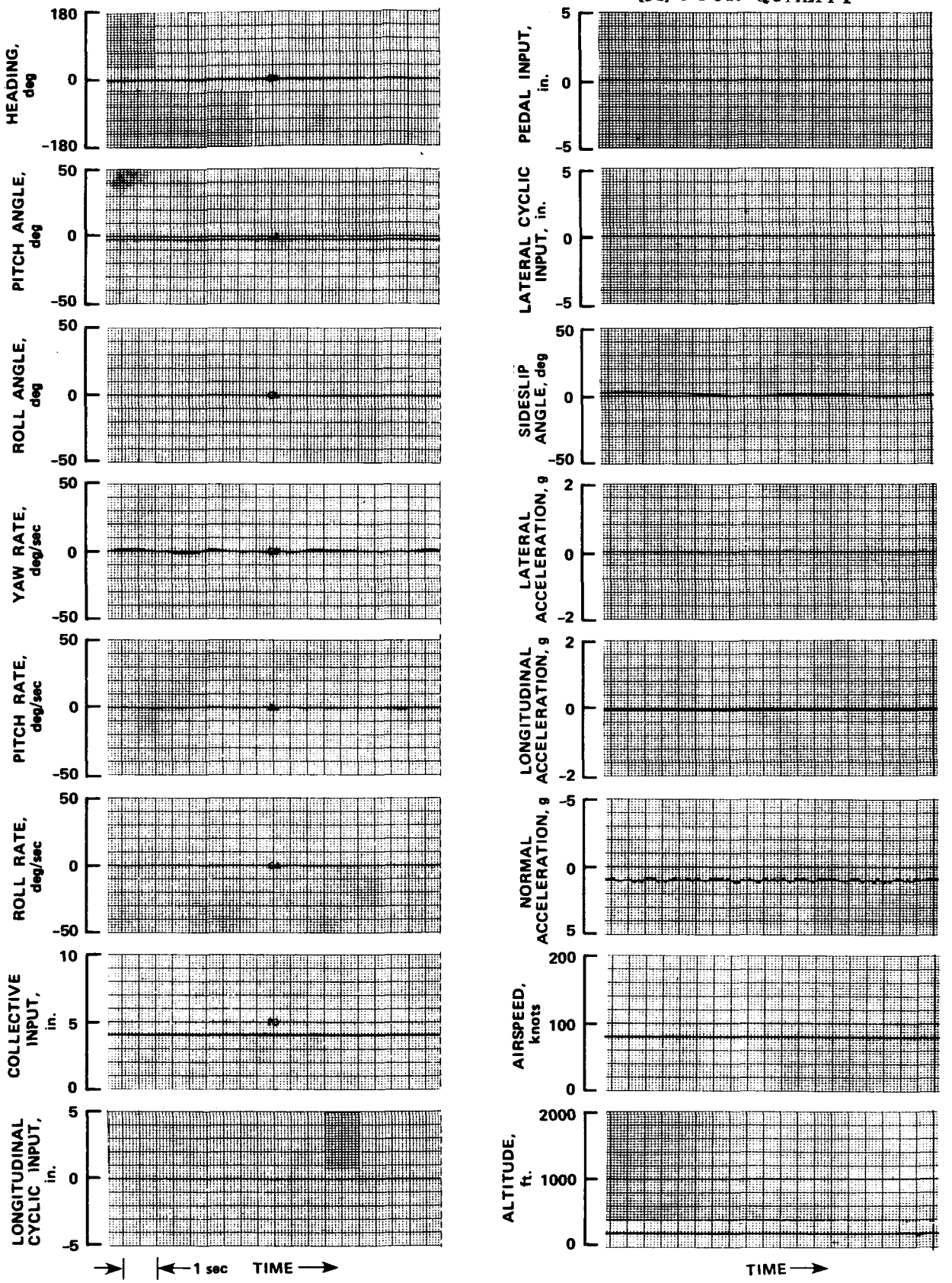

Figure 32.- Turbulence level and its effects.

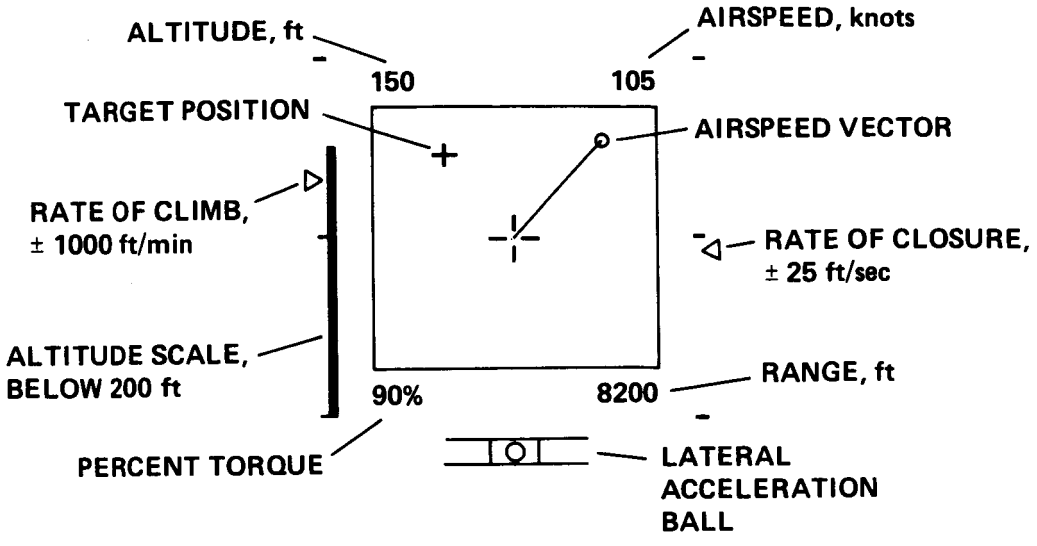

Figure 33.- Head-up display.

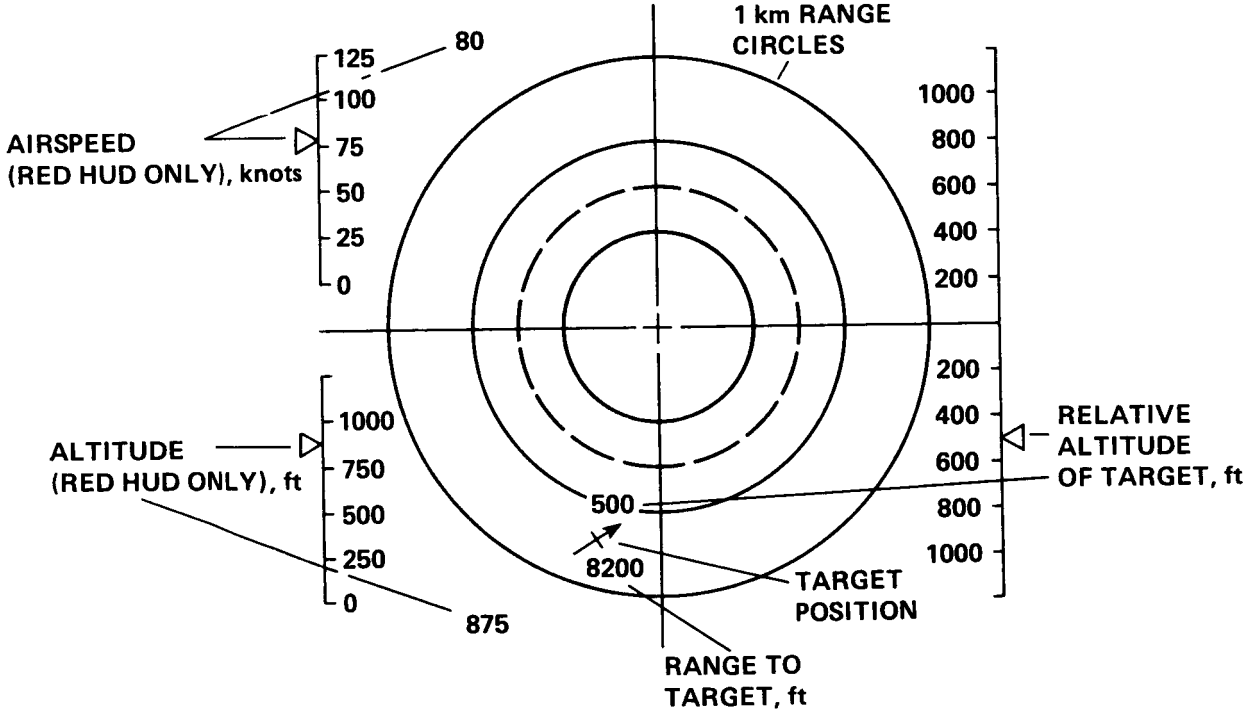

Figure 34.- Blue panel-mounted and red head-up displays.

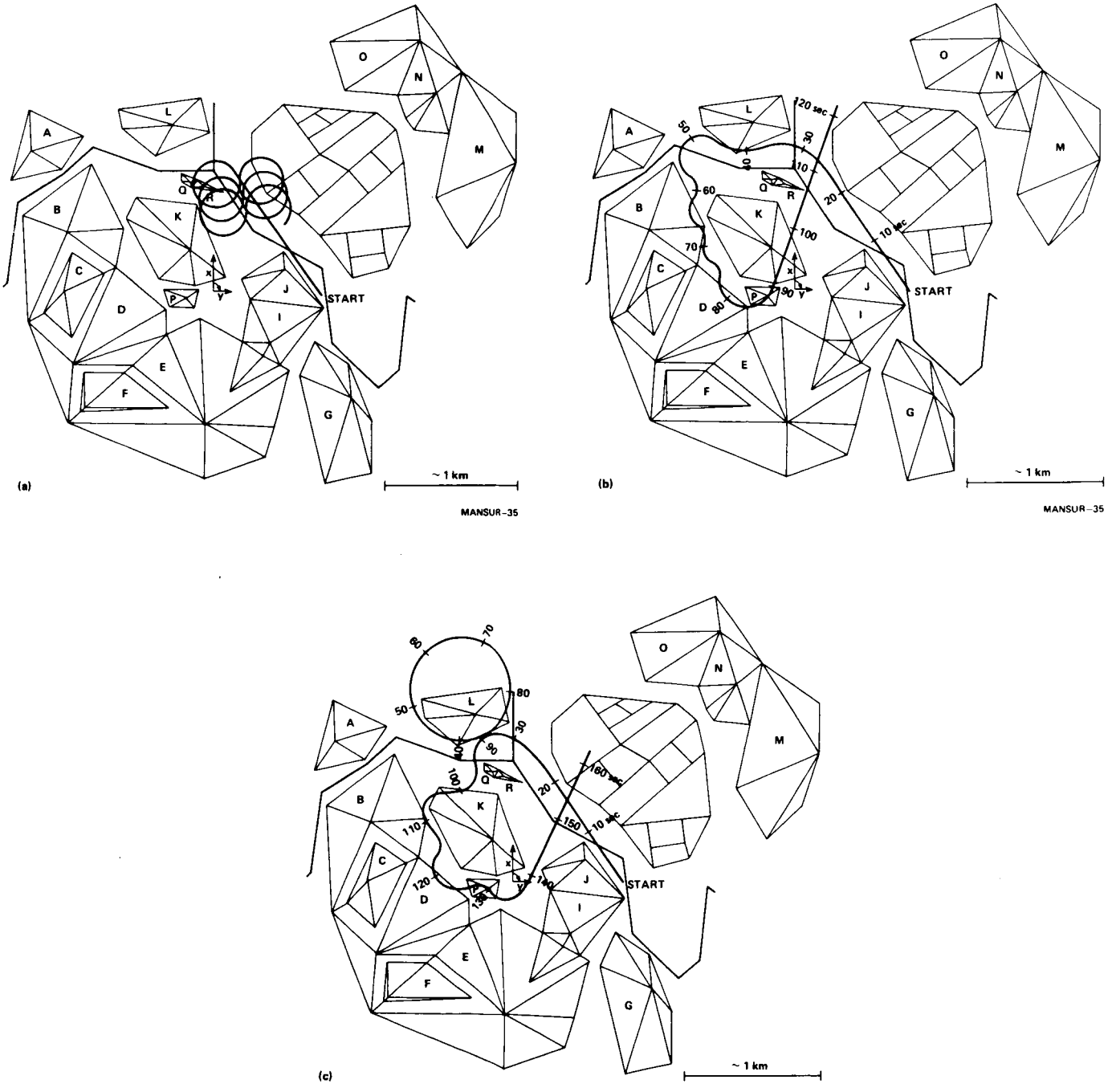

Figure 35.- Automatic target flightpaths. (a) Target path 1. (b) Target path 2. (c) Target path 3.

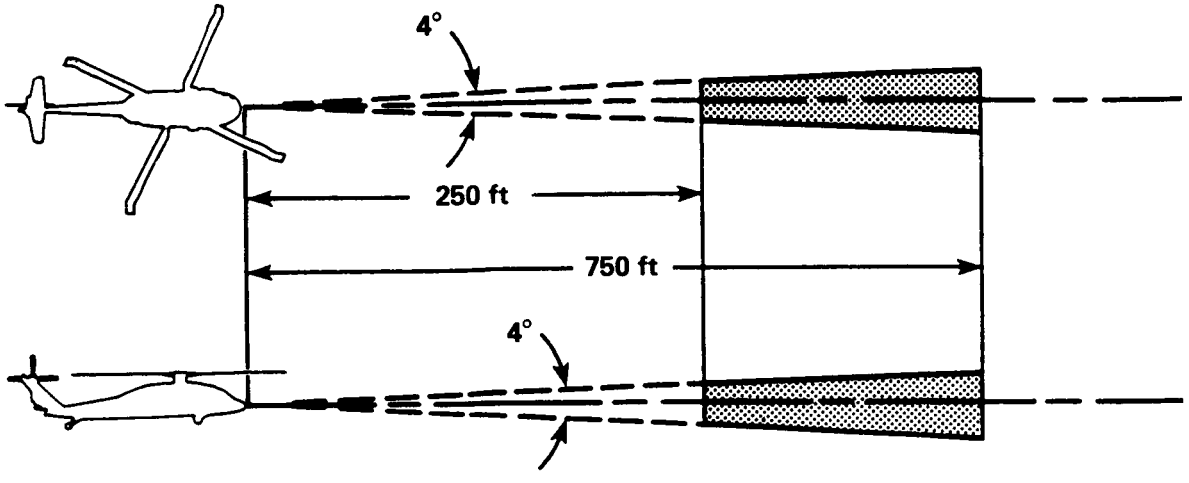

Figure 36.- Simulated weapon envelope.

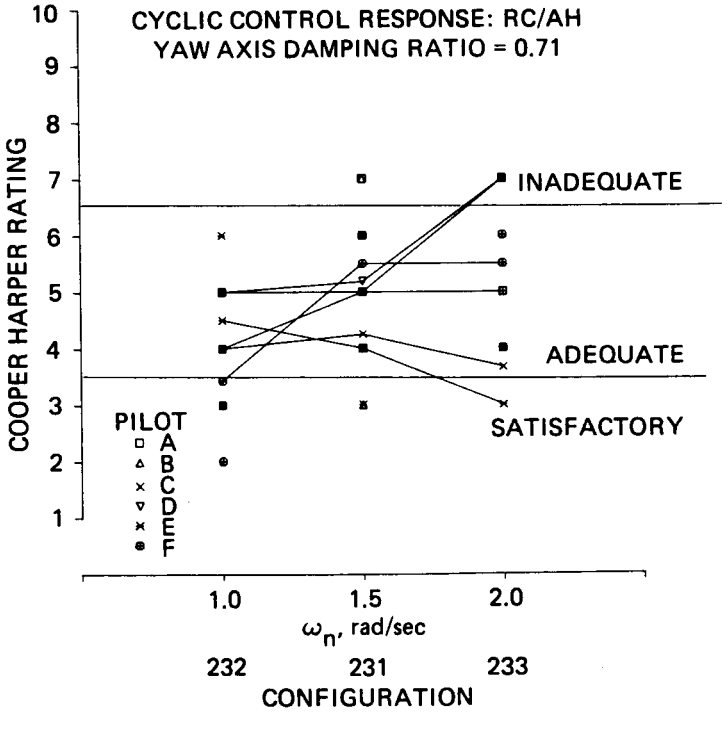

Figure 37.- Effect of directional axis natural frequency on pilot rating.

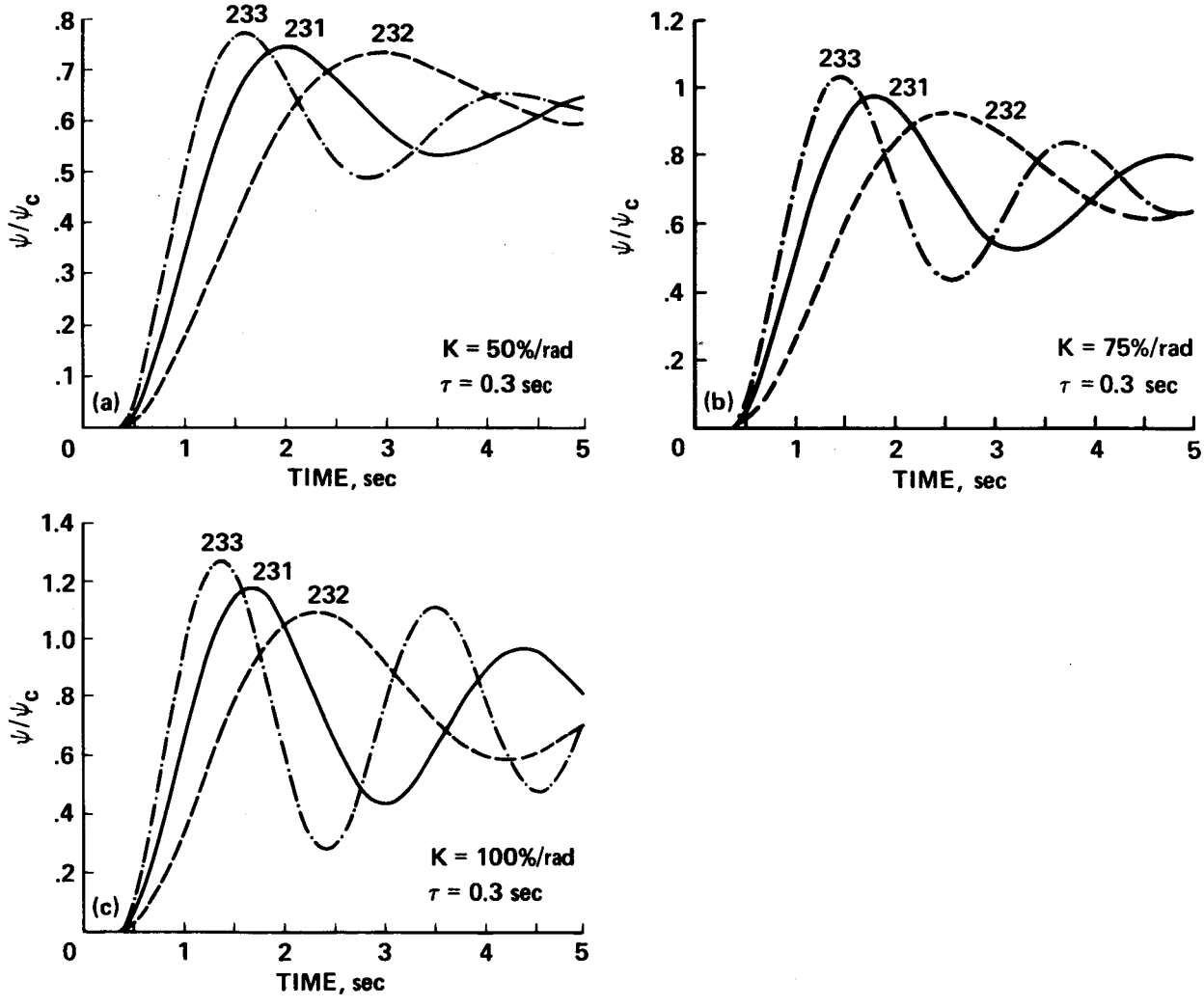

Figure 38.- Closed-loop analysis of the effects of changes in the directional axis natural frequency. (a) $K = 50$, $\tau = 0.3$ *sec*. (b) $K = 75$, $\tau = 0.3$ *sec*. (c) $K = 100$, $\tau = 0.3$ *sec*.

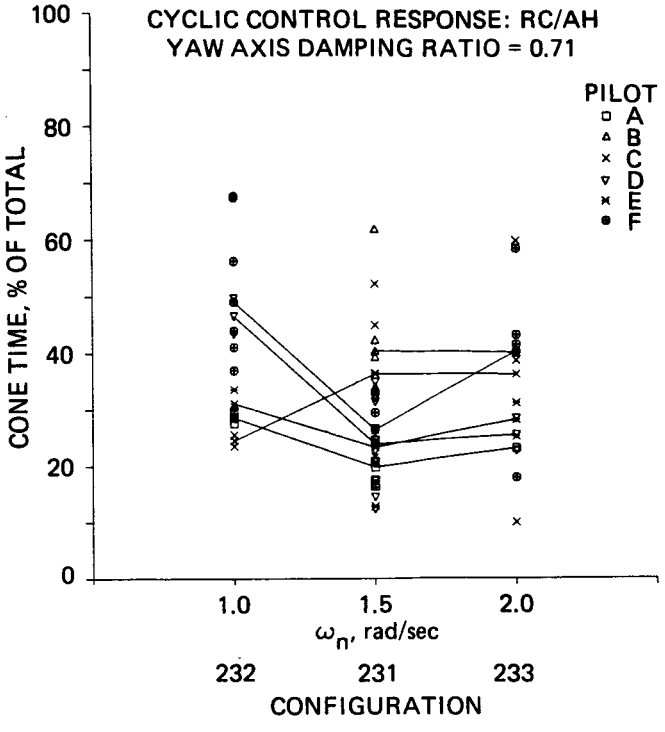

Figure 39.- Effect of directional axis natural frequency on tracking success.

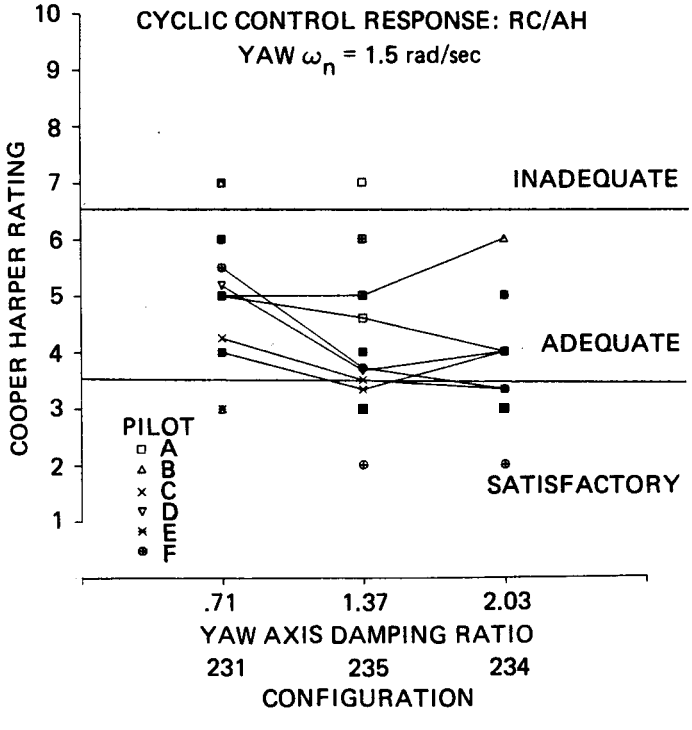

Figure 40.- Effect of yaw damping ratio on pilot rating, $\omega_n = 1.5\ rad/sec$.

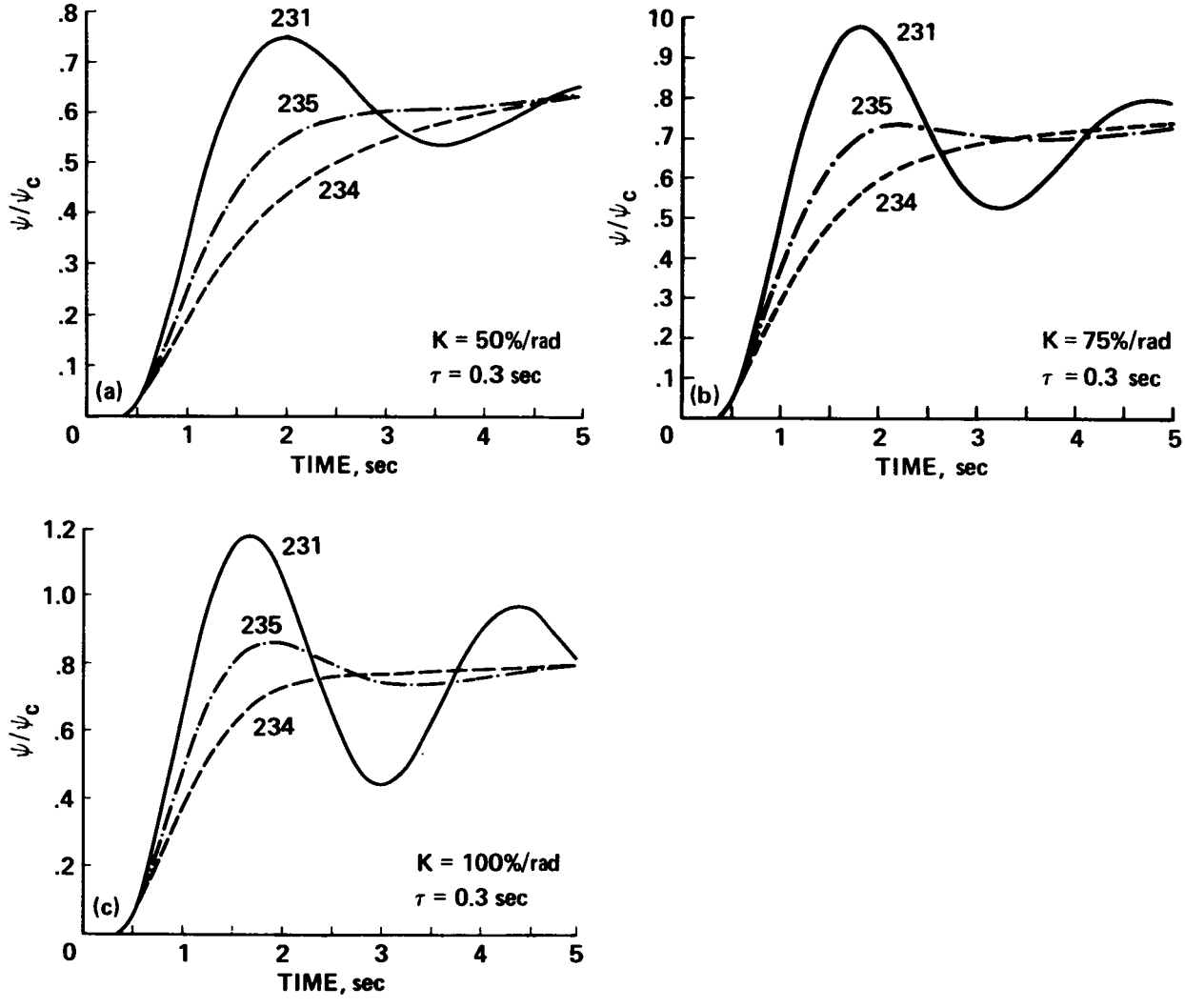

Figure 41.- Closed-loop analysis of the effects of changes in the directional axis damping ratio. (a) $K = 50$, $\tau = 0.3$ *sec*. (b) $K = 75$, $\tau = 0.3$ *sec*. (c) $K = 100$, $\tau = 0.3$ *sec*.

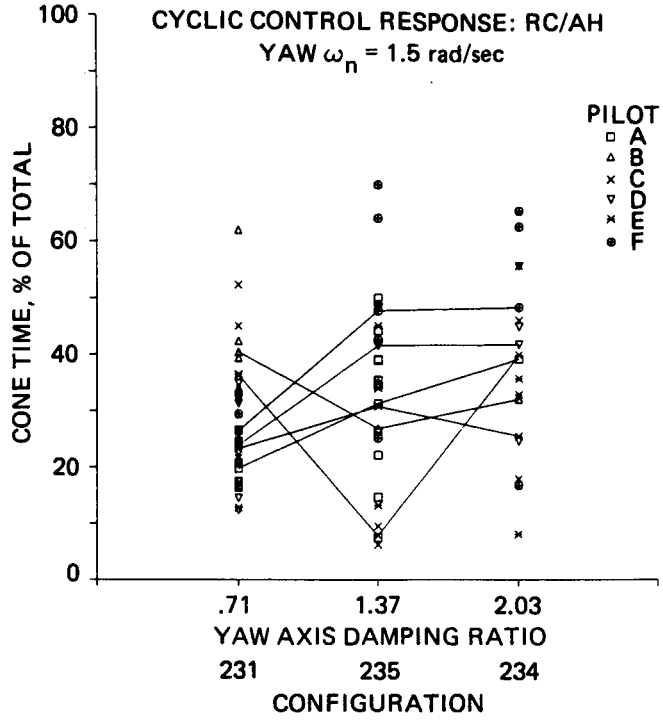

Figure 42.- Effect of directional axis damping ratio on tracking success, $\omega_n = 1.5\ rad/sec$.

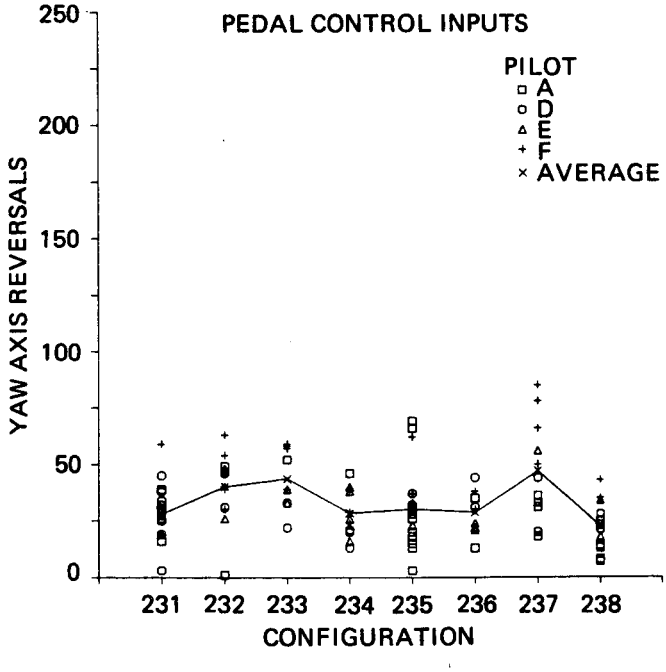

Figure 43.- Pedal control inputs, control reversals.

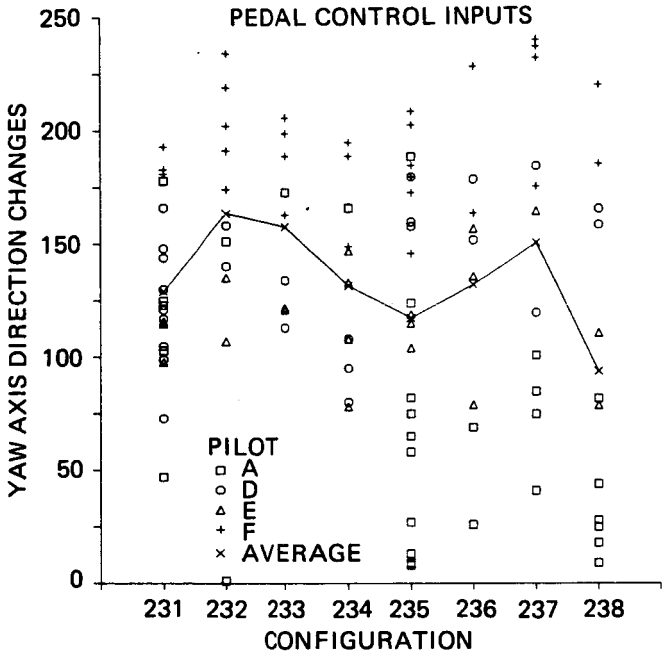

Figure 44.- Pedal control inputs, direction changes.

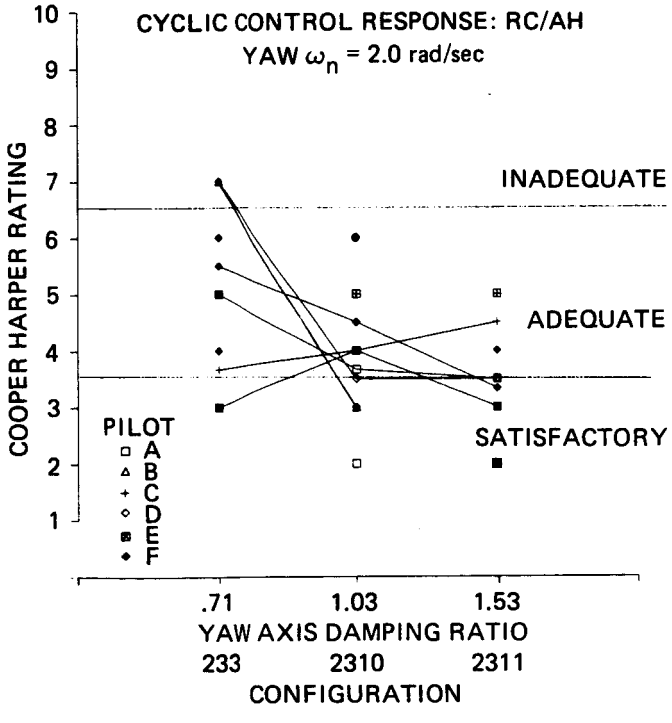

Figure 45.- Effect of directional axis damping ratio on pilot rating, $\omega_n = 2.0\ rad/sec$.

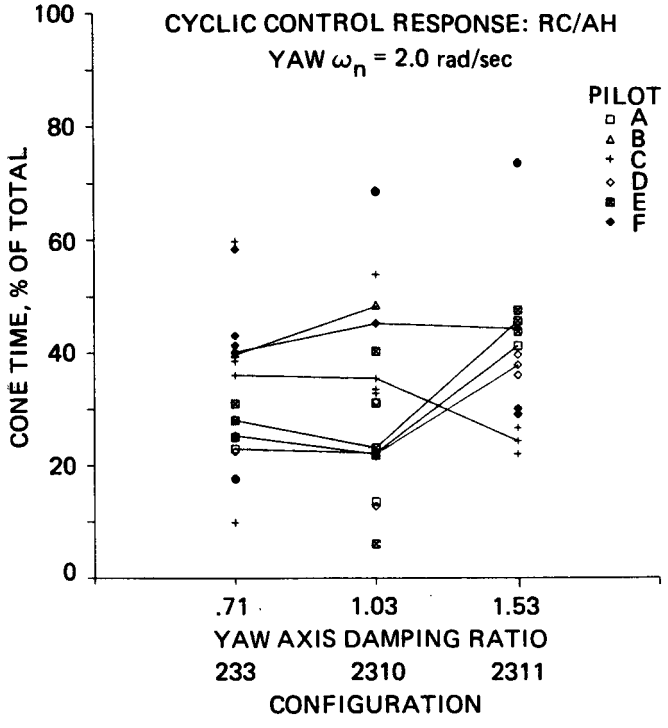

Figure 46.- Effect of directional axis damping ratio on tracking success, $\omega_n = 2.0\ rad/sec$.

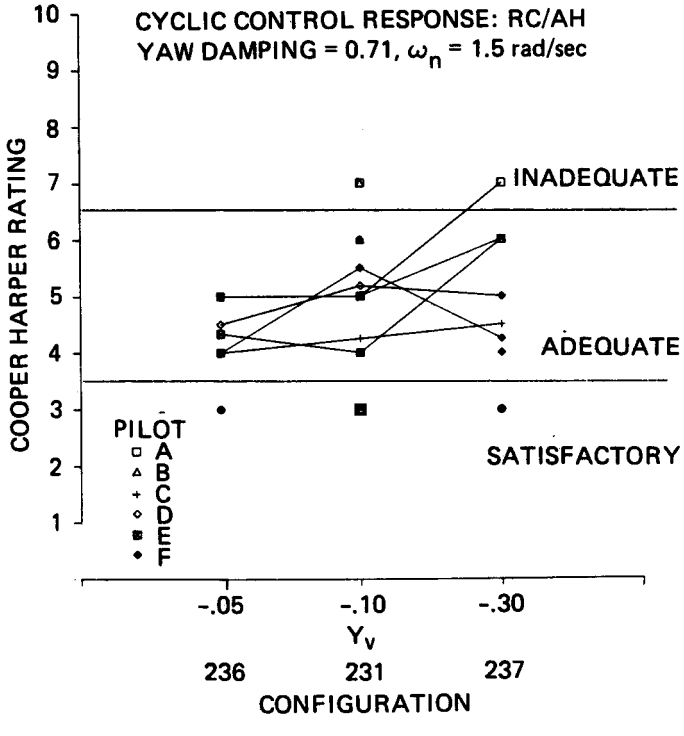

Figure 47.- Effect of sideforce caused by sideslip on pilot rating.

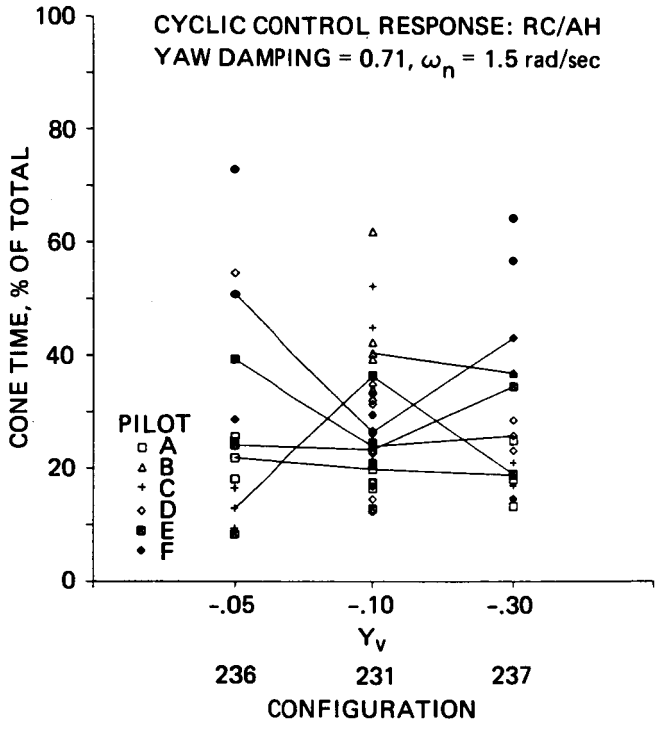

Figure 48.- Effect of sideforce caused by sideslip on tracking success.

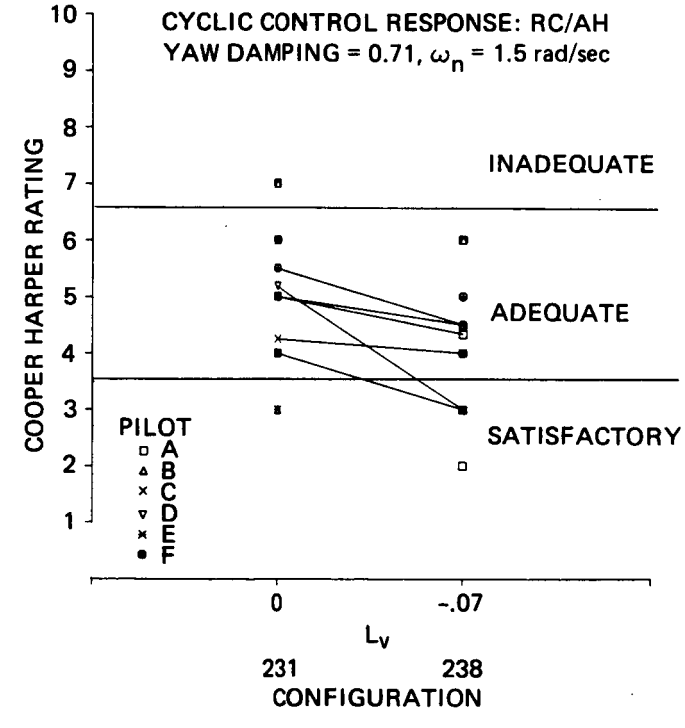

Figure 49.- Effect of dihedral coupling on pilot rating.

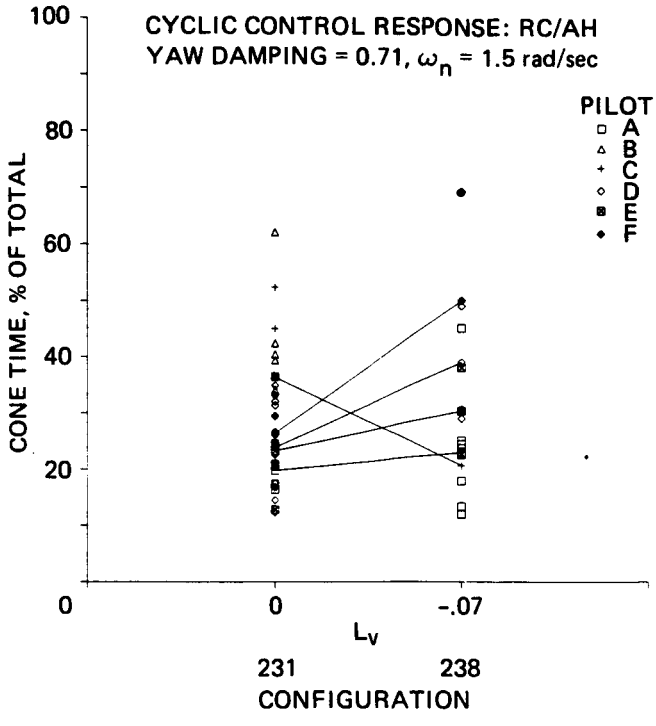

Figure 50.- Effect of dihedral coupling on tracking success.

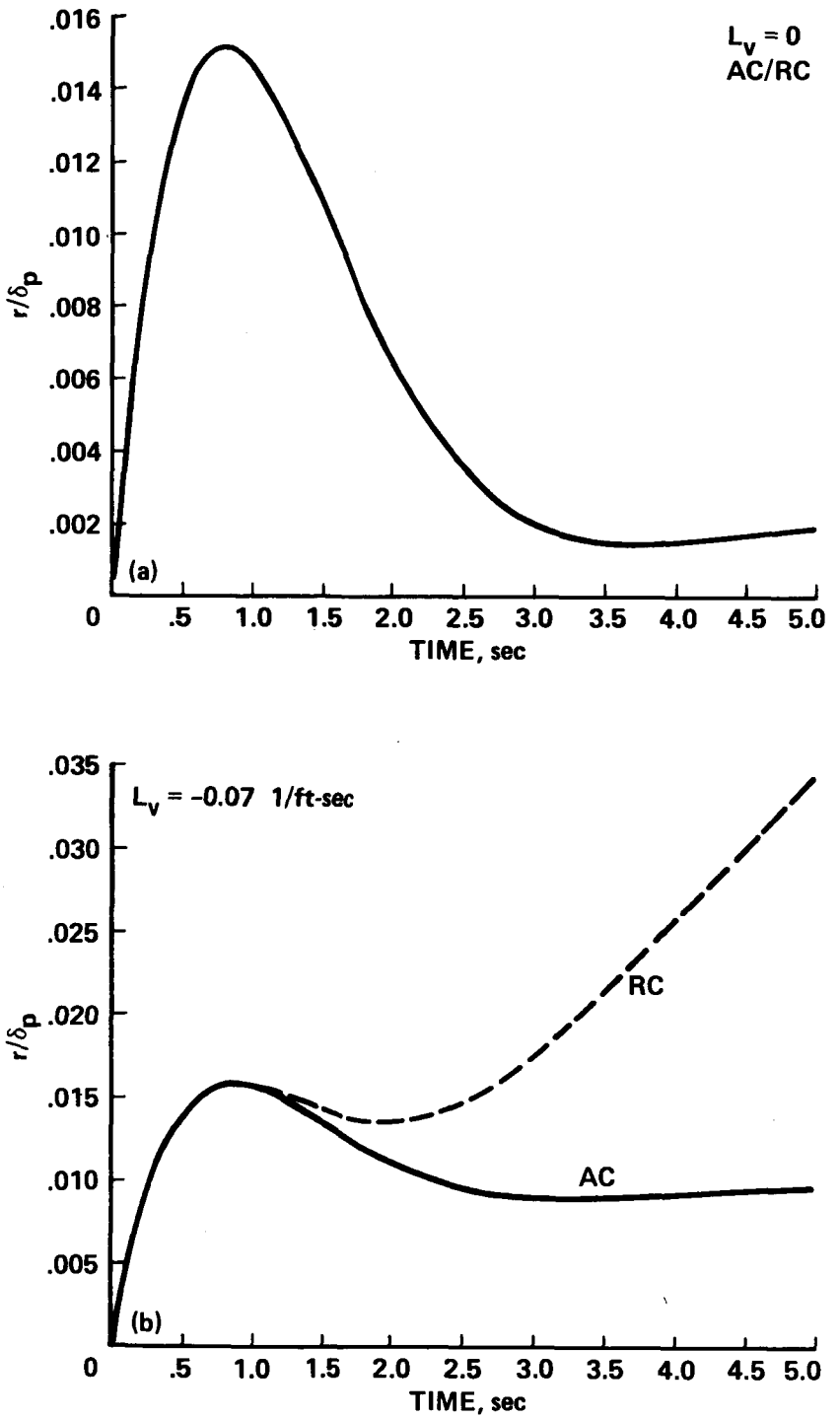

Figure 51.- Handling qualities effects of the addition of some effective dihedral. (a) Yaw rate response to step pedal input, no dihedral. (b) Yaw rate response to step pedal input, with dihedral.

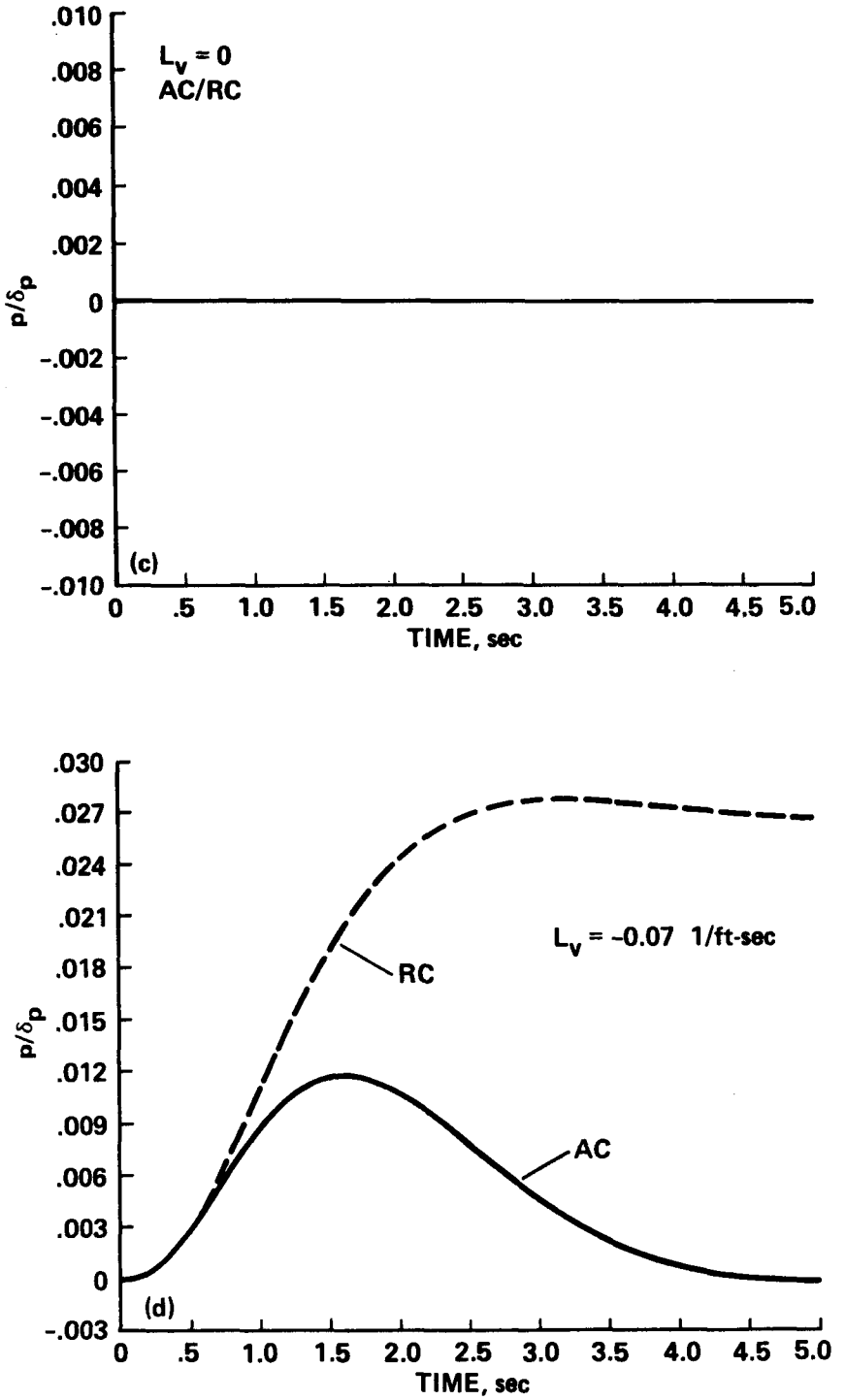

Figure 51.- Concluded. (c) Roll rate response to step pedal input, no dihedral. (d) Roll rate response to step pedal input, with dihedral.

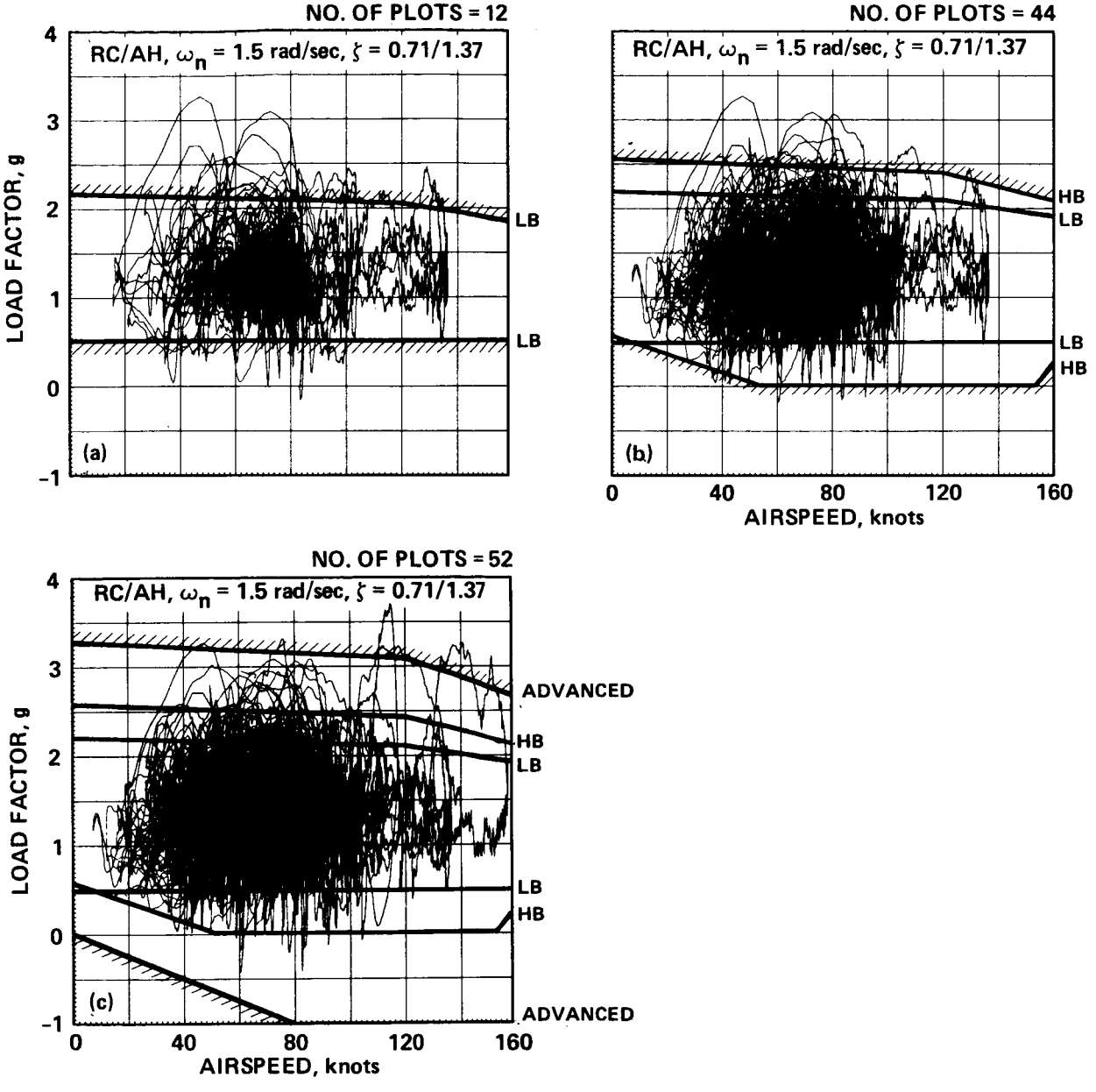

Figure 52.- Pilot usage of normal load factor envelope. (a) Low baseline. (b) High baseline. (c) Advanced.

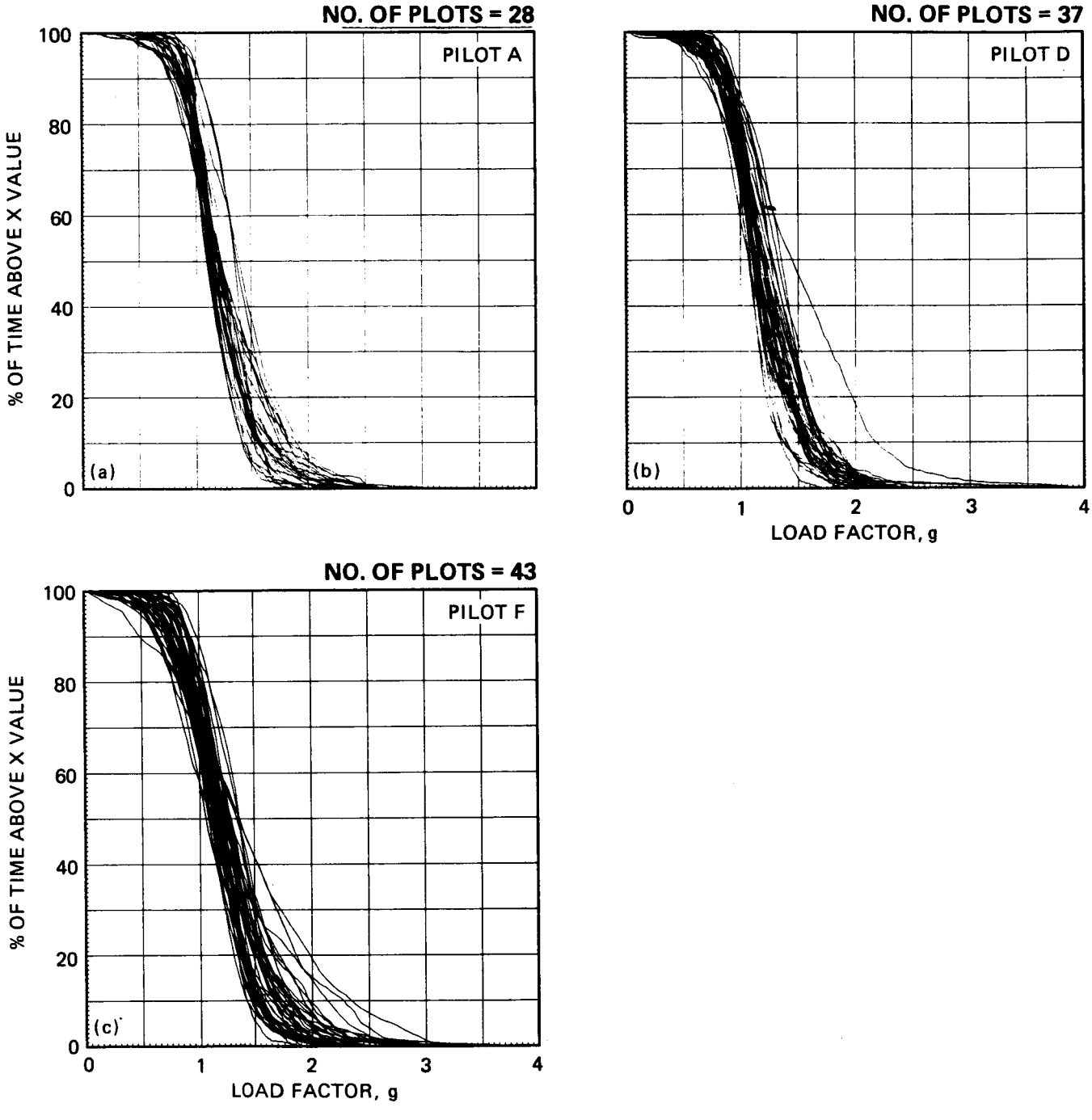

Figure 53.- Load factor time-percentage plot. (a) Pilot A. (b) Pilot D. (c) Pilot F.

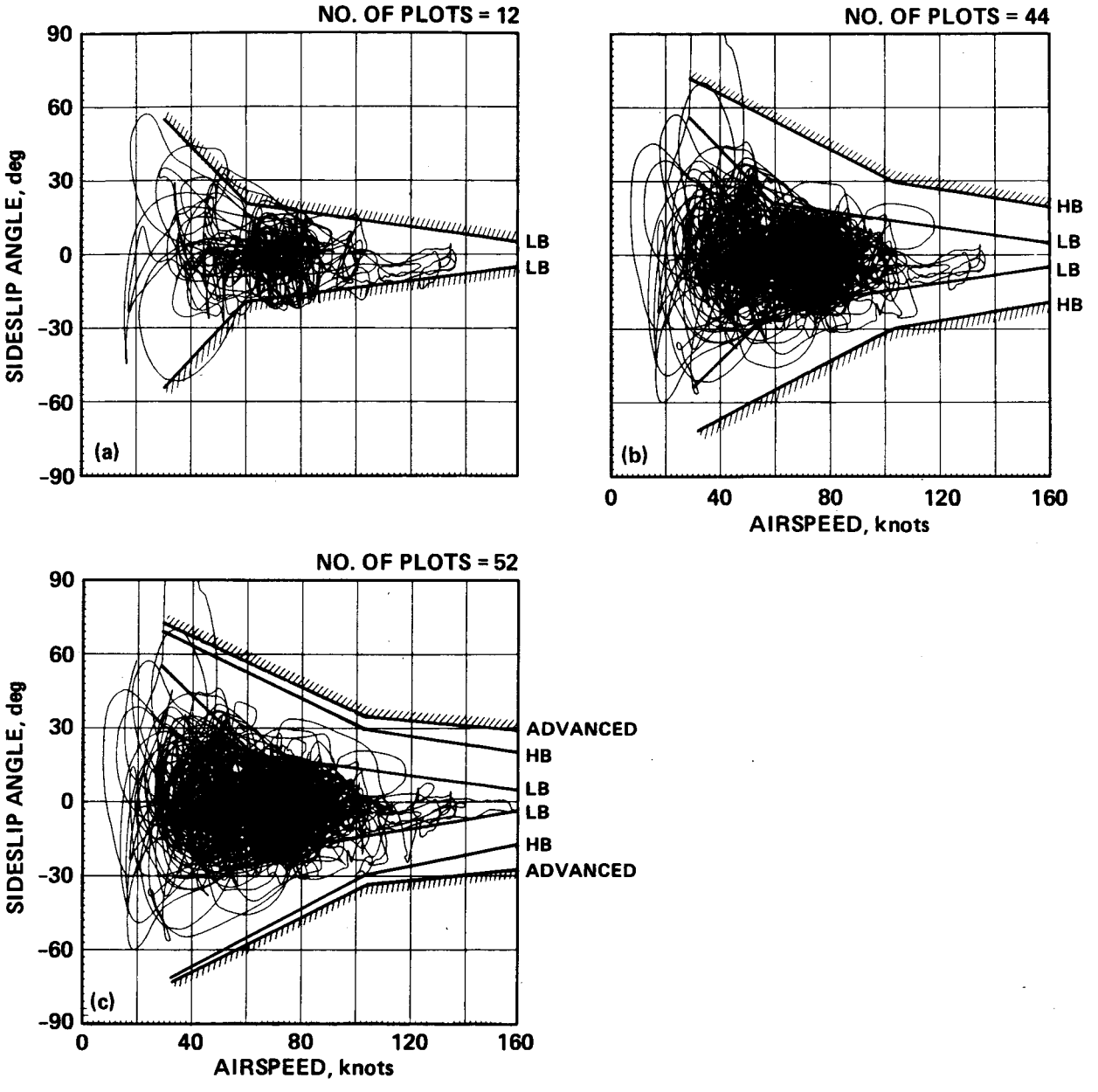

Figure 54.- Pilot usage of sideslip envelope. (a) Low baseline. (b) High baseline. (c) Advanced.

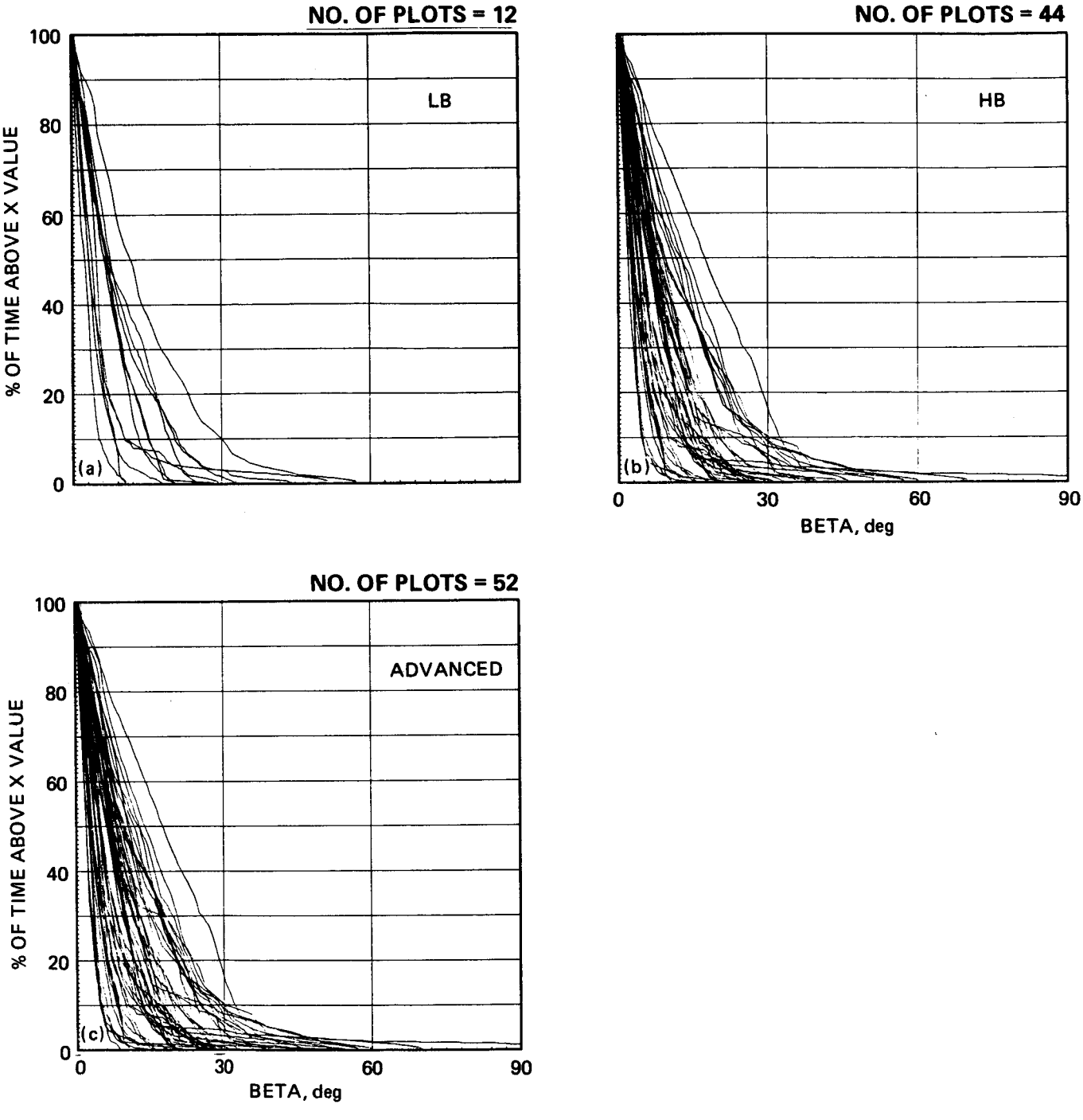

Figure 55.- Sideslip angle time-percentage plot. (a) Low baseline. (b) High baseline. (c) Advanced.

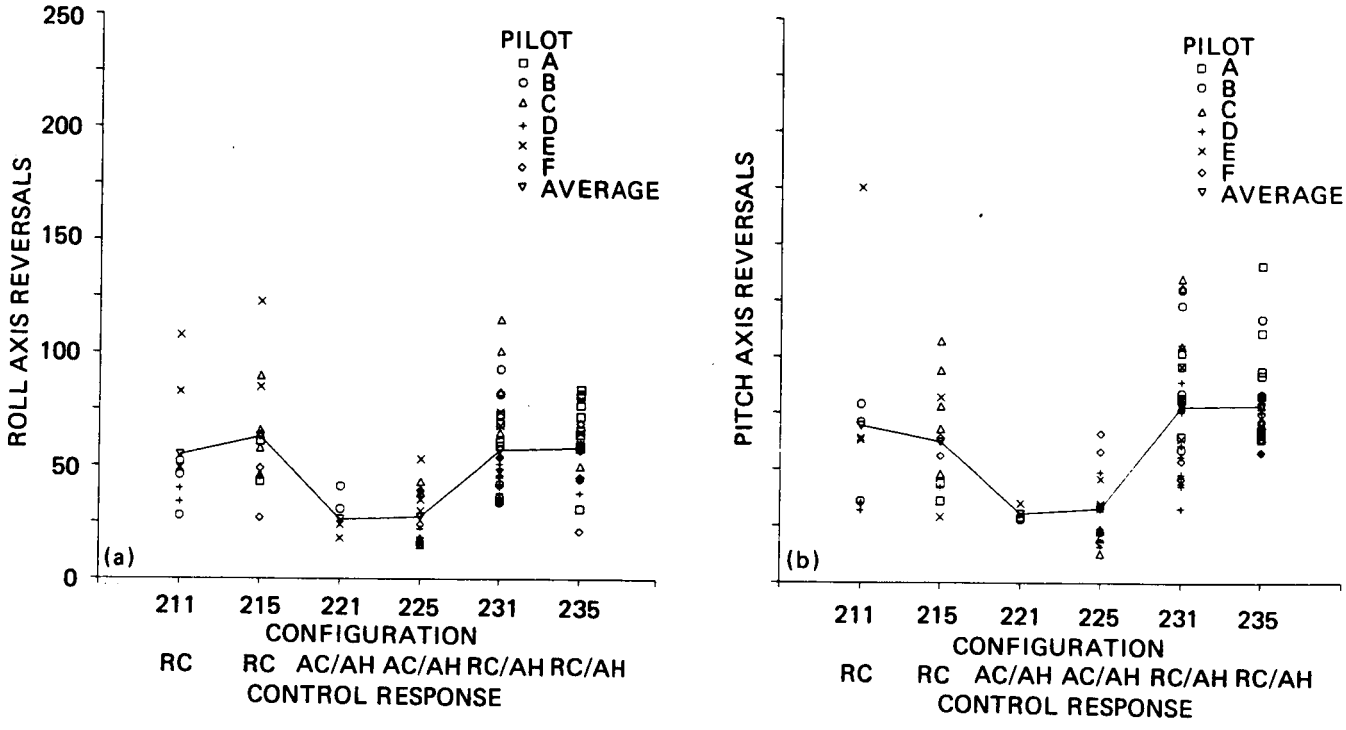

Figure 56.- Influence of control response type on: (a) roll axis control reversals; (b) pitch axis control reversals.

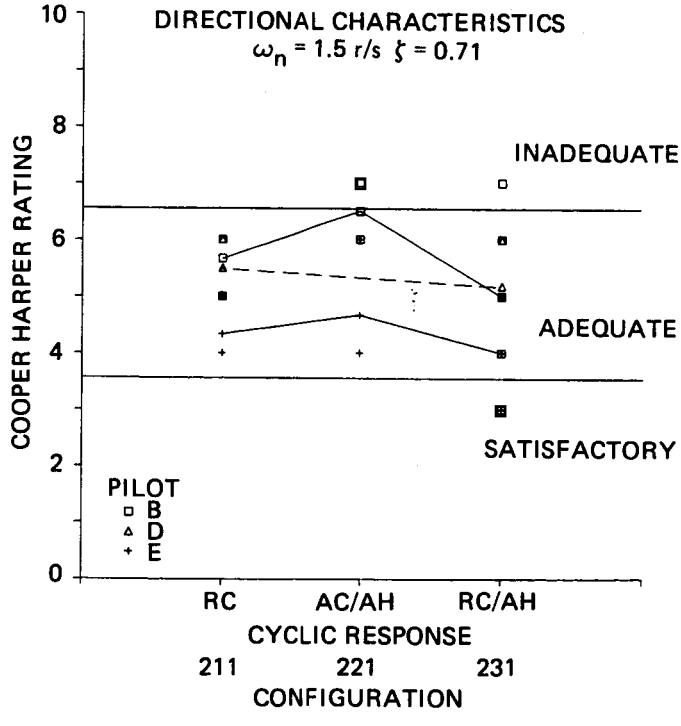

Figure 57.- Influence of pitch/roll control response type on pilot rating—low value of directional axis damping ratio.

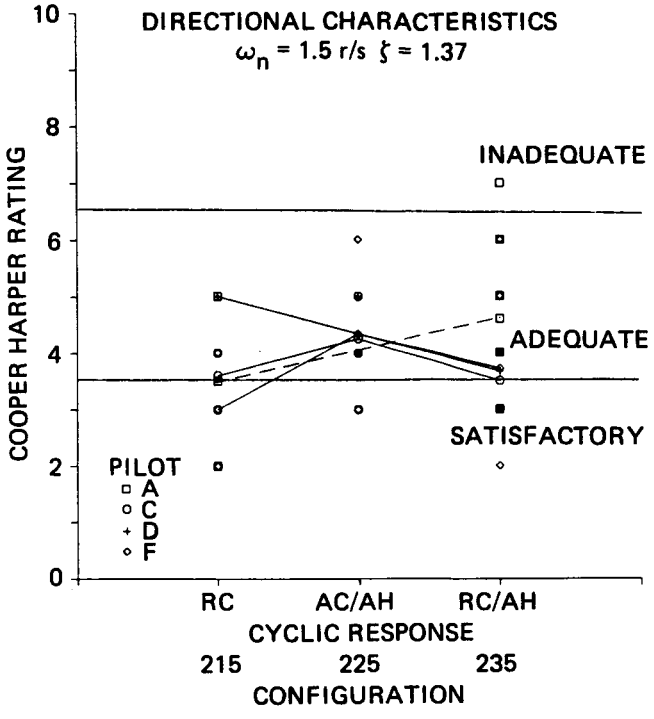

Figure 58.- Influence of pitch/roll control response type on pilot rating—high value of directional axis damping ratio.

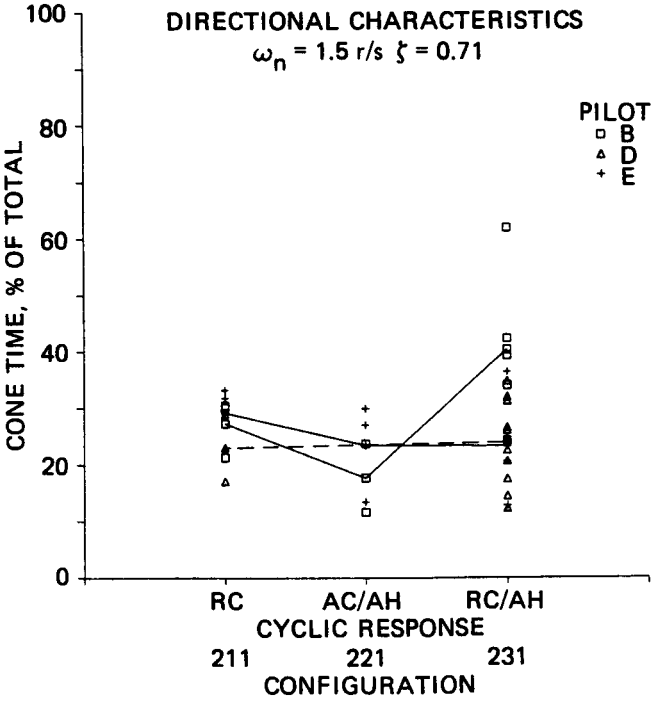

Figure 59.- Influence of pitch/roll control response type on tracking success—low value of directional axis damping ratio.

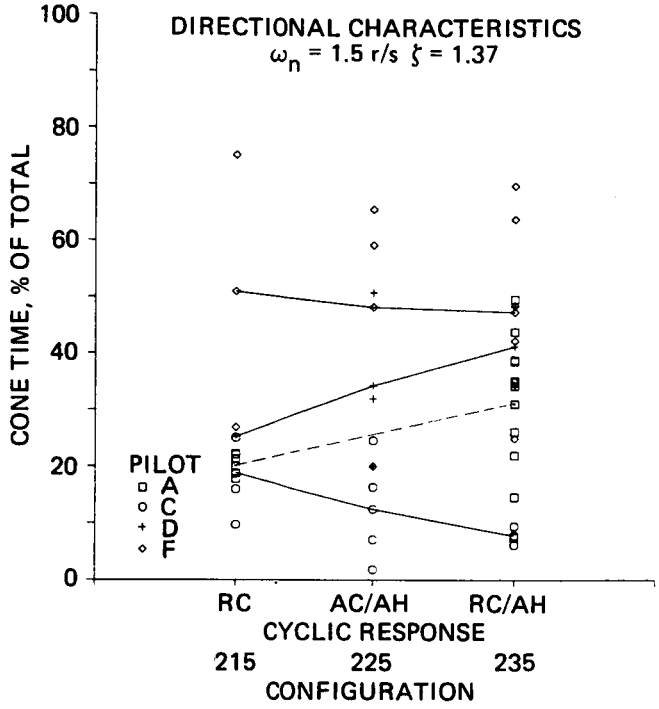

Figure 60.- Influence of pitch/roll control response type on tracking—high value of directional axis damping ratio.

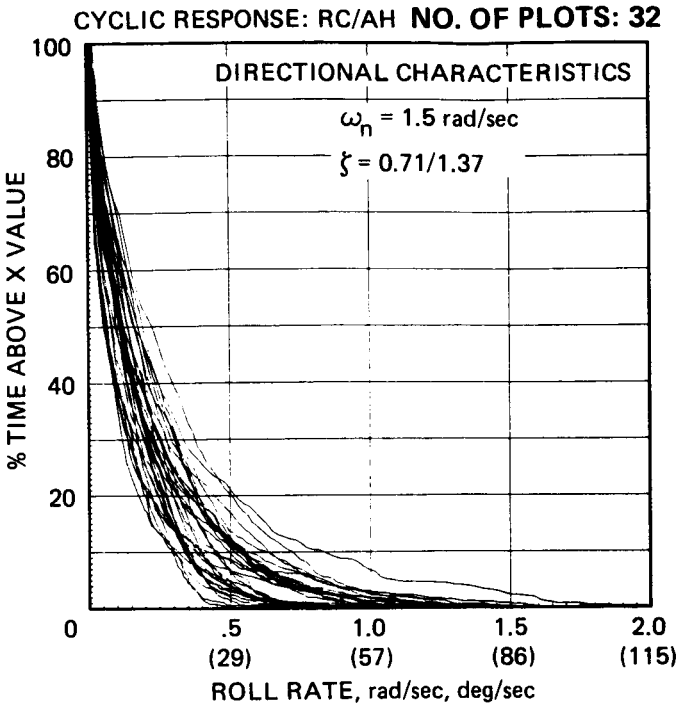

Figure 61.- Time-percentage plots of pilot usage of roll-rate—RC/AH response type in pitch and roll.

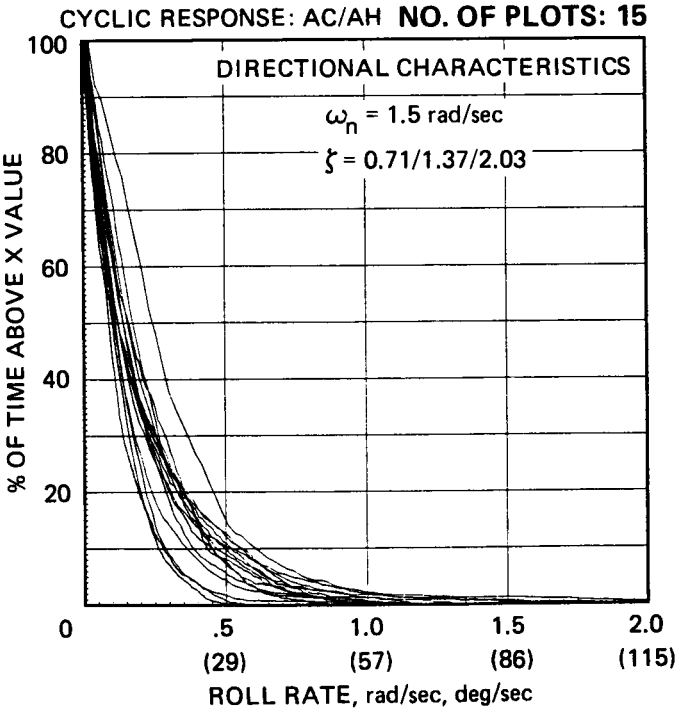

Figure 62.- Time-percentage plots of pilot usage of roll rate—AC/AH response type in pitch and roll.

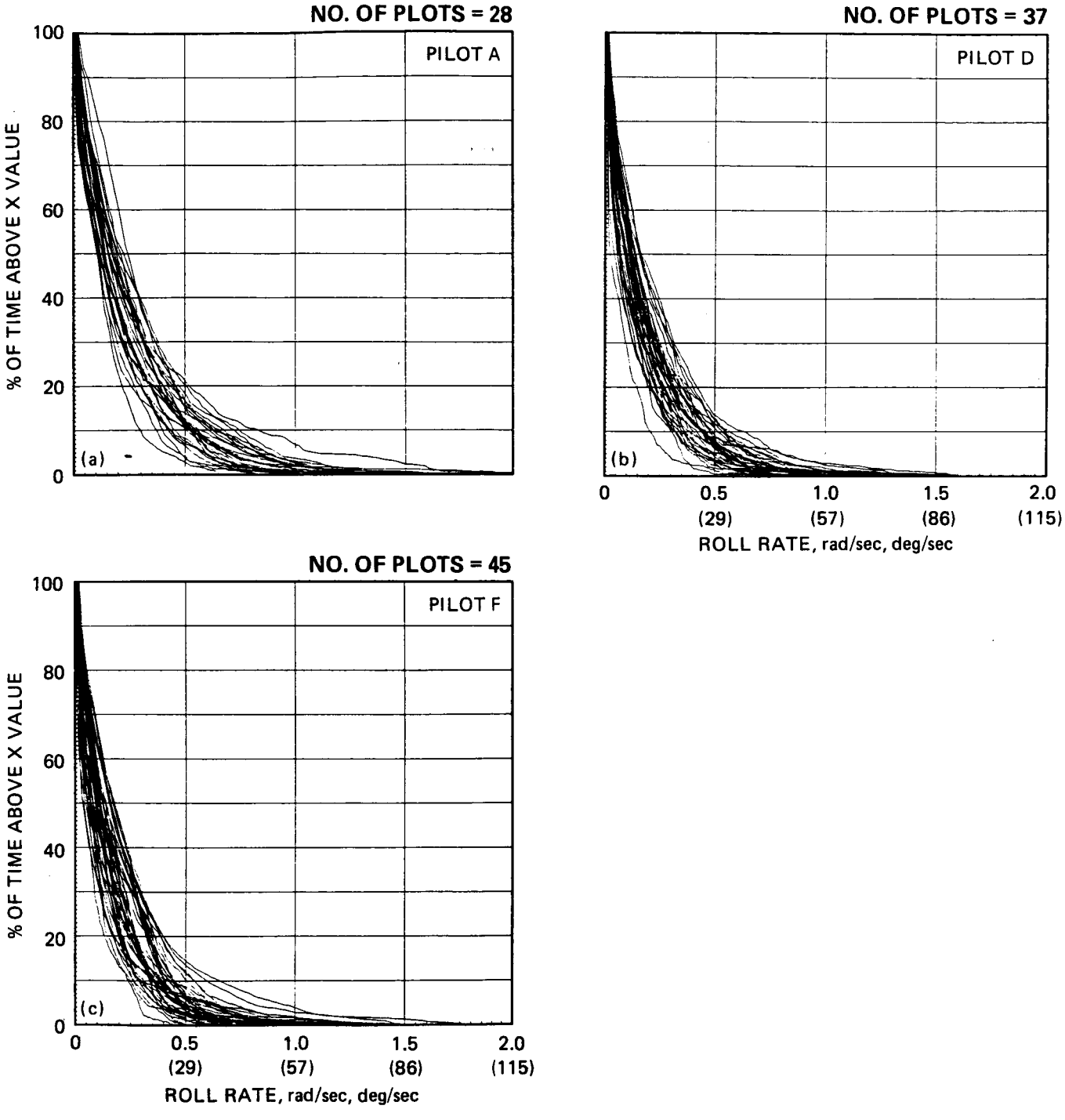

Figure 63.- Time-percentage plots of roll rate usage. (a) pilot A. (b) Pilot D. (c) Pilot F.

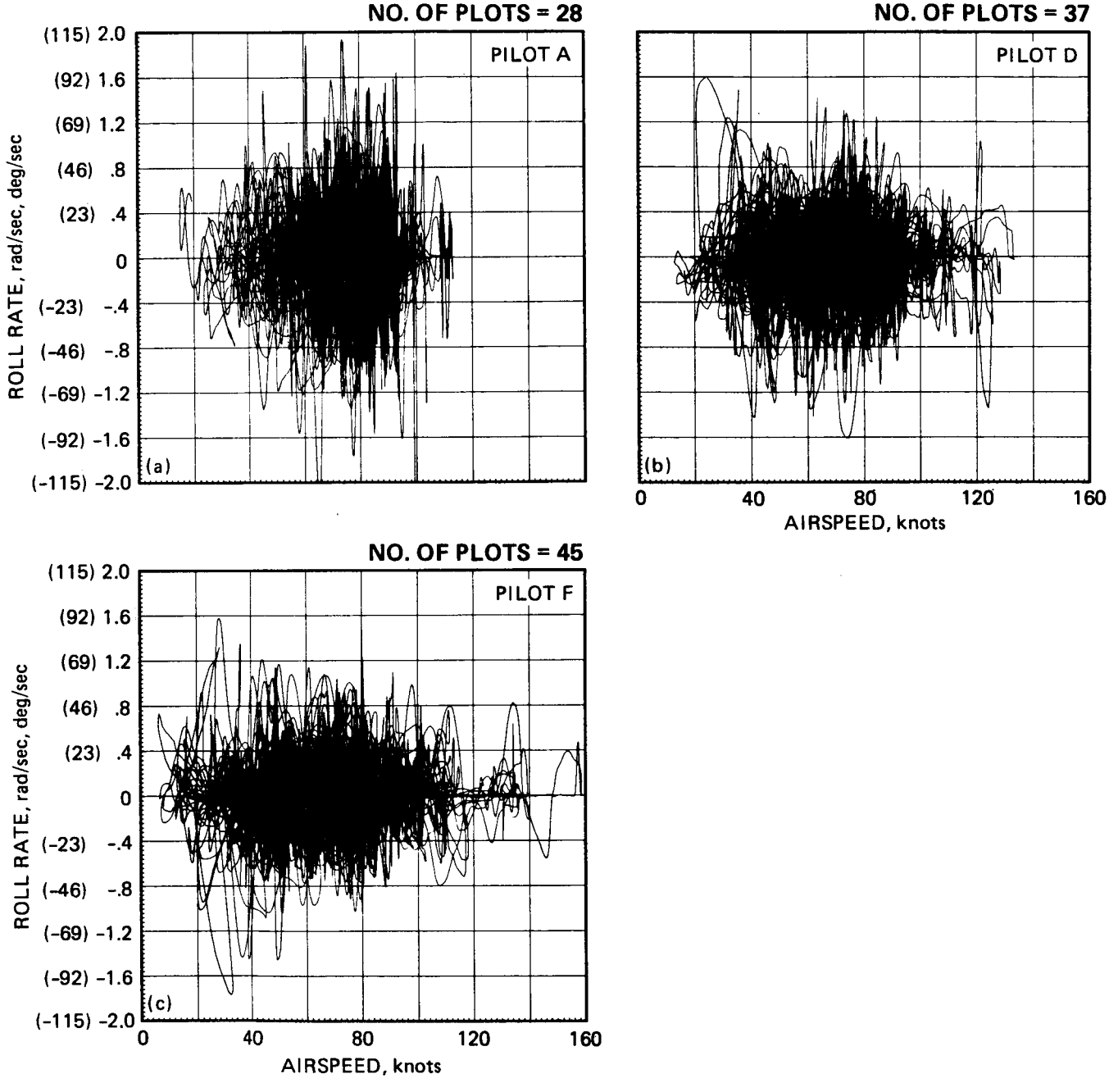

Figure 64.- Roll rate usage. (a) Pilot A. (b) Pilot D. (c) Pilot F.

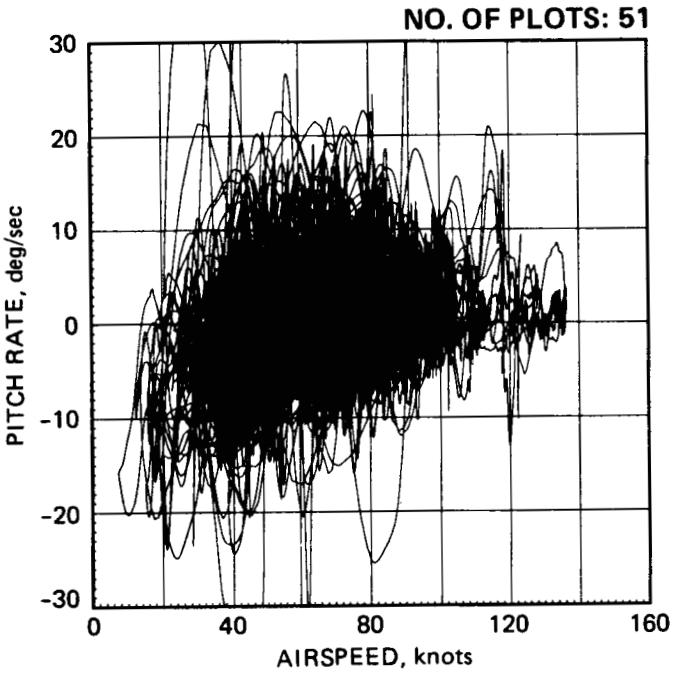

Figure 65.- Pitch rate usage, all pilots.

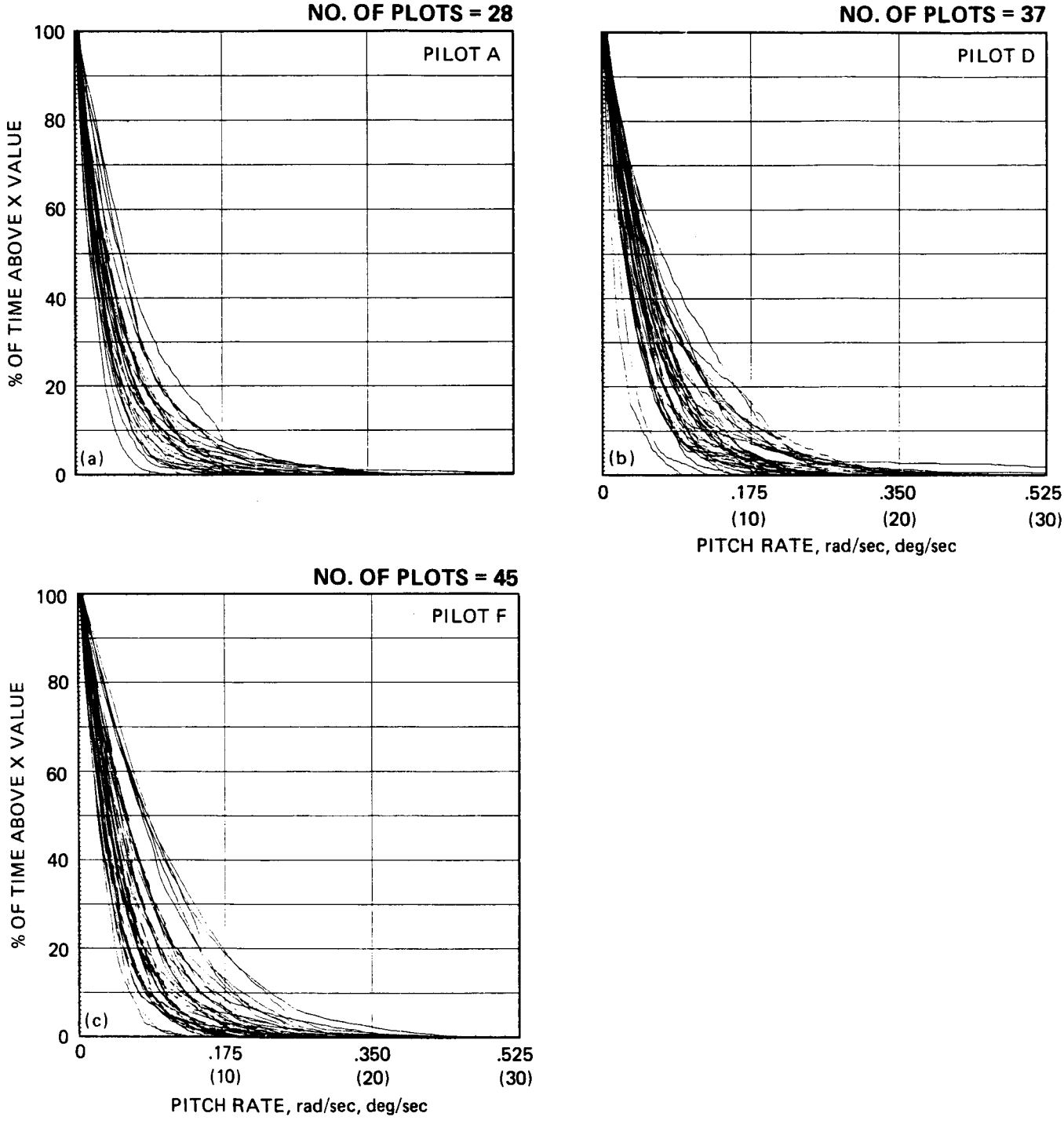

Figure 66.- Time-percentage plot of pitch rate usage. (a) Pilot A. (b) Pilot D. (c) Pilot F.

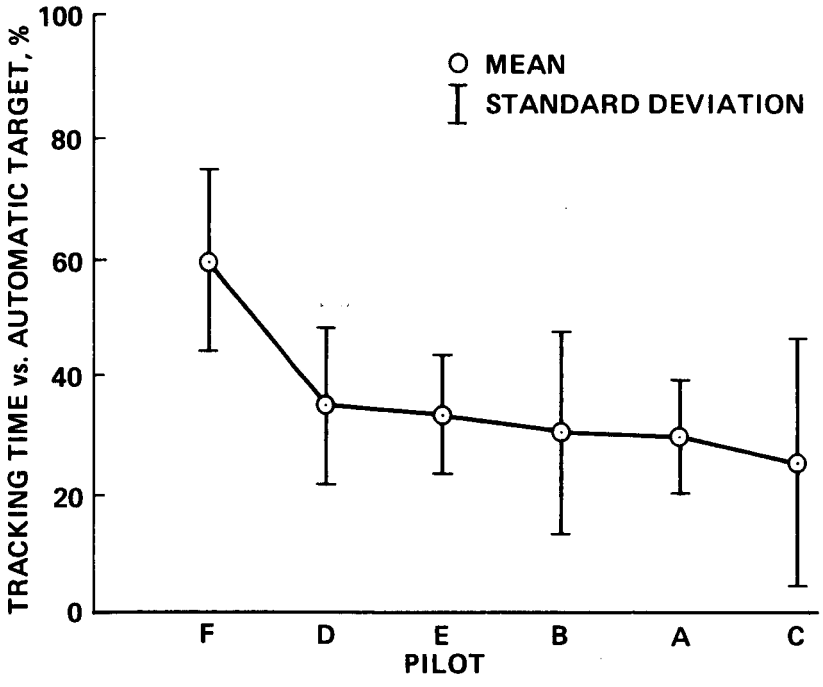

Figure 67.- Tracking scores for prerecorded target runs.

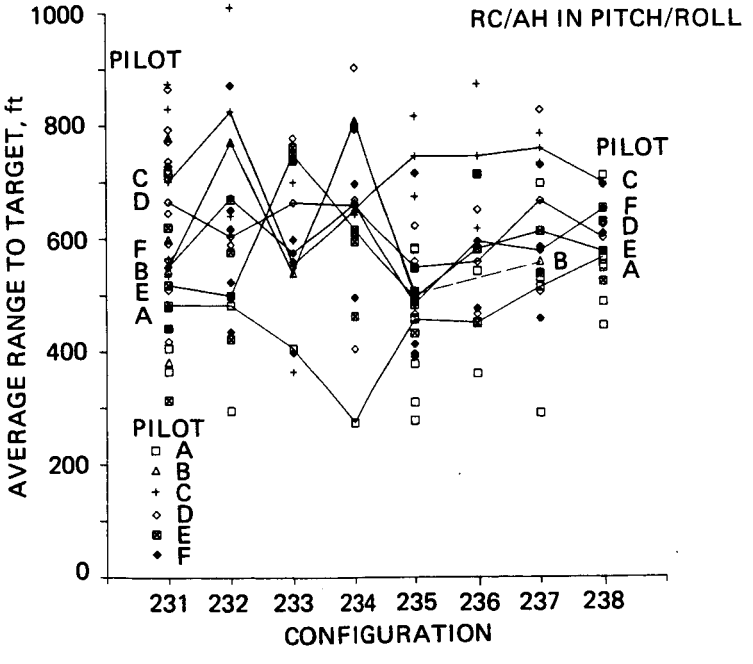

Figure 68.- Average tracking range used by evaluation pilots.

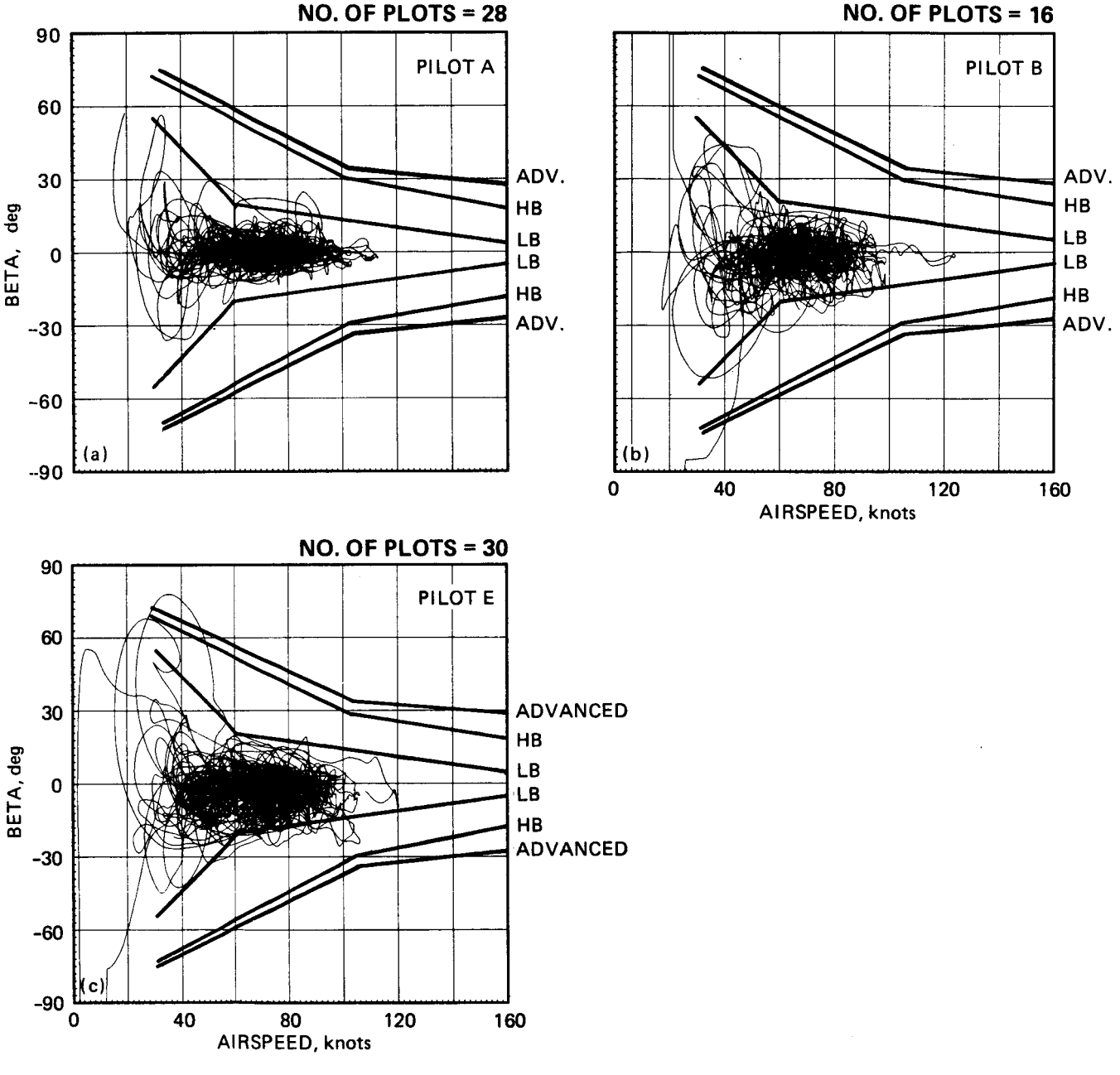

Figure 69.- Sideslip usage. (a) Pilot A. (b) Pilot B. (c) Pilot E.

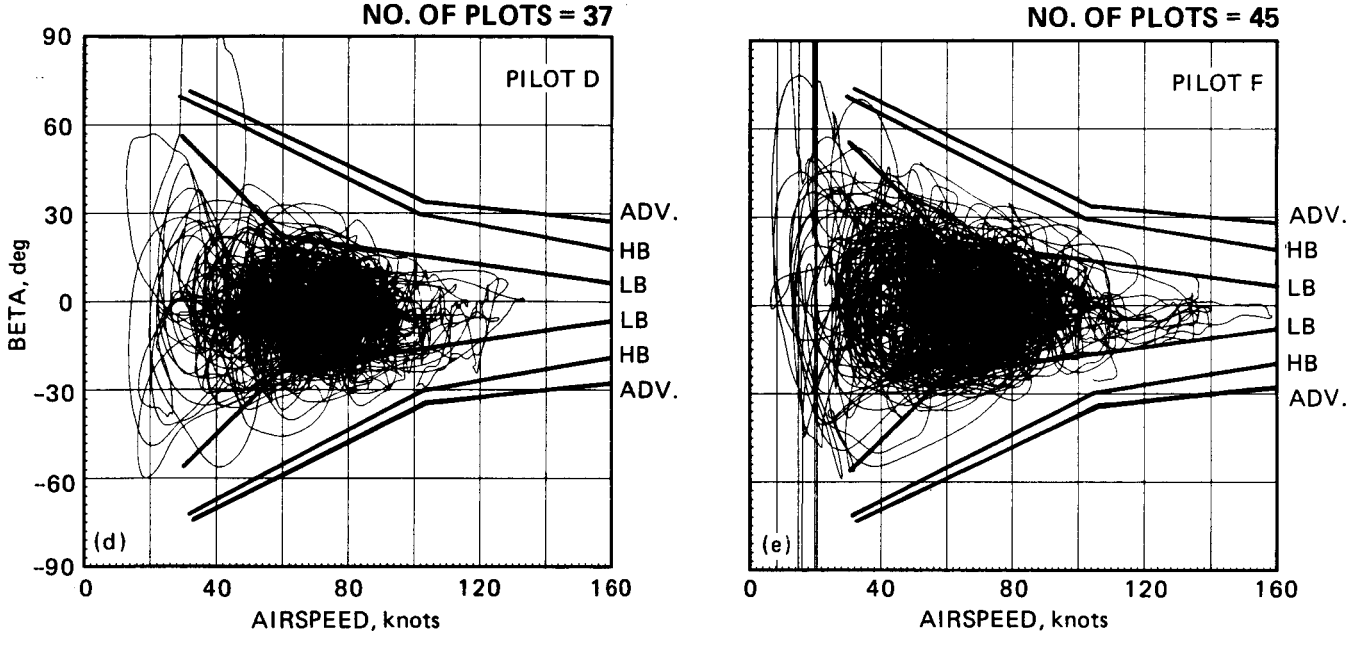

Figure 69.- Concluded. (d) Pilot D. (e) Pilot F.

END

DATE

DEC. 9, 1987

NASA National Aeronautics and Space Administration

Report Documentation Page

1. Report No.	2. Government Accession No.	3. Recipient's Catalog No.
NASA TM 89438 USAAVSCOM TM 87-A-3		

4. Title and Subtitle

A Piloted Simulation of Helicopter Air Combat to Investigate Effects of Variations in Selected Performance and Control Response Characteristics

5. Report Date

August 1987

6. Performing Organization Code

7. Author(s)

Michael S. Lewis,* M. Hossein Mansur,* and Robert T. N. Chen

8. Performing Organization Report No.

A-87147

10. Work Unit No.

505-61-51

9. Performing Organization Name and Address

Ames Research Center, Moffett Field, CA 94035 and
*Aeroflightdynamics Directorate, U.S. Army Aviation Research and Technology Activity, Ames Research Center, Moffett Field, CA 94035-1099

11. Contract or Grant No.

13. Type of Report and Period Covered

Technical Memorandum

12. Sponsoring Agency Name and Address

National Aeronautics and Space Administration Washington, DC 20546-0001 and U.S. Army Aviation Systems Command, St. Louis, MO 63120-1798

14. Sponsoring Agency Code

15. Supplementary Notes

Point of contact: Michael S. Lewis, Ames Research Center, MS 211-2, Moffett Field, CA 94035, (415) 694-6115 or FTS 464-6115

16. Abstract

A piloted simulation study investigating handling qualities and flight characteristics required for helicopter air-to-air combat is presented. The Helicopter Air Combat system (developed on the vertical motion simulator at NASA Ames Research Center) was used to investigate this important new role for Army rotorcraft.

Experimental variables for the study were the maneuver envelope size (load factor and sideslip), directional axis handling qualities, and pitch and roll control-response type. Over 450 simulated, low altitude, one-on-one engagements were conducted utilizing evaluation pilots from the Army, NASA, and industry.

Results from the experiment indicate that a well-damped directional response, low sideforce caused by sideslip, and some effective dihedral are all desirable for weapon system performance, good handling qualities, and low pilot workload. An angular rate command system was favored over the attitude-type pitch and roll response for most applications, and an enhanced maneuver envelope size over that of current generation aircraft was found to be advantageous. Pilot technique, background, and experience are additional factors which had a significant effect on performance in the air combat tasks investigated. The implication of these results on design requirements for future helicopters is presented.

17. Key Words (Suggested by Author(s))	18. Distribution Statement
Handling qualities Helicopter air combat Simulation Flight envelope	Unlimited - Unclassified Subject category: 08

19. Security Classif. (of this report)	20. Security Classif. (of this page)	21. No. of pages	22. Price
Unclassified	Unclassified	97	A05

NASA FORM 1626 OCT 86

For sale by the National Technical Information Service, Springfield, Virginia 22161